Head Office: Università degli Studi di Padova
Department of Molecular Medicine

Ph.D. COURSE IN MOLECULAR MEDICINE
CURRICULUM: REGENERATIVE MEDICINE
SERIES XXXII

Zebrafish as a model for dissecting the in *vivo* roles of Collagen VI

Coordinator: Prof. Stefano Piccolo
Supervisor: Prof. Stefano Piccolo
Co-Supervisor: Prof. Paolo Bonaldo

Ph.D. student: Valentina Tonelotto

Index

Abstract

My PhD project was focused on using *Danio rerio* (zebrafish) as an *in vivo* model to dissect the expression and function of Collagen VI (COL6), a key extracellular matrix component found in several tissues and involved in a range of physiological and pathological processes. Mutations of COL6 genes in humans can cause different forms of inherited muscular diseases, including Bethlem myopathy and Ullrich congenital muscular dystrophy. A number of animal models were generated for COL6-related myopathies, displaying a spectrum of phenotypes. In particular, studies carried out in COL6 knockout (*Col6a1*$^{-/-}$) mice provided a valuable tool for throwing light on the *in vivo* roles of COL6. Indeed, those studies demonstrated that COL6 exerts several cytoprotective functions, which span from counteracting apoptosis and oxidative damage, to the regulation of cell differentiation and autophagy. Despite this, no study until now ever assessed in detail which functions COL6 plays during development and in regulating intracellular signalling pathways. To gain further insights into these aspects, we decided to exploit zebrafish, a model that has been widely used for studies of vertebrate development and gene function. Indeed, thanks to its transparency and rapid development, zebrafish represents a powerful tool to visualize the expression pattern of a gene in the whole organism. In addition, the availability of transgenic biosensor lines makes zebrafish an ideal tool for the *in vivo* study of signaling pathways.

During the first part of my PhD, I characterized in detail the spatio-temporal expression pattern and distribution of COL6 in zebrafish embryos, larvae and adults. The results I obtained demonstrate that zebrafish COL6 genes exhibit features that are very similar to those found in their mammalian orthologs. In particular, by exploiting a new antibody generated against zebrafish COL6, I was able to characterize precisely the expression pattern of this distinctive ECM protein during zebrafish development and adult life. These data are of major relevance since they provide the basis for functional studies in this animal model, and they have been collected in a manuscript entitled "Spatio-temporal expression and distribution of collagen VI during zebrafish development", which is currently under revision.

In the second part of my PhD, I carried out a number of functional studies exploiting a novel zebrafish *col6a1* null line generated through CRISPR/Cas9 site-specific mutagenesis. The ablation of COL6 in this zebrafish model allowed me to identify

neuromuscular defects and distinctive alterations in the three-dimensional architecture of craniofacial cartilages. In addition, knockout of COL6 affected Wnt signaling during embryogenesis, thus pointing at a potential role of COL6 in regulating this major signalling pathway.

Altogether, the zebrafish *col6a1* null line represents a valuable tool to unveil previously unknown links between molecular and signaling defects and COL6 deficiency. Indeed, the data reported in this thesis underline how zebrafish represents a very useful *in vivo* model for increasing our understanding of the role of this major ECM protein in different physiological and pathological contexts, both during development and adult life. Moreover, the zebrafish *col6a1* null line represents a suitable tool for future drug testing aimed at finding novel treatments for COL6-related diseases.

Riassunto

ll mio progetto di dottorato si è basato sull'utilizzo del modello animale *Danio rerio* (zebrafish) al fine di analizzare l'espressione e la funzione del collagene VI (COL6), un componente chiave della matrice extracellulare presente in vari tessuti e coinvolto in numerosi processi fisiologici e patologici. Mutazioni a carico dei geni codificanti per le catene del COL6 sono note causare diverse forme di malattie muscolari ereditarie nell'uomo, tra cui la miopatia di Bethlem e la distrofia muscolare congenita di Ullrich. Diversi modelli animali sono stati generati al fine di studiare queste miopatie. In particolare, gli studi condotti su topi knockout per il COL6 (*Col6a1*$^{-/-}$) hanno permesso di mettere in luce alcuni dei ruoli chiave che questa proteina esercita *in vivo*. Tali lavori hanno infatti dimostrato che il COL6 svolge importanti funzioni citoprotettive, che vanno dal contrastare l'apoptosi e i danni ossidativi alla regolazione del differenziamento e dell'autofagia. Ciò nonostante, nessuno studio ha finora mai indagato a fondo quali siano le funzioni del COL6 durante lo sviluppo embrionale e nella regolazione delle vie di segnalazione intracellulari. Pertanto, allo scopo di ottenere ulteriori conoscenze su questi aspetti, abbiamo deciso di utilizzare lo zebrafish, un modello ampiamente impiegato negli studi sullo sviluppo dei vertebrati e sulla funzione genica. Grazie infatti alla sua trasparenza e al suo rapido sviluppo, lo zebrafish rappresenta un ottimo modello per visualizzare il pattern di espressione di un gene nell'intero organismo. Inoltre, la disponibilità di numerose linee transgeniche reporter rende lo zebrafish uno strumento ideale per lo studio *in vivo* delle vie di segnalazione intracellulare.

Durante la prima parte del mio lavoro di dottorato, ho analizzato in dettaglio il pattern di espressione spazio-temporale e la distribuzione delle diverse catene del COL6 in embrioni, larve e adulti di zebrafish. I dati ottenuti dimostrano che i geni COL6 presentano un pattern di espressione nello zebrafish molto simile a quella dei rispettivi ortologhi in mammifero. In particolare, sfruttando un nuovo anticorpo che riconosce in maniera specifica il COL6 di zebrafish, ho potuto caratterizzare in dettaglio la distribuzione della proteina in questo organismo, sia durante lo sviluppo embrionale che in età adulta. Tali dati sono di notevole interesse, in quanto forniscono una base essenziale per poter effettuare degli studi funzionali in questo modello animale. I risultati ottenuti sono stati quindi raccolti in un lavoro intitolato "Spatio-temporal expression and distribution of collagen VI during zebrafish development", il quale è attualmente in fase di revisione.

Nella seconda parte del mio dottorato ho svolto studi funzionali sfruttando una nuova linea di zebrafish priva di COL6, generata nel laboratorio attraverso la tecnologia di mutagenesi sito-specifica CRISPR/Cas9. In tale linea ho individuato numerosi difetti neuromuscolari e peculiari alterazioni nella struttura tridimensionale delle cartilagini craniofacciali. Inoltre, ho identificato che l'assenza di COL6 causa alterazioni nella via di segnale di Wnt, suggerendo un ruolo del COL6 nel regolare questa via di segnalazione intracellulare.

Complessivamente, i dati ottenuti dimostrano che la linea di zebrafish non esprimente il COL6 rappresenta un valido modello *in vivo* per svelare connessioni ancora poco conosciute tra carenza di COL6 e deficit molecolari e di vie di segnalazione. Le evidenze riportate in questa tesi sottolineano infatti come lo zebrafish sia estremamente utile nello studio del ruolo di questa proteina di matrice in diversi contesti fisiologici e patologici, sia durante lo sviluppo che nella vita adulta. Inoltre, il modello zebrafish COL6 knockout rappresenta lo strumento ideale per effettuare studi farmacologici volti ad identificare nuovi trattamenti per le malattie associate ad alterazioni del COL6.

1. Introduction

1.1. The extracellular matrix

The extracellular matrix (ECM) is a complex network of proteins and polysaccharides found in all solid tissues. Each tissue has an ECM with a unique composition and topology. The composition and organization of the ECM is finely regulated during tissue development through a dynamic and reciprocal interaction between the different cellular components (e.g. fibroblasts, adipocytes, endothelial and epithelial cells) and the evolving cellular and protein microenvironment. The ECM provides essential physical scaffolding for the cellular constituents, giving rise to a three-dimensional network in which cells are layered and anchored to form specialized tissues and organs. Moreover, it initiates crucial biochemical and biomechanical cues that are required for tissue morphogenesis, differentiation and homeostasis (Hay, 1981; Frantz et al., 2010).

1.1.1. ECM components: structure, interactions, and function

The major constituents of ECMs are various classes of proteins, such as collagens, elastin, fibronectin, laminins and other glycoproteins, as well as proteoglycans and glycosaminoglycans, which are highly acidic and hydrated molecules. These matrix components bind to each other as well as to cell adhesion receptors, forming a complex network into which cells reside in all tissues and organs. The remodeling of this highly dynamic network is mediated by several matrix-degrading enzymes.

Proteoglycans (PGs) are among the most important structural and functional macromolecules in tissues. They can be classified into four families, namely intracellular (e.g. serglyclin, present in secretory compartments), cell surface (e.g. syndecans, glypicans), pericellular-basement membrane (e.g. perlecan), and extracellular ones (e.g. small leucine-rich proteoglycans, SLRPs), according to their cellular and subcellular location, gene/protein homology, and the presence of specific protein modules within their respective protein cores (Theocharis et al., 2010; Iozzo and Schaefer, 2015). They consist of a core protein onto which one to several hundred glycosaminoglycan (GAG) chains of the same or different types are covalently attached. GAGs are long, highly negatively charged heteropolysaccharides composed of repeating disaccharide units [sulfated N-aceltylglucosamine or N-acetylgalactosamine, D-glucuronic or L-iduronic acid and galactose (4 N-

acetylglucosamine-β1,3-galactose-β1)] that can be divided further into sulfated (chondroitin sulfate, heparan sulfate and keratan sulfate) and non-sulfated (hyaluronic acid, HA) GAGs (Frantz et al., 2010; Schaefer and Schaefer, 2010). HA is the only GAG not covalently linked to PGs, but it does assemble with aggregating PGs and the interaction between the two components are critical for the formation of pericellular matrices (Heldin and Pertoft, 1993). Moreover, HA can act as a signalling molecule interacting with its receptors, such as CD44 (Turley et al., 2002). Sizes of PG core proteins range from 10 kDa to 500 kDa, rendering them a complex and heterogeneous group of macromolecules (Silbert and Sugumaran, 1995). These molecules are extremely hydrophilic, and thus adopt highly extended conformations that are fundamental for hydrogel formation and enabling matrices formed by these molecules to sustain high compressive forces (Frantz et al., 2010). Besides acting as structural components, PGs also interact with numerous growth factors, cytokines and chemokines, proteases, cell surface receptors and other ECM molecules either via their core proteins or through their GAG side chains, participating in several cell mechanisms, such as cell signaling, proliferation, migration, differentiation, apoptosis, and adhesion. Thus, PGs and GAGs play important roles in normal physiology and development of various diseases, since their biosynthesis is highly modified during ECM remodeling in different pathologies (Iozzo and Sanderson, 2011).

The main fibrous ECM proteins are collagens, elastin, fibronectin and laminins.

Elastic fibers are large ECM structures that provide recoil to tissues which undergo repeating stretching forces, such as large elastic blood vessels, lungs, heart, elastic ligaments, skin, bladder, and elastic cartilage (Theocharis et al., 2010). Importantly, elastin stretch is limited by tight association with collagen fibrils, which give tensile strength and limit tissue stretching, avoiding damage (Wise and Weiss, 2009). Genesis of elastic fibers involves deposition of tropoelastin (the precursor of elastin) on a preformed template of microfibrils made of specific glycoprotein, mainly fibrillins (Davis and Mecham, 1998). Secreted tropoelastin molecules assemble into fibers and become highly cross-linked to one another via their lysine residues by members of the lysyl oxidase enzyme family (Lucero and Kagan, 2006).

Another distinct fibrous member of the ECM is fibronectin (FN), a glycoprotein involved in directing the organization of the ECM and in mediating cell attachment and function. FN consists of two subunits, each with a size of almost 250 kDa, that are covalently connected with disulfide bonds at their C-termini. Cell-surface binding

of the soluble FN dimer is essential for its assembly into longer fibrils (Pankov, 2002). FN has several binding sites to collagen, to heparin and also to cell-surface integrin receptors (Pankov, 2002). The interaction with integrins, in particular, results in pleiotrophic changes in cellular behavior and implicate FN as an important extracellular player in mechanotransduction processes (Smith et al., 2007). FN is important to promote neural crest differentiation along the smooth muscle lineage during development and has been implicated in cardiovascular disease and tumor metastasis (Costa-Silva et al., 2009; Tsang et al., 2010).

Together with fibronectin, laminins are the best-studied ECM glycoproteins. Laminins comprise a family of large heterotrimeric cross-shaped glycoproteins, which are assembled into basement membranes along with other ECM molecules, such as collagen type IV, nidogens and perlecan. Each laminin heterotrimer is composed by one α, one β and one γ chain, each of which is encoded by individual genes (Aumailley et al., 2005). Five α, four β, and three γ laminin chains have been identified, which can combine to form 15 different isoforms (Hallmann et al., 2005). The distribution of laminin isoforms is tissue-specific, suggesting the involvement of distinct laminins in tissue functions. In particular, they influence cell differentiation, adhesion, and migration and are vital for the maintenance and survival of tissues (Hallmann et al., 2005).

Besides fibrous components, PGs and GAGs, ECM also includes enzymes involved in the remodeling that occurs during physiological and pathological conditions, as they modulate the structure and properties of ECMs in multiple ways. Matrix metalloproteases (MMPs), a-disintegrin-and-metalloproteases (ADAMs) and ADAMs with thrombospondin motifs (ADAMTSs) are some of the major enzymes involved in the proteolytic degradation of ECM components. Of note, these proteases also release growth factors and cytokines from the ECM, while their actions on matrix molecules, including collagens, elastin, various PGs, and cell membrane receptors, generate bioactive molecules known as matrikines (Wells et al., 2015) and modulate cell–cell communication and tumor progression (McCawley and Matrisian, 2001).

Cells embedded into ECM interact with this macromolecular network through their surface receptors, such as integrins, discoidin domain receptors (DDRs), cell surface PGs, and the HA receptor CD44. These receptors are able to transduce signals into cells from ECM, thus regulating different intracellular processes, such as survival, growth, migration, and differentiation at developmentally and physiologically relevant times (Theocharis et al., 2016). Importantly, soluble factors (e.g. growth

factors, cytokines, and chemokines) can be stored in the ECM, which acts as a reservoir, and in the presence of appropriate forces or after proteolytic degradation, they can be released from the ECM for the subsequent binding to their cell surface receptors (McCawley and Matrisian, 2001).

Altogether, it is becoming increasingly clear that ECM protein networking has a crucial role in modulating cell behaviour and homeostasis. At the same way, abnormal changes in ECM composition and structure can lead to pathological conditions, such as tumorigenesis, inflammation processes, and neuromuscular diseases (Tsang et al., 2010). Therefore, detailed understanding of the different biological activities and properties of the ECM components will be fundamental for developing novel targeted therapeutic interventions for disease treatment. In this regard, mutant and knockout animal models for ECM molecules provide a valuable tool for translational studies and for the mechanistic understanding of human diseases linked to ECM defects.

1.1.2. Collagens

Collagens are the most abundant class of fibrous proteins in the interstitial ECM, and they represent up to 30% of the total protein mass of a multicellular animal. A large part of ECM deposited collagens is secreted by fibroblasts that reside in the stroma or are recruited from neighboring tissues (De Wever et al., 2008). The collagen superfamily is composed of at least 28 different collagen types that are formed by at least 46 distinct polypeptide subunits (called α chains) in vertebrates (Kadler et al., 2007). The characteristic feature of collagens is a structural motif in which three polypeptide (α) chains display a polyproline II-type helical conformation and coil with each other, forming a right-handed triple helix (Brodsky and Persikov, 2005). In each α chain, a repeated Gly-Xaa-Yaa amino acid triplet unit is present, where the Xaa and Yaa positions are frequently occupied by proline and 4-hydroxyproline, respectively. This repeating structure forms stable, rod-like, trimeric coiled coils, which can vary in lengths (Brodsky and Persikov, 2005). According to their common domain homology and functions, collagens can be classified into seven categories, namely fibrillar collagens, network-forming collagens, FACITs (fibril-associated collagens with interrupted triple helices), MACITs (membrane-associated collagens with interrupted triple helices), anchoring fibrils, beaded filament-forming collagens, and multiplexin (multiple triple-helix domains and interruptions)/endostatin-producing collagens (Shoulders and Raines, 2009).

The organization, distribution and density of collagen fibrils and networks is different between tissues, influencing the direction and magnitude of forces to which a given tissue is subjected. These proteins are the principal tensile element of tissues such as tendon, cartilage, bone and skin. Moreover, they are located in specialized basement membranes, such in the kidney glomerulus, where they are involved in molecular filtration. Thus, collagens are important for a broad range of functions, including tissue scaffolding, cell adhesion, cell migration, cancer, angiogenesis, tissue morphogenesis and tissue repair (Rozario and DeSimone, 2010). Several mutations have been identified in collagens, where they can affect trimerization, three-dimensional folding, formation of matrix networks, or interaction with other ECM molecules or cell surface receptors. These mutations have been linked with various clinical pathologies, such as Ehlers–Danlos syndrome (collagen types I, III, V), osteogenesis imperfecta and osteoporosis (collagen type I), osteoarthrosis (collagen types II, IX, XI), chondrodysplasias (collagen types II, IX, X, XI), arterial aneurysms (collagen type III), epidermolysis bullosa acquisita (collagen type VII), Bethlem myopathy and Ullrich muscular dystrophy (collagen type VI) (Theocharis et al., 2016).

1.2. Collagen VI

Collagen VI (COL6) is a unique type of collagen forming a distinctive microfilamentous network in several tissues, such as skeletal muscle, skin, cornea, lung, blood vessels, tendons, intervertebral disks, peripheral nerves, lungs, heart, adipose tissue, skin and cartilages (Keene, 1988; Kuo et al., 1997; Cescon et al., 2015).

1.2.1. COL6 structure, assembly and interactions

Three genetically distinct COL6 chains were originally identified and named α1(VI), α2(VI) and α3(VI), which are respectively encoded by the *COL6A1*, *COL6A2* and *COL6A3* genes in humans (Chu et al., 1988; Bonaldo et al., 1989; Bonaldo et al., 1990; Doliana et al., 1990). COL6 monomers are constituted by three polypeptide chains in a 1:1:1 stoichiometric ratio (Bonaldo et al., 1987). More recently, three other genes coding for COL6 chains were identified and annotated as *COL6A4*, *COL6A5* and *COL6A6*, showing high sequence homology and shared domain structure with α3(VI). In humans, a large chromosome inversion broke the *COL6A4* gene into two separate non-processed pseudogenes (Gara et al., 2008). The fact that the α4(VI), α5(VI) and α6(VI) chains share a similar structure with α3(VI) indicate that they represent alternative polypeptides for the assembly of COL6 subunits into α1–α2–αX triple-

helical monomers (where αX is either α3, α4, α5 or α6), thus increasing the structural and functional versatility of this ECM component (Gara et al., 2011; Maaß et al., 2016). The *COL6A1* and *COL6A2* genes are located on chromosome 21q22.3, in a head-to-tail orientation, while the *COL6A3* gene maps to chromosome 2q37 (Lampe and Bushby, 2005). *COL6A4*, *COL6A5* and *COL6A6* are located in tandem on chromosome 3q21. All COL6 chains are constituted by a short central triple helical region of 335–336 amino acid residues, which is flanked by large N- and C-terminal globular regions sharing similarity with the von Willebrand factor type A (VWA) module (Colombatti and Bonaldo, 1991). The α1(VI) and α2(VI) chains are approximately 130–150 kDa in size, while α3(VI), α4(VI), α5(VI) and α6(VI) are much larger, ranging from 220 kDa to over 300 kDa (Bonaldo et al., 1987; Gara et al., 2008). The α1(VI) and α2(VI) chains contain one N-terminal and two C-terminal VWA modules (N1, and C1 and C2, respectively) (Bonaldo et al., 1989). Conversely, each longer chain comprises more N-terminal VWA modules (N1 to N10 in α3; N1 to N7 in α4, α5 and α6), and two C-terminal VWA modules (C1 and C2), followed by unique regions (C3–C5). The C3 domain comprises a proline-rich sequence, which in the α6(VI) chain is also the C-terminal end. In the α3(VI) chain, C4 is a fibronectin-type-III domain, and C5 is a Kunitz-like domain (Bonaldo et al., 1990). The murine α4(VI) chain presents a stretch of 17 amino acid residues at the C-terminal end (C4) which is similar to a partial Kunitz-like domain. The C-terminus of α5(VI) presents an additional VWA domain (C4), followed by another unique domain (C5) (Bonaldo and Colombatti, 1989; Bonaldo *et al*., 1990; Fitzgerald *et al*., 2008; Gara *et al*., 2008). The C5 domain of α3 chain is needed for microfibril formation (Lamandé et al., 2006), from which it is then cleaved off (Aigner et al., 2002). The resulting peptide, named endotrophin, is capable of promoting the growth of breast cancer cells in a process that is triggered by the interaction of adipocytes with tumor and stromal cells (Aigner et al., 2002; Park and Scherer, 2012). Recently it has been demonstrated that the extracellular metalloproteinase bone morphogenetic protein 1 (BMP-1) is involved in endotrophin release and the BMP-1 cleavage site has been identified (Heumüller et al., 2019). Endotrophin-containing fragments were found in various tissues and body fluids, pointing out the possibility to use them as biomarkers of disease progression (Heumüller et al., 2019).

Several alternatively spliced variants that involve some VWA modules were also described for the α3(VI) and α2(VI) chains. For instance, in the α3(VI) chain, the N10, N9 and N7 domains are subjected to alternative splicing, and transcript variants missing one or more of these N-terminal domains have been detected in mouse

tissues and human cells (Doliana *et al*., 1990; Dziadek *et al*., 2002). Conversely, alternative splicing of the human α2(VI) transcript was found to generate three different protein variants, called α2C2, α2C2a and α2C2a′ (Saitta *et al*., 1990).

COL6 has a unique intracellular assembly process made of distinct steps (Figure 1), where three different chains associate intracellularly to form disulfide-bonded monomers (~500 kDa), dimers (~ 1000 kDa), and tetramers (~ 2000 kDa) before secretion (Colombatti and Bonaldo, 1987; Colombatti et al., 1987). These tetramers are finally secreted and, in the extracellular space, they associate end-to-end through non-covalent bonds to form the characteristic beaded microfilaments with a periodicity of 105 nm, as revealed by electron microscopy studies (Furthmayr et al., 1983; Knupp et al., 2006; Cescon et al., 2015).

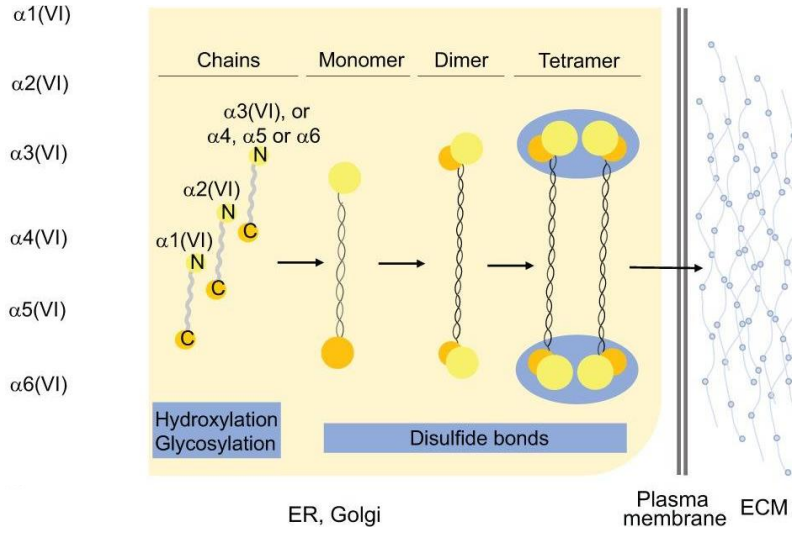

Figure 1. Diagram displaying COL6 assembly and secretion. Modified from (Gregorio et al., 2018).

In the extracellular microenvironment, COL6 forms a network which interact with a range of other ECM molecules, thus supporting tissue 3D architecture and anchoring large interstitial structures. In particular, it allows the establishment of a proper link between muscle cells and ECM by binding to collagen IV and perlecan in the basal lamina (Kuo et al., 1997). It also interacts with other collagens, such as collagen types I, II and XIV (Bonaldo et al., 1990; Bidanset et al., 1992; Brown et al., 1994), and other ECM molecules, among which microfibril-associated glycoprotein MAGP1 (Finnis and Gibson, 1997), matrilin-1 (Wiberg et al., 2001), fibulin-2 (Sasaki et al., 1995), lumican (Takahashi et al., 1993), heparin, hyaluronan (Specks et al., 1992) and decorin (Bidanset et al., 1992). Biglycan and WARP are thought to play a role in stabilizing and regulating COL6 secretion and assembly in the extracellular space (Hansen et al.,

2012), while the absence of COL6 was found to affect fibronectin deposition in cultured fibroblasts (Sabatelli et al., 2001). Furthermore, COL6 interacts with several membrane receptors involved in intracellular signaling pathways. Among them there are various integrins, including α1β1, α2β1, α3β1, α10β1, α11β1 and αvβ3 (Pfaff et al., 1993; Doane et al., 1998; Tulla et al., 2001), the chondroitin sulfate proteoglycan-4 (CSPG4; also known as NG2) (Stallcup et al., 1990; Sardone et al., 2016), and the anthrax receptors ANTXR1/TEM8 and ANTXR2/CMG2 (Nanda et al., 2004; Bürgi et al., 2017). Despite these various data and information, it remains unclear how COL6 extracellular signals are transduced within cells.

1.2.2. COL6 tissue expression during embryogenesis and adult life in mammals

A distinctive pattern of expression during development is a common feature of most genes coding for ECM components. Consistently, COL6 expression pattern is dynamically regulated throughout life. Studies in mice revealed that the transcription of the *Col6a1* gene in different tissues is regulated by separate enhancer elements organized in a modular arrangement within a large genomic region spanning about 20 kb at the 5' end of the transcribed region, thus conferring a remarkable flexibility in the spatio-temporal control of COL6 expression during development (Braghetta et al., 1996). Moreover, all COL6 chains display restricted patterns of expression among different tissues, thus highlighting the concept of tissue-specific roles for this ECM component (Marvulli et al., 1996; Gara et al., 2011).

During mouse embryogenesis, *Col6a1* transcripts are first detected at embryonic day (E) 10.5, predominantly in mesenchymal cells of different tissues, including branchial arches, large blood vessels, myotomes and meninges (Marvulli et al., 1996). From E16.5, *Col6a1* expression is also found in joints, intervertebral disks, perichondrium, periostium, dermis, skeletal muscle and heart valves, whereas lower amounts of the transcript are found in cartilage and bone. In several organs, among which are lung, salivary glands and the digestive tract, *Col6a1* is deposited underneath epithelia (Dziadek et al., 1996; Marvulli et al., 1996). The pattern of distribution of the α1(VI) protein well reflects that of the *Col6a1* mRNA, with abundant ECM deposition in skeletal muscles and adrenal glands, and in the salivary, nasal, oral, gastric and intestinal mucosa. In the nervous system, α1(VI) is found in the peripheral branches of nerves, where it forms a sheath around axon bundles (Marvulli et al., 1996), and in the mesenchyme of the developing murine choroid plexus (Dziadek et al., 1996).

Abundant α1(VI) deposition is also found in the eye, where the protein is present in the cornea and sclera and in the mesenchyme of conjunctiva. Interestingly, high levels of *Col6a1* mRNA are also observed in rabbit fetal corneas (El-Shabrawi et al., 1998). Thus, during development COL6 mainly defines the boundaries of distinct domains in connective tissues. In adult mice, tissues in which *Col6a1* transcript is still abundant are lung, skin, adrenal gland, heart, skeletal muscle, tail and fat (Marvulli et al., 1996). The expression of *Col6a2* transcript during mouse embryogenesis is very similar to that of *Col6a1*, as it accumulates predominantly in mesenchymal structures (Dziadek et al., 1996), with abundant expression in lungs, heart, liver, skin and brain starting from E12 (Dziadek et al., 1996). This overlapping distribution between *Col6a1* and *Col6a2* transcripts is in agreement with the fact that the synthesis and secretion of COL6 requires the assembly into α1–α2–αX monomers.

Concerning the other COL6 chains, a more recent study in mouse compared the tissue distribution of the novel chains (α4, α5, α6) with that of α3(VI) (Gara et al., 2011). Interestingly, and at difference from the broadly expressed α3 chain, the novel chains show a more restricted and sometimes complementary expression. In E14.5 mouse embryos, all the novel chains are present in bronchi and partly co-localize with α3(VI). The α4 and α5 chains are more abundant in the muscular and epithelial layers of the developing bronchial wall, whereas they are display weak expression in the parenchyme of the lung. Intriguingly, the α6 chain displays the opposite pattern of distribution. In the inner wall of the developing stomach the α4 chain is distributed exactly where the α3 chain is absent or weakly expressed, while no expression of α5 and α6 chains is found in stomach. In adult mice, the α3 chain is expressed in the muscular, inner and sub-mucosal layers of intestine, while α4 chain is abundant in the sub-mucosal and mucosal layers but is absent in the muscular layer. The α6 chain is not present in smooth muscles, whereas its expression is abundant in the perimysium and epimysium of skeletal and cardiac muscles. The α3 and α5 chains are present in all three muscle tissue types, with a strong deposition of α5 in the basement membrane at the neuromuscular junction (Gara et al., 2011).

Further studies revealed that the distribution of the novel chains in mouse does not always overlap with that found in humans. For instance, the α6 chain is present in the territorial matrix of human articular cartilage (Fitzgerald et al., 2008), while no expression of the novel chains is detected in mouse cartilage. Moreover, while the α5 chain in humans is mainly found in the papillary dermis, the mouse α5 chain is present in the basement membranes surrounding blood vessels in the dermis,

mimicking the distribution of the human α6 chain in the skin (Sabatelli et al., 2011). The differences observed in tissue distribution of the novel chains between humans and mouse may be due to the loss of a functional gene for the α4 chain in humans, as a consequence of the chromosome inversion that broke the *COL6A4* gene into two pseudogenes (Gara et al., 2008).

1.2.3. COL6 functions

COL6 exerts a broad range of functions, spanning from the fine regulation of mechanical properties to cytoprotective functions, such as inhibition of apoptosis and oxidative damage, promotion of tumor growth and progression, regulation of cell differentiation and of the autophagic machinery, and maintenance of cell stemness (Cescon et al., 2015).

1.2.3.1. COL6 function in skeletal muscle

As described above, COL6 is one of the major components of muscle ECM and is found in the basement membrane of myofiber endomysium (Bönnemann, 2011b). The deposition of COL6 in muscle is mainly provided by interstitial fibroblasts, whereas it is not produced by myoblasts and myofibers. However, the presence of myogenic cells is required for the transcriptional induction of the *Col6α1* gene in mesenchymal cells (Braghetta et al., 2008).

The importance of COL6 for the proper structure and function of skeletal muscle is underlined by the evidence that altered expression or mutations in the genes encoding its chains can cause several human disorders, collectively known as "COL6-related myopathies". These include Ullrich congenital muscular dystrophy (UCMD), Bethlem myopathy, (BM) and myosclerosis myopathy (Bönnemann, 2011b; Cescon et al., 2015).

UCMD (MIM #254090) presents with signs and symptoms that are readily apparent at birth or during the first years of life. Clinical manifestations at birth include hypotonia and weakness associated with distal joint laxity, while contractures and skeletal deformities can be seen in more proximal joints in about 50% of the patients (Bönnemann, 2011a). In the most severe cases walking is never achieved, but more commonly children with UCMD achieve the capacity to walk, sometimes only with the use of assistive devices (Nonaka et al., 1981; Voit, 1998). Walking then is typically lost again during childhood, around 10 years of age (Nadeau et al., 2009). Beside musculoskeletal system, also the skin is significantly affected, leading to excessive

scar formation including the formation of large keloids (Bönnemann, 2011a). Feeding and swallowing difficulties have been observed in several affected infants. Some of them required transient nasogastric tube feeding, while a minority receive G-tube feeding later in life to avoid the risk of nutritional deficiency and dehydration (Nadeau et al., 2009). The rapid progression of UCMD symptoms usually leads to early death in the first or second decade of life, mainly as a result of respiratory failure due to weakness of the diaphragm and accessory muscles as well as stiffness of the chest wall (Mercuri et al., 2002; Briñas et al., 2010).

In BM (MIM #158810) the onset of the disease may also be congenital, but children are affected to a much milder degree (Lampe and Bushby, 2005). Muscle weakness often shows a proximal predominance, but there can be distal weakness as well. The weakness is stable or may improve in puberty, but a slowly progressive increase in wasting is usually found in the third to fourth decades of life. Thus, most patients need assistance for ambulation at around 50 years of age (Jöbsis et al., 1999). Foot dorsiflexion contractures and torticollis have been noted at birth in most affected infants (Jöbsis et al., 1999). As in UCMD, development of keloidal scars is often observed (Nadeau and Muntoni, 2008). A potential complication is the development of respiratory insufficiency, resulting from the combination of stiffness of the rib cage and diaphragmatic muscle weakness (Haq et al., 1999).

So far, all COL6 mutations associated with UCMD and BM spectra of disorders were described in the *COL6A1*, *COL6A2* and *COL6A3* genes (Bönnemann, 2011b). UCMD occurs through both recessive and dominant genetic mechanisms, the latter most typically as *de novo* autosomal-dominant mutations. Recessive mutations mostly lead to complete absence of COL6 in the ECM of muscle and of dermal fibroblast cultures (Camacho Vanegas et al., 2001). Of note, haploinsufficiency was also described, even if carriers of these null mutations are not significantly affected clinically (Camacho Vanegas et al., 2001; Foley et al., 2009). As regard BM, although initially researchers thought that only dominant mutations caused the disease, recessive mutations were also described in BM, thus suggesting the presence of a spectrum of COL6-associated disorders, with a broad range of clinical and genetic heterogeneity (Foley et al., 2009; Caria et al., 2019).

A further type of COL6-related myopathy is autosomal recessive myosclerosis (MIM #255660), a rare myopathy characterized by moderate weakness, "woody consistency" of muscles and progressive contractures of multiple joints, including masseter muscles, neck, shoulders, elbows, fingers, knees, and Achilles tendons. This

mostly contractural phenotype was associated with mutations in the *COL6A2* gene (Merlini et al., 2008).

1.2.3.1.1. *Col6a1* knockout mouse: a model of COL6 deficiency

To gain insight into the *in vivo* roles of COL6, a *Col6a1* knockout (*Col6a1*$^{-/-}$) mouse model lacking COL6 was generated. In this mouse, the second exon of the of *Col6a1* gene, coding for the signal peptide of the α1(VI) chain, was inactivated by targeted gene disruption, leading to the complete absence of the α1(VI) chain. As a consequence, even if α2(VI) and α3(VI) chains are translated, the formation of COL6 monomers is compromised, thus no triple helical COL6 molecules can be synthesized and secreted in the *Col6a1*$^{-/-}$ mice (Bonaldo et al., 1998).

This mouse model largely contributed to unveil many of the COL6 *in vivo* functions, throwing new light on the relevance of this matrix component, but also of the ECM in general, in regulating several cellular pathways.

Col6a1$^{-/-}$ mice display several signs of myopathy such as muscle necrosis, an increase in centrally nucleated myofibers and a pronounced variation in myofiber diameter (Bonaldo et al., 1998). Additionally, COL6-deficient myofibers undergo spontaneous apoptosis, due to an accumulation of swollen and dysfunctional mitochondria (Irwin et al., 2003). Indeed, studies carried out in *Col6a1*$^{-/-}$ myofiber cultures showed that mitochondria are not able to maintain their membrane potential, due to increased sensibility to opening of the permeability transition pore (PTP), leading to the release of cytochrome *c*, a major intermediate in apoptosis (Irwin *et al*., 2003*).* Of note, the same pathological process of increased apoptosis because of a dysfunctional PTP was also found in muscle cell cultures and biopsies from BM and UCMD patients (Angelin et al., 2007). Further work demonstrated that the persistence of defective organelles in *Col6a1*$^{-/-}$myofibers is caused by an altered regulation of the autophagic machinery (Grumati et al., 2010). Autophagy is an evolutionarily conserved process in which cytoplasmic components are sequestered by double-membraned vesicles called autophagosomes and delivered to lysosomes, where they are degraded into biomolecules that are recycled for further cellular use (Mathai et al., 2017). One of the 'gold standard' approaches currently used to evaluate the autophagic flux is based on the quantification of microtubule-associated protein light chain 3 (LC3) lipidation. The lipidated form of LC3 (LC3-II) is bound to the autophagosome membrane, where it remains until the fusion with the lysosome, and for this reason LC3 lipidation is considered an excellent marker of autophagy (Klionsky et al., 2016; Mizushima et al.,

2010). Skeletal muscles of *Col6a1*$^{-/-}$ mice display a lower amount of LC3-II, pointing at an impairment autophagic flux. Moreover, a lower induction of Beclin-1 and Bnip3, which are key effectors in the initiation of autophagy, and defective formation of autophagosomes after starvation, have been found in both *Col6a1*$^{-/-}$ mice and BM/UCMD patients (Grumati et al., 2010). Interestingly, a recent work in *Col6a1*$^{-/-}$ mice demonstrated that autophagy regulation is compromised not only in muscle fibers, but also in fibroblasts. Indeed, fibroblast cultures from COL6-deficient mice display defects in the autophagy/lysosome machinery, with impaired clearance of autophagosomes and altered lysosomal function. Therefore, this recent study strongly support a new concept, in which fibroblasts are likely contribute to the pathophysiological features of COL6-related diseases (Castagnaro et al., 2018).

The translational impact of these studies for human COL6-related myopathies has been very high, since the pathomolecular features revealed by *Col6a1*$^{-/-}$ mice were also detected in UCMD and BM patients. Therefore, *Col6a1*$^{-/-}$ mice are a valuable tool for dissecting the pathomolecular mechanisms of COL6-related myopathies and developing effective therapeutic approaches. In particular, the *in vivo* treatment with cyclosporin A, an inhibitor of cyclophilin D that desensitizes PTP opening, was able to rescue the latent mitochondrial dysfunction and spontaneous apoptosis of both *Col6a1*$^{-/-}$ mice and UCMD/BM patients (Irwin et al., 2003; Merlini and Bernardi, 2008). Further work demonstrated that administration of spermidine, a non-toxic cationic polyamine, reactivated autophagy in a dose-dependent manner in *Col6a1*$^{-/-}$ mice, leading to a significant amelioration of the histological and ultrastructural muscle defects (Chrisam et al., 2015). More recently, a pilot clinical trial was designed to assess the efficacy of a one-year low-protein diet in reactivating autophagy in skeletal muscle of patients affected by COL6 myopathies (Castagnaro et al., 2016).

Additional work revealed that COL6 is a key component of the niche of adult muscle stem cells (also known as satellite cells). Indeed, these studies showed that satellite cells express COL6 genes in a regulated manner and that COL6 markedly influences their activity by finely modulating muscle stiffness. Notably, the absence of COL6 in *Col6a1*$^{-/-}$ mice causes impaired self-renewal capabilities of satellite cells and defective muscle regeneration (Urciuolo et al., 2013). These findings demonstrated a critical role for COL6 in the homeostasis of muscle stem cells and opened further perspectives on the etiology and treatment of COL6-related myopathies.

Intriguingly, COL6 was recently found to be part of the specialized ECM of the neuromuscular junction (NMJ) of mice and humans, where it is required for the

structural and functional integrity of this compartment. Indeed, COL6 deficiency causes fragmentation of acetylcholine receptor (AChR) clusters and altered neuromuscular transmission in both *Col6a1*$^{-/-}$ mice and UCMD patients (Cescon et al., 2018). Thus, this study revealed a novel role for COL6 in the NMJ, pointing at the involvement of NMJ alterations in the clinical features of patients affected by COL6-related myopathies.

1.2.3.2. COL6 function in the central and peripheral nervous system

A number of findings based on work in animal models and genetic studies in humans have shown that COL6 plays a key role in the central nervous system (CNS) and in the peripheral nervous system (PNS).

COL6 deposition in brain was initially described in the adventitia of the meningeal vessels and of the larger intraparenchymal arteries and veins (Roggendorf et al., 1988). Abundant deposition of COL6 was also detected in the choroid plexus of both human and mouse brain samples (Roggendorf et al., 1988; Dziadek et al., 1996).

In the last decade different studies revealed the involvement of COL6 in CNS diseases, thus shedding new light on the roles of COL6 in this tissue. In particular, a key study highlighted a link between COL6 expression and Alzheimer's disease. Indeed, the mRNA and protein levels for COL6 were found to be elevated in the hippocampal neurons of Alzheimer's disease patients and in a transgenic mouse model of Alzheimer's disease expressing mutant human amyloid precursor protein (APP) (Cheng et al., 2009). Interestingly, neuronal cultures derived from *Col6a1*$^{-/-}$ mice display increased apoptosis when treated with Aβ-peptides, which are involved in the etiology of Alzheimer's disease. Therefore, these experiments revealed a neuroprotective role for COL6 against Aβ-peptide toxicity (Cheng et al., 2009). In another study, expression of COL6 genes was reported to increase upon UV irradiation of cultured murine primary hippocampal neurons (Cheng et al., 2011). Addition of soluble COL6 to the medium of neuronal cultures was able to rescue UV-induced apoptosis and limited dendrite decrease, suggesting once again a neuroprotective function for COL6 upon stress (Cheng et al., 2011). More recently, *Col6a3* mRNA expression was detected in different brain areas of adult wild-type mice, including motor regions thought to have a central role in the pathogenesis of dystonia, a neurological disorder characterized by involuntary muscle contractions (Zech et al., 2015). Interestingly, compound heterozygous mutations of *COL6A3* were

found in patients suffering from autosomal recessive early-onset isolated dystonia, suggesting that biallelic mutations of this gene could be an autosomal-recessive cause of dystonia (Zech et al., 2015). The mutations were identified in exons 36, 41 and 42 of *COL6A3*, that encode for the C1 and C4 domains at the C-terminal end of the α3(VI) chain. *In vivo* studies revealed that zebrafish embryos injected with a morpholino that inhibits the splicing of *col6a3* exon 42 display motor neuron pathfinding, branching, and extension errors. Thus, it seems reasonable that the C4 domain of the α3(VI) chain might be implicated in the organization of structural plasticity and in the maintenance and/or stability of neural circuits (Zech et al., 2015). Another neurodegenerative disorder that has been linked to COL6 alterations is the progressive myoclonus epilepsy, which is characterized by ataxia, myoclonic seizures and cognitive dysfunctions. Indeed, although its pathogenic role has not been clearly unveiled, a recent study reported a disease-segregating mutation in the *COL6A2* gene in a consanguineous family affected by this rare epilepsy syndrome (Karkheiran et al., 2013).

A recent work aimed at throwing light on the physiological roles of COL6 in brain showed the presence of distinctive neurodegenerative traits in aged *Col6a1*$^{-/-}$ mice (Cescon et al., 2017). Interestingly, and similarly to the cellular defects found in skeletal muscle, *Col6a1*$^{-/-}$ neural cultures were found to display an increased incidence of spontaneous apoptosis, a higher vulnerability to oxidative stress and an abnormal regulation of autophagy. These neurodegenerative hallmarks were accompanied by impaired motor and memory task performances in aged *Col6a1*$^{-/-}$ mice. Therefore, these findings highlighted a crucial neuroprotective role of COL6 also during physiological aging (Cescon et al., 2017).

Concerning the PNS, a pioneering work showed that COL6 is expressed by immature Schwann cells (SCs) upon stimulation by neuregulins, as part of the differentiation program of SCs from neural crest cells. Once SC precursors start to transcribe the *Col6a1* gene, transcriptional regulation becomes independent from neuregulins (Vitale et al., 2001). Additional findings confirmed the presence of COL6 in the connective tissue of endo-, peri- and epineurium, where it is secreted in the by SCs and perineural cells (Chen et al., 2014; Peltonen et al., 1997). Studies in *Col6a1*$^{-/-}$ mice revealed that COL6 is involved in the maintenance of proper PNS myelination and function of sciatic nerves. Indeed, COL6 ablation leads to hypermyelination of peripheral nerves, as a consequence of the activation of signaling pathways

promoting myelination and the inhibition of negative regulators (Chen et al., 2014). Besides structural alterations of myelin, *Col6a1*$^{-/-}$ display deficits in motor and sensory functions, with a reduced nerve conduction velocity (Chen et al., 2014).

Further studies revealed that COL6 also plays a pivotal role in nerve regeneration, by regulating macrophage recruitment and polarization. Indeed, COL6 expression in wild-type mice rapidly increases at the site where a sciatic crush injury is induced, via a mechanism that involves promoting the recruitment of macrophages and their polarization towards the pro-regenerative M2 phenotype. Intriguingly, *Col6a1*$^{-/-}$ mice undergo delayed sciatic nerve regeneration upon injury, with a decreased macrophage recruitment to the site of crush, due to a failure in recruiting polarized macrophages to the injury site (Chen et al., 2015a).

Although no PNS disease was thus far directly linked to mutations of COL6 genes, abnormal COL6 expression was reported in pathological states affecting the PNS. Among the peripheral disorders in which COL6 expression was found to be altered there is Hirschsprung's disease (HSCR), a congenital syndrome that affects the enteric nervous system, leading to a deficient innervation of the distal bowel (Amiel et al., 2007). In HSCR patients, increased amounts of COL6 were distinctly observed around the enteric ganglia, thus pointing at a COL6-dependent pathogenic mechanism for HSCR (Soret et al., 2015). Abnormal COL6 deposition was also described in diabetic peripheral neuropathy, a common complication of diabetes which is characterized by distal axonopathy, loss of nerve fibers and Wallerian degeneration (Yagihashi et al., 2007). Remarkably, COL6 expression was found to be increased even in Charcot-Marie-Tooth disease type I (CMT1), a demyelinating neuropathy that arises from mutations of different genes expressed by myelinating SCs (Palumbo et al., 2002).

Altogether, the data collected until now suggest that neurodevelopment could be a major field of future COL6 studies, to identify additional molecular and genetic defects of this ECM component linked to diseases affecting the nervous system.

1.2.3.3. COL6 function in the skeletal system

Despite the pivotal role in muscle and nervous systems, COL6 is also fundamental for the homeostasis of cartilage and bone.

Studies performed in *Col6a1*$^{-/-}$ mice revealed that the pericellular matrix (PCM), a narrow region that encapsulates chondrocytes, has significantly reduced mechanical properties when compared to wild-type controls (Alexopoulos et al., 2009). This mechanical defect, in turn, leads to an increased extent of chondrocyte swelling and

osmotically induced signalling via TRPV4 (transient receptor potential cation channel subfamily V member 4), a receptor that responds to a plethora of physical signals, including changes in osmolarity and deformation, thus serving as an integrator of various signals at the cell surface (Zelenski et al., 2015). These studies revealed that COL6 is involved in the transmission of mechanical and osmotic stresses from the interstitial matrix to the PCM, and, in the end, to the chondrocytes. Alexopoulous and coll. also reported that, with age, *Col6a1*$^{-/-}$ mice display accelerated development of osteoarthritic joint degeneration, suggesting that alterations in the mechanical environment of the chondrocytes can lead to the progression of osteoarthritis (Alexopoulos et al., 2009). Interestingly, a recent study defined the spatio-temporal dynamics of NG2/COL6 interactions during the progression of temporomandibular joint osteoarthritis, a clinical syndrome characterized by arthralgia and limited joint mobility (Yotsuya et al., 2019). Of note, it has been demonstrated that the use of soluble COL6 allows a rapid and efficient expansion of mesenchymal stem cells for potential use in cartilage regeneration and osteoarthritis (Smeriglio et al., 2017).
With regard to bone, *Col6a1*$^{-/-}$ mice have delayed secondary ossification process and reduced bone mineral density (Alexopoulos et al., 2009). Further studies aimed at investigating the role COL6 in the knee demonstrated that *Col6a1*$^{-/-}$ mice display abnormalities in the morphology of the knee trabecular bone structure, as revealed by the lower bone volume and the reduced trabecular number and thickness (Christensen et al., 2012). A further study showed that the femora of *Col6a1*$^{-/-}$ mice contain osteoblasts with altered shapes and disorganized arrangement of collagen fibrils, highlighting that COL6 is required for the normal morphology of osteoblasts and the maintenance of bone architecture (Izu et al., 2012).

1.3. Zebrafish as a model organism

Danio rerio (zebrafish) is a tropical freshwater fish that belongs to the *Cyprinidae* family, within the superclass of bony fish (*Osteichthyes*) and the class of ray-finned fish (*Actinopterygii*). Its natural habitat consists in rivers of South-East Asia, India, Pakistan, Bhutan and Nepal (Dahm and Geisler, 2006). In last years, this vertebrate model organism has been widely used to study the genetics underlying development, normal body function, and disease. Indeed, zebrafish presents several advantages, that mainly accrue from the embryonic and early larval stages. Zebrafish embryos are transparent and develop externally, allowing the use of non-invasive imaging techniques to track the impact of genetic manipulation or drug treatments (Howe et

al., 2013; Garcia et al., 2016). Moreover, embryos display a fast development. At 24 hours post fertilization (hpf) the body axes have already been established, allowing to distinguish eyes, somites, the vascular system and an organized nervous system. At 5 days post fertilization (dpf), the heart, liver, brain, pancreas and other organs are fully developed and embryos have become swimming and feeding larvae (Figure 2). At 3-4 months they reach sexual maturity and display a large capacity for generating offspring, thus offering the opportunity for a high availability of animals for research purposes, such as the screening of wide libraries of compounds (Kimmel et al., 1995; Dahm and Geisler, 2006; Garcia et al., 2016).

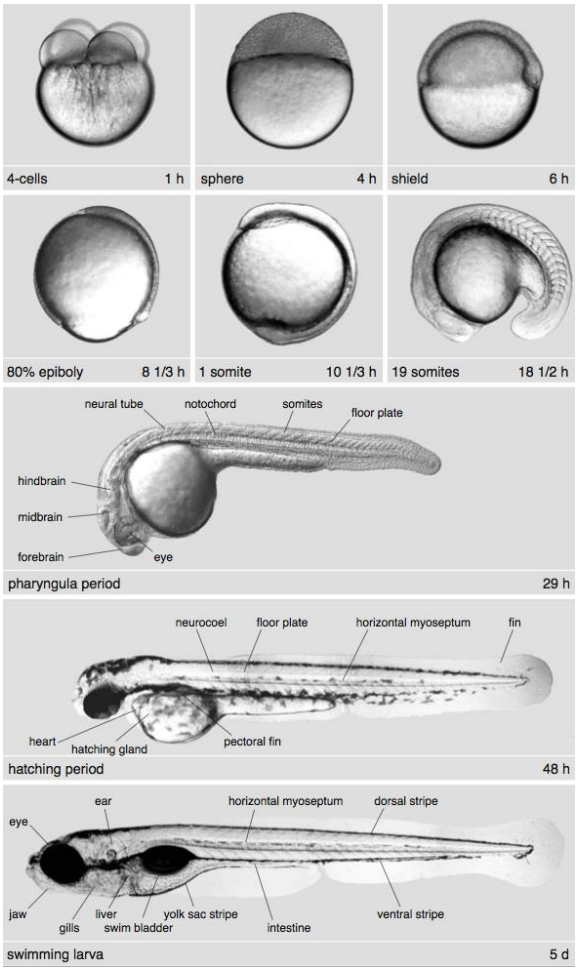

Figure 2. Stages of zebrafish development from 1 hpf to 5 dpf. From (Haffter et al., 1996).

Despite the evolutionary distance between human and zebrafish, the genetic features and the molecular mechanisms of embryonic development and physiology are largely conserved. A comparison with the human genome reveal that 70% of human genes and about 82% of potential disease-related genes have at least one obvious zebrafish

ortholog (Howe et al., 2013). Furthermore, many of the anatomical and physiological features of zebrafish are highly homologous to humans (Eimon and Rubinstein, 2009; Nishimura et al., 2016). Another advantage of this model relies on the availability of several reporter strains that are driven by specific promoters, which provide useful readouts for cell/tissue specificity and signaling pathways. *In vivo* live imaging of zebrafish reporter lines gives the possibility to extend the understanding of cell behaviour, by monitoring cells in their physiological environment. Indeed, cellular responses are strictly related to the physiological, mechanical and molecular stimuli deriving from the surrounding environment.

The high degree of conservation between zebrafish and humans make this vertebrate an ideal animal model to study several human diseases, including muscular dystrophies, cancer, neurodegenerative syndromes, diabetes and cardiovascular disorders (Ingham, 2009; Tavares and Santos Lopes, 2013). In the last 10 years, with the aim of unraveling the molecular mechanisms involved in human pathologies, novel gene targeting strategies have been developed, which totally revolutionized knockout in zebrafish.

1.4. The CRISPR/Cas9 genome editing technology

Several methods for altering gene expression have been developed and applied in zebrafish (Koster and Sassen, 2015). Among them, in the last years the CRISPR/Cas9 system has become the most used approach for *in vivo* targeted gene mutation in various species, including zebrafish.

The system is based on an immunity strategy adopted by archaea and bacteria to protect themselves against bacteriophage infection and plasmid transfer (Marraffini and Sontheimer, 2010). The CRISPR (Clustered Regularly Interspaced Shorts Palindromic Repeats) loci present in archaea and bacteria genome are organized in pattern made of palindromic repeats separated by protospacer regions. After the infection, short fragments of foreign DNA are integrated into the CRISPR repeat-spacer array in the chromosome of the host. These provides a genetic record of the infection, protecting the host from future invasion by the same invader (Barrangou et al., 2007). Indeed, since each CRISPR element is normally located close to the Cas nuclease locus, if the host is attacked by the same invader a second time, the CRISPR array is transcribed into a crRNA (CRISPR RNA) that guides the Cas enzyme to foreign DNA, thus triggering its sequence-specific destruction (Marraffini and Sontheimer, 2010; Jiang and Doudna, 2017).

The best studied CRISPR/Cas system is the one of *Streptococcus pyogenes* (Jansen et al., 2002; Barrangou et al., 2007; Cong et al., 2013a; Makarova et al., 2015), which has been widely used for targeted genome modifications in mammalian and zebrafish cells (Cong et al., 2013b; Li et al., 2016; Albadri et al., 2017). Briefly, the *S. pyogenes* Cas9 endonuclease performs its activity using two small RNA molecules, one target-recognizing CRISPR RNA (crRNA) and one auxiliary trans-activating RNA (tracrRNA). CrRNA is complementary to 20 bases of genomic DNA sequence and directs the cleavage through this sequence, while tracrRNA promotes sequence specific double-strand breaks (DBS) in a DNA target sequence (20 bp) followed by a protospacer adjacent motif (PAM). The generation of DBS is then repaired by endogenous DNA repair systems. The more common repair mechanism is the Non-Homologous End Joining (NHEJ), which leads to random insertions or deletions at the DSB site. This mechanism often generates knockout alleles, since it causes frameshifts and premature stop codons, thus destroying gene function. A second repair mechanism, the Homology Directed Repair (HDR), needs an exogenous template, that can be provided by the experimenter or can be the sister chromosome, to direct the filling of the gap. This second approach is considerably more difficult to achieve (Cong et al., 2013; Li et al., 2016).

The CRISPR/Cas9 system from *S. pyogenes* has been implemented in a variety of *in vivo* settings. One of the first modifications of this technology was the generation of a synthetic single-guide chimeric RNA (sgRNA), derived from the fusion of the crRNA and the tracRNA, that is able to guide Cas9 endonuclease for site-directed cleavage of target DNA (Jinek et al., 2012). Moreover, the Cas9 protein has also been modified by the addition of nuclear localization sequences, to maximize the transport into the nucleus in eukaryotes (Jao et al., 2013) . Notably, the CRISPR-Cas9 system was shown to be six-fold more efficient than other genome editing approaches in generating germline mutations in zebrafish (Varshney et al., 2015). In addition, in a recent work Cas9 nucleases with altered PAM specificities have been designed to generate somatic mutations in zebrafish, therefore increasing the number of targetable loci in the zebrafish genome (Kleinstiver et al., 2015). However, despite the fact that this genome editing technique is simple and economic, a significant limitation relies on the difficulty to have a precise readout of the mutated cells. Thus, the scientific community is currently developing new strategies to achieve NHEJ-based knock-in, in order to precisely modify a gene and study its function (Amitai and Sorek, 2016).

Chapter I

1. Background

COL6 is an ECM protein expressed in several tissues. Studies in mammals revealed that COL6 is present in skeletal muscle, skin, cornea, lung, blood vessels, tendons, intervertebral disks, peripheral nerves, lungs, heart, adipose tissue, skin and cartilages (Marvulli et al., 1996; Gara et al., 2011; Sabatelli et al., 2012a; Cescon et al., 2015b). In the past few years, some studies on COL6 were carried out in zebrafish, a powerful model organism for studying vertebrate development (Telfer et al., 2010; Radev et al., 2015; Ramanoudjame et al., 2015). Nevertheless, these studies provided only limited data on the expression and distribution of COL6 in this animal model. Thus, during my PhD, I characterized in detail the spatio-temporal expression pattern and distribution of COL6 chains in zebrafish embryos, larvae and adults. The data demonstrate that zebrafish COL6 genes exhibit features that are very similar to those found in their mammalian orthologs. In particular, by exploiting a new antibody we generated against zebrafish COL6, I could characterize in detail the expression pattern of this distinctive ECM protein during zebrafish development and adult life. These data are of major relevance since they provide the basis for functional studies in this animal model. Indeed, zebrafish represents an ideal tool to throw light into the signaling pathways and tissues affected by the absence of this major ECM component, and thus to dissect the pathomolecular mechanisms underlying COL6-related diseases.

The data I obtained during this part of my PhD work were collected in a manuscript entitled "**Spatio-temporal expression and distribution of collagen VI during zebrafish development**". This manuscript has been submitted to the journal *Scientific Reports* and is currently under revision.

Spatio-temporal expression and distribution of collagen VI during zebrafish development

Valentina Tonelotto[1, †], Valeria Trapani[1, †], Sandrine Bretaud[2], Stefanie Elisabeth Heumüller[3], Raimund Wagener[3], Florence Ruggiero[2, *] and Paolo Bonaldo[1, 4, *]

[1] Department of Molecular Medicine, University of Padova, Padova 35131, Italy.

[2] Institut de Génomique Fonctionnelle de Lyon, ENS de Lyon, UMR CNRS 5242, Université Lyon 1, Lyon 69364, France.

[3] Center for Biochemistry and Center for Molecular Medicine Cologne (CMMC), Medical Faculty, University of Cologne, Cologne 50931, Germany.

[4] CRIBI Biotechnology Center, University of Padova, Padova 35131, Italy.

[†] These authors contributed equally to this work.

Authors for correspondence: Paolo Bonaldo, Department of Molecular Medicine, University of Padova, Via Ugo Bassi 58/B, 35131 Padova, Italy, email: bonaldo@bio.unipd.it; Florence Ruggiero, Institut de Génomique Fonctionnelle de Lyon, ENS de Lyon, UMR CNRS 5242, Université Lyon 1, 69364 Lyon Cedex 07, France, email: florence.ruggiero@ens-lyon.fr

Running title: Collagen VI in zebrafish

Key words: Extracellular matrix; Collagen VI; Zebrafish; Embryonic development; *In vivo* expression.

Summary statement: Collagen VI is a key matrix protein exerting critical roles in different tissues. Here, we show that collagen VI has a dynamic and tightly regulated expression during development in zebrafish.

Collagen VI (ColVI) is an extracellular matrix (ECM) protein involved in a range of physiological and pathological conditions. Zebrafish (*Danio rerio*) is a powerful model organism for studying vertebrate development and for *in vivo* analysis of tissue patterning. Here, we performed a thorough characterization of ColVI gene and protein expression in zebrafish during embryogenesis and postnatal life. Bioinformatics analyses confirmed that zebrafish genome contains single genes encoding for α1(VI), α2(VI) and α3(VI) ColVI chains and duplicated genes encoding for α4(VI) chains. At 1 day post-fertilization (dpf) ColVI transcripts are expressed in myotomes, pectoral fin buds and developing epidermis, while from 2 dpf abundant transcript levels are present in myosepta, pectoral fins, axial vasculature, gut and craniofacial cartilage elements. Using newly generated polyclonal antibodies against zebrafish α1(VI) protein, we found that ColVI deposition in adult fish delineates distinct domains in the ECM of several organs, including cartilage, eye, skin, spleen and skeletal muscle. Altogether, these data provide the first detailed characterization of ColVI expression and ECM deposition in zebrafish, thus paving the way for further functional studies in this species.

INTRODUCTION

ColVI is a major ECM protein forming a microfibrillar network in many tissues, including skeletal muscle, cartilage, tendon, lung, nervous system, adipose tissue, skin, eye, heart and vasculature (for a review see[1]). ColVI is a distinctive member of the superfamily of collagens, since only 20% of its structure is made of a triple helical region. In most tissues ColVI consists of three chains, α1(VI), α2(VI) and α3(VI), which are respectively encoded by the *COL6A1*, *COL6A2* and *COL6A3* genes in tetrapods[2–5]. More recently, three other genes were identified, annotated as *COL6A4*, *COL6A5* and *COL6A6*, whose expression is restricted to specific tissues[6,7]. In humans, a large chromosome inversion broke the *COL6A4* gene into two separate non-processed pseudogenes[8]. The domain structure of the α4(VI), α5(VI) and α6(VI) chains and the shared homology with α3(VI) indicate that they represent alternative polypeptides for the assembly of ColVI subunits into α1–α2–αX triple-helical monomers (where αX is either α3, α4, α5 or α6), thus increasing the structural and functional versatility of this ECM component[7,9]. Of note, ColVI has a unique intracellular assembly process made of distinct steps, where three different chains associate intracellularly to form disulfide-bonded monomers, dimers and tetramers before secretion[10,11]. In the extracellular microenvironment, ColVI forms a network of beaded microfilaments which interact with a range of other ECM molecules, including fibronectin, collagen IV, decorin and perlecan[1]. Moreover, ColVI is able to bind several cell surface receptors, such as the α1β1, α2β1, α3β1, α10β1 and αvβ3 integrins, the chondroitin sulfate proteoglycan-4 (CSPG4, also known as NG2), and the anthrax toxin receptors 1 and 2 (ANTXR1/TEM8 and ANTXR2/CMG2)[12–14].

Several human disorders have been linked to altered expression or mutations of the genes encoding ColVI chains. In particular, ColVI is critical for the proper structure and function of skeletal muscle, and inherited mutations of the *COL6A1-COL6A3* genes cause different forms of myopathies in humans, including Ullrich congenital muscular dystrophy (UCMD) and Bethlem myopathy (BM) (for a review, see[15]). A number of animal models have been generated for myopathies with a spectrum of phenotypes[16]. The generation of a *Col6a1* null mouse model provided a valuable tool for the dissection of the *in vivo* functions of ColVI[17],

thereby highlighting the relevance of this ECM component in regulating several key cellular pathways. Indeed, ColVI exerts different functions in the tissues where it is expressed, including protection from apoptosis and from oxidative damage, regulation of autophagy, promotion of tumor growth and progression, and maintenance of cell stemness [1]. ColVI knockout mice display a myopathic phenotype characterized by structural and functional defects in skeletal muscles[17]. In particular, ColVI-deficient myofibers undergo spontaneous apoptosis, with accumulation of dysfunctional mitochondria and altered organelles [18]. Further studies demonstrated that the persistence of abnormal organelles in ColVI knockout muscles is caused by defective regulation of the autophagic machinery[19]. Of note, the pathomolecular defects identified in *Col6a1* null mice were also confirmed in muscle biopsies and primary muscle cultures of UCMD and BM patients[19,20]. Treatment with cyclosporin A was able to rescue the latent mitochondrial dysfunction and myofiber apoptosis of both ColVI knockout mice and UCMD/BM patients[18,21]. Further work demonstrated that administration of spermidine, a non-toxic cationic polyamine, reactivates autophagy in a dose-dependent manner in ColVI knockout mice, leading to a significant amelioration of muscle defects[22]. More recently, a pilot clinical trial was carried out, showing the efficacy of a one-year low-protein diet in reactivating autophagy in skeletal muscle of patients affected by ColVI myopathies [23].

Danio rerio (zebrafish) has been widely used for studies of vertebrate development and gene function. Indeed, thanks to its transparency and rapid development, zebrafish represents a powerful tool to visualize the expression pattern of a gene in the whole organism. Moreover, this animal model allows the dissection of different aspects associated with specific gene functions, providing valuable data for a better understanding of human development and disease mechanisms, such as for collagenopathies[24,25]. Although some studies on ColVI in zebrafish were carried out in the past few years[26–28], only limited data are available concerning the expression and distribution of ColVI during fish development and adult life. In this work, we investigated the spatio-temporal expression pattern of ColVI genes and the distribution of ColVI protein in zebrafish embryos, larvae and adults. The data demonstrate that zebrafish ColVI genes exhibit features that are

very similar to those reported for their mammalian orthologs[7,29]. In particular, by exploiting a new antibody we generated against zebrafish ColVI, we found that the expression pattern of this distinctive ECM protein is dynamically regulated during zebrafish development and adult life. These data are of major relevance since they provide the basis for further functional studies in this animal model.

RESULTS

Phylogenetic analysis of fish ColVI genes.

Five genes coding for ColVI chains were identified in zebrafish[25,27,30,31], one ortholog each for the α1, α2 and α3 chains and two for the α4 chain (see also Fig. S1). The two orthologs coding for the α4(VI) chain are designated *col6a4a* and *col6a4b* and are located on chromosome 16 and 13, respectively. However, it has not been determined how *col6a4a* and *col6a4b* evolved. Therefore, we performed a phylogenetic analysis based on protein parsimony and protein distance methods and confirmed earlier results[27] indicating that the two zebrafish α4 chains do not belong to the α5/α6 chain branch (Fig. 1A). The question remained whether the duplication of the two α4 genes is the result of the whole genome duplication[32] that occurred in the teleost linage, or if these two genes were independently duplicated. Close inspection of the gene loci revealed that *col6a4a*, but not *col6a4b*, is in synteny with the locus coding for the α4(VI) chain in other vertebrates. In amphibians, reptiles, birds and mammals, the genes *ldlrap1b* and *fndc5a* that flank *col6a4b* on zebrafish chromosome 13 lack a neighboring gene coding for a ColVI chain (Fig. 1B). Moreover, the synteny of orthologue *col6a4b* genes with *ldlrap1b* or *fndc5a* is only present in cyprinids (Cyprinidae) (Fig. 1b), also commonly called the "carp family", clearly indicating that these ColVI α4 chains are unique for this family. The genomes of other teleosts, like salmon, fugu or medaka, and that of the spotted gar[33] , which belongs to the infraclass of holostei, do not contain a *col6a4b* gene (Fig 1b). Consequently, in carps *col6a4a* and *col6a4b* are paralogue genes independently of the teleost whole genome duplication. Interestingly, in *Cyprinus carpio* (common carp) and *Carassius auratus* (goldfish), *col6a4b* is further duplicated in tandem (Fig. 1B).

ColVI expression and distribution in developing zebrafish embryos and larvae.

To assess the expression of ColVI genes during fish development, we performed qRT-PCR at different developmental stages from 12 hpf to 4 dpf. ColVI transcripts were first detected at 24 hpf. Notably, *col6a1* and *col6a2* mRNA levels were the most abundant at all developmental stages included in the analysis. Moreover, among the transcripts encoding the longer chains, the levels of *col6a3* and *col6a4b* mRNAs gradually increased between 24 hpf and 72 hpf, whereas *col6a4a* mRNA was barely detectable before 72 hpf (Fig. 2A).

To further investigate the spatio-temporal expression of ColVI transcripts during development, we performed *in situ* hybridization in zebrafish embryos and larvae from 1 dpf to 3 dpf, using digoxigenin-labeled antisense riboprobes for *col6a1*, *col6a2* and *col6a3*. Interestingly, at 1 dpf all three ColVI transcripts were restricted to the surface of the myotome and pectoral fin buds (Fig. 2B and Fig. S2a). Of note, although ColVI is generally described as a dermal collagen, *col6a1* transcripts were clearly detected in the cuboid epithelial cells of the developing fish epidermis (Fig. S2b). Moreover, at 2 dpf strong signals for ColVI transcripts were displayed by myosepta, pectoral fins, axial vasculature and the gut. Expression of ColVI genes encoding the three main chains was also found in the connective tissue surrounding the eye and in the craniofacial cartilage elements at 2 and 3 dpf (Fig. 2B and Fig. S2a).

We next investigated the levels and distribution of ColVI protein during fish development. As available antibodies for human and murine ColVI did not provide adequate cross-reaction with the zebrafish protein, we generated specific antibodies for zebrafish ColVI (see also Materials and Methods). Western blot analysis with the newly generated anti-α1(VI) antibodies in protein extracts from 24-hpf to 10-dpf embryos showed an abundant band at about 130 kDa, corresponding to the expected migration for the α1(VI) polypeptide. ColVI protein levels were already abundant at 1 dpf, and their levels increased throughout development (Fig 2C). Whole-mount immunofluorescence of embryos and larvae at different developmental stages from 2 to 10 dpf allowed to ascertain the distribution of ColVI protein during development. At 2 dpf, ColVI labeling was detected in the

connective tissue surrounding the eye, in the pectoral fin and in the myosepta (Fig. 2D). A similar pattern of ColVI deposition was detected in 3-dpf embryos, which also displayed strong ColVI labeling in the developing craniofacial cartilages (Fig 2D). In 6- and 10-dpf larvae, abundant ColVI labeling was present in the connective tissues of eyes and olfactory pits and in the gut (Fig. 2D).

Further immunofluorescence analyses of whole-mount samples, as well as of frozen and paraffin-embedded sections, allowed to get additional insights on ColVI deposition during early development. At 3 dpf, transverse sections of the trunk (Fig. 3a-f) and whole-mount larvae (Fig. 3g, h) showed ColVI deposition in skin, gut, skeletal muscles and vertical myosepta. Interestingly, orthogonal views of whole-mount larvae labeled with antibodies against collagen XII, a marker of myosepta [34], revealed that ColVI was restricted to the myoseptal surface and was absent in deep vertical myosepta (Fig. 3h), pointing at a specific role of the protein in the myoseptum, a structure functionally equivalent to tetrapod tendon. Aorta and vein were also positive for ColVI (Fig. 3a), but these structures were highly autofluorescent in the controls (not shown), making it difficult to discern bona fide signal from autofluorescence. However, staining of vessels in the head were not autofluorescent (Fig. S2c). Since *in situ* hybridization showed that *col6a1* transcripts were present in different cell types (Fig. 2A and Fig. S2b), we further examined ColVI protein deposition in various areas at 3 dpf. Zoomed images of skeletal muscles co-stained for ColVI and actin revealed that muscle cells might contribute to the deposition of ColVI at least at early larval stages (Fig. 3b, c). In agreement with *in situ* hybridization data, the basal layer of epidermis displayed strong ColVI labeling in skin (Fig. 3d). ColVI deposition in epidermis was confirmed by double immunolabeling for cadherin, a marker of epithelial cells (Fig. 3d). In the developing cartilages, double immunofluorescence for ColVI and collagen XII showed distinct co-labeling in the perichondrium. On the other hand, strong ColVI immunoreactivity was also detected at the level of chondrocytes (Fig. 3e, f).

Sagittal sections of 5-dpf larvae revealed abundant ColVI deposition in the skin, in the connective tissue surrounding the craniofacial cartilage elements, in the liver and in the head and trunk skeletal muscles (Fig. 3i). A strong ColVI labeling

delineated the intestine (Fig. 3i), and costaining with the F-actin marker phalloidin showed ColVI deposition in the smooth muscle layer of the developing intestine (Fig. 3j). Detailed views confirmed ColVI immunoreactivity in the connective tissue surrounding the craniofacial cartilage elements and in the skeletal muscles of the head and trunk, as revealed by co-staining with phalloidin (Fig. 3k-m). Zoomed images of 5-dpf trunk co-stained for ColVI and actin showed strong staining surrounding muscle fibers. Strikingly, ColVI staining of muscle fibers alternated with actin staining, resulting in a costameric-like periodic pattern of ColVI immunoreactivity (Fig. 3l, m).

In order to determine more precisely ColVI distribution at later developmental stages, we exploited different zebrafish transgenic reporter lines. First, we characterized ColVI deposition in the developing connective tissue of craniofacial structures by using the *Tg(fli1:EGFP)* line, in which *fli1* promoter drives EGFP expression in cranial neural crest derivatives, such as the aortic arch mesenchyme and the developing jaw cartilage[35]. Analysis of 6-dpf *Tg(fli1:EGFP)* larvae revealed ColVI deposition in the proximity of EGFP-positive cells within Meckel's and palatoquadrate cartilages (Fig 4a-d). Since one of the main molecular players involved in chondrogenesis is the Wnt signaling pathway, we also exploited *Tg(7xTCF-Xla.Siam:GFP)ia4*, a reporter line in which the expression of GFP is under the control of seven TCF responsive elements upstream the minimal promoter of *Xenopus* siamois gene, a direct b-catenin target[36]. At 6 dpf, ColVI was detected in close proximity to Wnt responsive cells of the jaw joint (Fig. 4e-h). Of note, it was previously demonstrated that such Wnt-responding cells include chondrocytes of the jaw joint and along the palatoquadrate ligaments and tendons[37]. Immunofluorescence of 7-dpf sections confirmed ColVI deposition in branchial arches and chondrocranium (Fig. 4i-l). In particular, co-staining with wheat germ agglutinin (WGA) and anti-light meromyosin antibodies revealed that ColVI is localized in the perichondrium surrounding the cartilage of each pharyngeal arch, as well as in the connective tissue of the adjacent skeletal muscle (Fig. 4m,n). To deepen the characterization of ColVI deposition in the developing craniofacial structures, we also took advantage of *Tg(osx:nuGFP)* reporter larvae, in which GFP expression mirrors endogenous *sp7* gene expression in the otic placode, and in the

developing skeletal structures[38]. Analysis of 6-dpf *Tg(osx:nuGFP)* larvae revealed ColVI labeling in the connective tissue surrounding the dentary bone and ceratobranchial arches (Fig. 4o-q). In the developing nervous system, ColVI was detected in brain blood vessels and in the meninges (Fig. 4r-u). Finally, by exploiting the *Tg(fli1:EGFP)* reporter line, in which *fli1* promoter also drives the expression of the EGFP in all blood vessels[35], we found that ColVI labeling followed the pattern of EGFP-positive cells at the level of the intestine, suggesting that ColVI is part of the connective tissue that underlies the epithelium of intestinal folds (Fig. 4u-x).

Characterization of ColVI expression and deposition in adult zebrafish tissues.

To assess the levels of the ColVI transcripts during adulthood, we performed qRT-PCR on various tissues dissected from adult fish. Higher levels of the mRNAs coding for the three main ColVI chains were displayed by skeletal muscle, cartilage, skin, eye and spleen (Fig. 5A). Conversely, transcripts coding for the α4(VI) chain were expressed at much lower abundance in these tissues. Interestingly, higher levels of the *col6a4* transcript were detected in the intestine (Fig. 5A), thus confirming previous results obtained for the murine α4(VI) chain[7]. Western blot analysis of protein extracts prepared from adult (8- to 12-mpf) tissues showed higher abundance of the α1(VI) chain in cartilage, eye, skin, spleen and skeletal muscle (Fig. 5B).

To further characterize the pattern of ColVI deposition in adult animals, we performed immunolabeling on sagittal sections of adult fish, followed by haematoxylin-eosin staining (Fig. 5c-k). ColVI immunoreactivity was abundant in the endomysium of skeletal muscle (Fig. 5e). In particular, the endomysial basement membrane was heavily stained, whereas the interstitial ECM displayed much lower ColVI labelling (Fig. S2c). Cross sections of adult skin showed accumulation of ColVI filaments in the dermis (5d, Fig. S2c), indicating a cell switch of ColVI production in the skin at later stages, when fibroblasts are present in the dermis, as it was shown for collagen I[39]. Strong ColVI immunoreactivity was also displayed by the intestinal folds (Fig. 5g), in particular at the level of mucosa

and muscular layers (Fig. S2c). Of note, all these areas were shown to have abundant deposition of ColVI also in mice[7,29,40]. Moreover, ColVI signal was detected also in corneal stroma (Fig. 5c), in the adipose tissue (Fig. 5f), in brain blood vessels (Fig. 5h), in the craniofacial cartilage elements (Fig. 5i,j), and at the basal level of the olfactory epithelium (Fig. 5k). Interestingly, this analysis also revealed some fish-specific expression domains, such as bony scales and gill arches (Fig. 5d and 5j, respectively).

Taken together, these data demonstrate that, as in tetrapods, ColVI has a dynamic expression and is broadly distributed in zebrafish during development and adult life, pointing at a role of this distinctive ECM component in the differentiation and specification of different tissues and organs.

DISCUSSION

Zebrafish is increasingly used as an animal model for investigating the function of collagen genes in development, regeneration and disease[25]. However, only partial data are currently available on the spatio-temporal expression patterns of the different collagens at the transcript and protein levels in zebrafish, in spite of the fact that such information is a fundamental prerequisite for undertaking functional studies in this animal model. In the present study, thanks to the generation of specific antibodies against zebrafish ColVI, we carried out a thorough characterization of the spatiotemporal expression and distribution of ColVI in zebrafish from early embryogenesis to adult life.

As in mammals, the fish genome contains several genes coding for distinct ColVI chains. Bioinformatics and phylogenetic analyses in zebrafish revealed the presence of single genes (*col6a1*, *col6a2* and *col6a3*) encoding the three major ColVI chains (α1, α2 and α3, respectively), and of two homologous genes (*col6a4a* and *col6a4b*) encoding α4 chains[26,27] (see also Fig. S1). These chains were earlier designated α4a and α4b[27]. However, the use of "a" and "b" is misleading in this context, as *col6a4a* and *col6a4b* are not ohnologs originating from the whole genome duplication that occurred in the teleost lineage. Ohnolog genes, generated by whole genome duplication and designated by "a" and "b" appendices, are

common in zebrafish[41]. Only one of the two ohnolog genes, each encoding for ColVI chains, was maintained in zebrafish after the whole genome duplication. Nevertheless, a duplication of the *col6α4* gene occurred, but only in the carp family and not in the context of whole genome duplication. Interestingly, *col6α4* belongs to the subgroup of ColVI long-chain encoding genes[8] that in very different species are independently duplicated, indicating a susceptibility for duplication events. The basis for this susceptibility remains unclear. As the two zebrafish ColVI α4 chains are differentially expressed and the corresponding knockdown fish display different phenotypes[27], caution is required when using results obtained from the study of zebrafish ColVI α4 chains to understand functions of α4(VI) in higher vertebrates, as one of the chains may have gained a novel function, unique for the carp family.

As for tetrapods, expression of ColVI genes in zebrafish is dynamically regulated during embryonic and adult life. ColVI transcripts are first detected in 1-dpf fish embryos, and their expression increases throughout development. *In situ* hybridization of 1- to 3-dpf embryos showed the presence of *col6a1*, *col6a2* and *col6a3* transcripts in myotomes and developing craniofacial cartilages, as well as in eyes and gut. Interestingly, this expression pattern is comparable to that of the mammalian orthologs[7,29], suggesting that the spatial and temporal regulation of ColVI genes expression is conserved among vertebrates. In particular, *col6a1* and *col6a2* transcript levels are the most abundant at all developmental stages, in agreement with the requirement of α1(VI) and α2(VI) for the 1:1:1 stoichiometric association with one of the longer chains. On the other hand, *col6a3* and *col6a4a* expression levels gradually increase between 1 and 3 dpf, whereas *col6a4b* levels increase between 3 and 4 dpf. This temporally regulated expression likely reflects different requirements of each of the longer ColVI chain in specific tissues during development. For instance, at 3 dpf, *col6a3* transcripts are abundant in pharyngeal cartilage elements, suggesting that the α3(VI) chain may be involved in craniofacial cartilage development, which typically occurs at this developmental stage[42]. In support of this notion, *col6a4b* expression also appears to be tissue-specific. Indeed, during larval stages *col6a4b* transcripts are first detected between 3 and 4 dpf, when gut differentiation is taking place[42], and in adult animals *col6a4b* is mainly expressed in intestine.

Thanks to specific antibodies raised against the zebrafish α1(VI) chain, we were able to characterize ColVI protein distribution in both larvae and adults. In the developing zebrafish, ColVI is abundant in the anterior body region, including the connective tissues surrounding the eye, the brain and the olfactory epithelium, as well as in craniofacial cartilages and pectoral fins. In the trunk region, the protein is found in the intestine and in the myosepta. Immunostaining of zebrafish transgenic biosensor reporter lines allowed define more exhaustively the distribution of ColVI in different organs and tissues, showing ColVI deposition in the perichondrium surrounding Meckel's and palatoquadrate cartilages and in the cartilaginous compartments of branchial arches. Interestingly, previous studies in mice showed that ColVI is abundant in the pericellular matrix of cartilage, where it is involved in the proper adhesion and function of chondrocytes[43]. ColVI is also present around the dentary bone and ceratobranchial arches of 6-dpf fish larvae. These results are in line with those reported in humans, where ColVI is found on the bone surface during development[44], and also in mice, showing ColVI deposition in the mesenchymal region at the surface of skeletal elements[29]. One of the major molecular players involved in the control of vertebrate chondrogenesis is the Wnt signaling pathway[45]. Interestingly, in 6-dpf fish larvae ColVI displays abundant deposition in the jaw, near some clusters of cells expressing Wnt reporter activity. A recent study showed that Wnt responsive cells include chondrocytes at the jaw joint and along the palatoquadrate cartilage, as well as ligament and tendon fibroblasts[37]. These cells are located in areas subjected to high levels of tensile and compressive strain and include cell types known to respond to biomechanical stimuli, such as chondrocytes and tenocytes[37]. Based on these results, in the next future it will be interesting to carry out targeted functional studies in zebrafish, in order to ascertain if ColVI is required for cartilage development and maintenance and whether there is a link between this ECM protein and Wnt signaling in regulating such processes. Concerning tendons, our data also revealed strong ColVI reactivity in the myotome of zebrafish larvae. In particular, the protein is found at the level of vertical and horizontal myosepta, the teleost homolog of tendons. In mammals ColVI is localized in the pericellular region surrounding tendon fibroblasts[46]. Interestingly, previous studies showed that the tendons of *Col6a1*$^{-/-}$ mice have disrupted microdomains and abnormal fibrillogenesis, with a decrease in

maximum load and stiffness, thus indicating that ColVI contributes to the maintenance of the mechanical properties of tendons[46].

Another tissue where ColVI is abundant in developing fish larvae is the mesenchyme surrounding brain, eyes and olfactory pits. At later stages, the protein is abundantly deposited in the corneal stroma and in the connective tissue that underlies olfactory epithelium. This distribution once again is in good agreement with what has been reported in mammals, where ColVI deposition was found in meningeal cells[29,47] in the ECM of cornea[29,48] and in the mesenchyme underneath the epithelium of nasal cavity[29]. Our immunofluorescence experiments also showed ColVI deposition in brain blood vessels both during development and in adulthood. In particular, ColVI is found in close apposition to Wnt-positive cells, previously reported as endothelial cells[36]. Given the fact that endothelial Wnt/β-catenin signaling regulates the induction and maintenance of blood-brain barrier features during embryonic and postnatal development[49,50], it will be interesting to investigate whether ColVI plays a role in trapping and accumulating Wnt ligands, thus contributing to the fine regulation of Wnt/β-catenin signaling within the blood-brain barrier.

During adult life ColVI is broadly distributed in various tissues in mammals[1], and other tissues showing ColVI labeling in zebrafish include intestine, adipose tissue, skin and skeletal muscles. Interestingly, we detected the protein in the connective tissue underlying the epithelium of intestinal folds not only in early larval stages but also in adult fish, as previously reported in mice[7,29]. Moreover, ColVI is abundant in the ECM surrounding adipocytes of adult fish, in agreement with the deposition pattern reported in humans[1]. In this respect, it has been demonstrated that adipocyte-derived ColVI promotes early mammary tumor progression by binding the NG2/CSPG4 cell surface receptor and triggering the activation of the Wnt/β-catenin pathway[51]. These data once again strongly suggest that the interaction between ColVI and Wnt signaling may play crucial roles in both physiological and pathological conditions. Concerning skin, in mammals ColVI is abundantly secreted by dermal fibroblasts, and *Col6a1* null mice represent a useful model for the study of skin pathology in patients affected by ColVI-related myopathies[52,53]. In zebrafish, *col6a1* transcripts are clearly detectable in the cuboid

epithelial cells of developing epidermis. This is not surprising since the dermis remains acellular at early stages of skin development in zebrafish, and epithelial cells were found to be responsible for the deposition of collagen I and other ECM proteins in the dermis during development[39]. In adult fish, ColVI is strongly expressed in in the dermis, indicating a cell type switch of ColVI production in the skin at later stages, when fibroblasts are present in the dermis, as it was previously shown for collagen I[39]. In addition, adult fish displayed abundant ColVI deposition in bony scales, dermal derivatives involved in protection and hydrodynamics of swimming[54]. One of the main tissues showing ColVI expression in different species is skeletal muscle[1]. Interestingly, our data revealed a costameric-like periodic pattern of ColVI immunoreactivity in muscles of developing fish, suggesting that muscle fibers may contribute to ColVI deposition during early larval stages. In adult fish, ColVI is deposited in the endomysium and perimysium of muscle cells, where it is most likely produced by interstitial fibroblasts, as shown in mammals[7,15,55,56]. Of note, ColVI was recently found to be part of the specialized ECM of the neuromuscular junction (NMJ) of mice and humans, where it is required for the structural and functional integrity of this compartment[57]. Those studies revealed a novel role for ColVI in the NMJ, pointing at the involvement of NMJ alterations in patients affected by ColVI-related myopathies. Since NMJ development is very similar in zebrafish and humans[58], it will be interesting to determine if ColVI is also present in fish NMJ and whether it has a critical role in regulating NMJ development. Indeed, the zebrafish model represents a valuable tool for such studies, as indicated by previous literature studies on the role of the ECM in motor axon pathfinding and neuromuscular development[58,59].

Taken together, our results provide novel information on the dynamic expression and tissue-specific distribution of ColVI in zebrafish during development and adult life. In the next future, loss-of-function studies in this animal model will help dissecting the roles played by ColVI in various tissues, not only under physiological but also in pathological conditions. For this purpose, zebrafish represents an ideal model, given its rapid development and the availability of different transgenic biosensor lines. In this respect, our data represent a valuable basis for future work focused on the targeted inactivation of ColVI genes in

zebrafish and aimed at shedding new light on the molecular mechanisms underlying the roles of this major ECM component in the modulation of signaling pathways and in tissue homeostasis during development and adulthood.

MATERIALS AND METHODS

Bioinformatics. For the analysis of gene loci, the NCBI genome data viewer (https://www.ncbi.nlm.nih.gov/genome/gdv/) was used. Multiple sequence alignments of the C1 and C2 domains of ColVI chains[1] were performed using the Pileup algorithm of the Wisconsin Package™. The phylogenetic analysis was done by protein distance and protein parsimony as described in PHYLIP v3.69.

Animals. Maintenance and staging of AB/TU wild-type and transgenic [*Tg(osx:nuGFP)*, *Tg(fli1:EGFP)* and *Tg(7xTCF-Xla.Siam:GFP)ia4]* zebrafish were carried out using established protocols[42]. Fish were raised in a 14 h light cycle at approximately 28.5° C. From 24 h post-fertilization (hpf), embryos were treated with phenylthiourea to block pigmentation. All animal manipulations were performed in agreement with EU Directive 2010/63/EU and were authorized by the University of Padova, Body for the Protection of Animals (OPBA-Project Number 1030/2015).

Quantitative real-time PCR (qRT-PCR). Organs were dissected from anesthetized adults. Total

RNA of embryos, larvae (~30 for each experiment) and adult organs was extracted using TRIzol Reagent (Life Technologies), following the manufacturer's protocol. One µg total RNA was retrotranscribed using the SuperScript III First-Strand Synthesis System for RT-PCR (Life Technologies), following manufacturer's instructions. Resulting cDNAs were used to perform qRTPCR with Rotor-Gene SYBR Green PCR Kit mastermix (Qiagen) and a RotorGeneQ instrument (Qiagen). Primer sequences are shown in Table S1. Data on embryos and larvae were normalized to the *arp* housekeeping gene and the expression levels of the different genes were compared to *col6a1* expression at 1 dpf, which was arbitrarily set to 1. Data on adults were normalized to expression of the *eif1axb* housekeeping gene.

Whole-mount *in situ* hybridization. Whole-mount *in situ* hybridization was performed following established protocols[60]. Digoxygenin uridine-5′-triphosphate-labelled RNA probes targeting the *col6a1*, *col6a2* and *col6a3* genes were generated. The primers used are listed in Table S2. Transverse sections (30 µm) were made with a Leica VT1000S vibratome. Stained embryos were analyzed under a Leica DMR compound/Nomarski microscope equipped with a Leica DC500 digital camera.

Expression of recombinant zebrafish α1(VI) C-terminal globular domain and generation of specific antibodies. A cDNA construct encoding the C-terminal globular domains of the α(VI) chain was generated by PCR on total RNA from zebrafish larvae and cloned with 5′-terminal *Spe*I and 3′-terminal *Xho*I restriction sites, using the following primers: zfC6α1(f), 5'– gca act agt ATG CAC ATG TGG ACC CTT GGA –3'; zfC6α1(r), 5'– aac ctc gag CCC TCT CGT CTC CAG GGA AA –3'. The amplified PCR product was inserted into a modified pCEP-Pu vector containing an Nterminal BM-40 signal peptide and a C-terminal One-STrEP tag downstream the restriction sites[61]. Using FuGENE 6 transfection reagents (Roche), the recombinant plasmid was introduced into HEK293-EBNA cells (Invitrogen) according to manufacturer's protocol. Selection was carried out with puromycin (1 µg/ml) and cells producing the One-STrEP-tagged protein were transferred to serum free medium for harvesting. Following filtration and centrifugation, the cell culture supernatants were applied to a Streptactin column (1.5 ml, IBA GmbH) and eluted with 2.5 mM desthiobiotin, 10 mM Tris-HCl, pH 8.0. Purified recombinant α1(VI) C-terminal polypeptide was used for rabbit immunization, and the obtained antiserum was purified by affinity chromatography on a column with the antigen coupled to CNBr-activated Sepharose™ 4B (GE Healthcare Life Sciences). Bound antibodies were eluted with 0.1 M glycine, pH 2.5, and neutralized with 3 M TrisHCl, pH 8.8 and 5 M NaCl. The specificity of purified antibodies was determined by ELISA binding assay and immunoblotting.

Immunofluorescence. Immunohistochemical stainings of whole zebrafish embryos and larvae at 2, 3, 6 and 10 dpf were performed by the One for All protocol[62]. Primary antibodies against zebrafish α1(VI) (1:50; except for Fig. 3g, 1:400; rabbit polyclonal) and GFP (1:400; ab13970, chicken polyclonal, Abcam)

were used, followed by anti-rabbit Cy3/Cy5 (1:500; Jackson Immunoresearch) or anti-chicken Alexa Fluor 488 (1:500; Abcam) secondary antibodies. Nuclei were stained with Hoechst 33258 (1.5 µg/ml; Sigma). Whole mount immunohistochemical staining of Fig. 3c was performed following the protocol in[34]. Anti- zebrafish α1(VI) (1:400) and anti-collagen XII (1:250; guinea pig**)** were used as primary antibodies. Conjugated secondary antirabbit Alexa546 and anti-guinea pig Alexa-488 antibodies (both from Life Sciences) were used at 1:500. Immunostaining of frozen tissue sections was performed as in[58], using antibodies against zebrafish α1(VI) (1:400), collagen XII (1:250[34]), E-cadherin (1:200; mouse BD Biosciences) and phalloidin-TRITC (1:100; Sigma). The secondary antibodies used were anti-rabbit Alexa546, anti-mouse Alexa488 and anti-guinea pig Alexa-488 (1:500, all from Life Sciences). Nuclei were stained as above. For some experiments, immunostaining was performed on paraffinized sections of 7-dpf and adult (8- to 12-mpf) zebrafish, obtained as in[63]. After deparaffination and rehydration, slices were covered with 10 mM sodium citrate buffer (pH 6.0) and placed in a steamer for 25 min, to promote antigen unmasking. In order to decrease autofluorescence, 50 mM NH_4Cl was then placed on each slice for 1 h. After washing with phosphate buffered saline (PBS), slices were incubated for 30 min with 5% goat/sheep serum in PBS. Primary antibodies were diluted in 5% goat/sheep serum and applied overnight at 4˚ C. In other experiments (Fig. 5 panels g and k), adult zebrafish were fixed overnight with 4% paraformaldehyde and then frozen in liquid nitrogen. Sagittal sections (50 µm) made with a cryostat were then permeabilized for 10 min in cold 50% methanol-50% acetone at -20 °C and dried. After washing with PBS, slices were incubated for 30 minutes with 5% goat/sheep serum in PBS. The primary antibodies were diluted in 5% goat/ sheep serum and applied overnight at 4˚ C. Primary antibodies against the following proteins were used: zebrafish α1(VI) (1:400); GFP (1:400; ab13970, chicken polyclonal, Abcam); light meromyosin (1:100; MF20, mouse monoclonal, DHS). After washing in PBS, sections were then incubated with secondary antibodies for 1 h at room temperature. The following secondary antibodies were used: anti-rabbit Cy3/Cy5 (1:500; Jackson Immunoresearch); anti-mouse FITC (1:500; Life Technologies); anti-chicken Alexa Fluor 488 (1:500; Abcam). After brief washes, slices were incubated with Hoechst 33258 (see above) and mounted using 50 to 80% glycerol. Images

were acquired with Leica SP5, Nikon C2 or Zeiss LSM 700 confocal microscopes and analyzed with the ImageJ/Fiji software.

Histology. Adult zebrafish and 7-dpf larvae were fixed for 24 h in Bouin's solution, following established protocols[63]. The samples were dehydrated progressively in ethanol and embedded in paraffin. Sagittal sections (7 µm) were made on Jung AG Heidelberg microtome. Slices were then deparaffinized, rehydrated and stained with haematoxylin and eosin. Finally, sections were mounted with Eukitt (BioOptica) for microscopic examination. In most cases, haematoxylin-eosin staining was performed on the same slices used for immunohistochemical experiments. Images were captured using a 5000B Leica microscope equipped with a DC500 digital camera.

Western blotting. Embryos and larvae were deyolked (except for 7- and 10-dpf larvae) and lysed using Tissue Extraction Reagent I (Invitrogen) and proteases inhibitors (Complete EDTA free, Roche). Lysates were then processed through mechanical homogenization and protein concentration determined by the BCA Protein Assay kit (Pierce). Adult tissues were dissected following established protocols[64], and lysis performed in Laemmli sample buffer containing 2M urea and 50 mM dithiothreitol. SDS-PAGE of protein lysates (40-50 µg) was carried out in 3-8% polyacrylamide Novex NuPAGE Bis-Tris gels (Invitrogen), followed by electrotransfer onto PDVF membrane (Millipore). Membranes were blocked for 1 h in 5% milk in Tris-buffered saline/0.1% Tween 20 (TBST) and incubated overnight at 4° C with antibodies against zebrafish α1(VI) (1:500) or β-actin (1:1000; mouse monoclonal, Sigma-Aldrich). Membranes were then washed three times with TBST and incubated for 1 h at room temperature with HRP-conjugated anti-rabbit or antimouse antibodies (1:1000; Amersham Bioscience). Detection was performed by SuperSignal West Pico or Dura Chemiluminescent Substrate with CL-XPosure Film (Thermo Scientific).

Statistics. Data were analyzed through GraphPad Prism software. Mann-Whitney tests were used for all pairwise comparisons. Values were expressed as mean ± standard error.

ACKNOWLEDGEMENTS

We are grateful to E. Moro for helpful discussion. We thank F. Argenton and the Zebrafish Facility at the Department of Biology, University of Padova. We thank L. Bernard and R. Renard for fish maintenance (PRECI, SFR Lyon-Biosciences-Gerland, ENS de Lyon, University of Lyon).

AUTHOR CONTRIBUTION STATEMENT

P.B. conceived the experiment(s); V.Tonelotto, V.Trapani, S.B., R.W. and S.E.H., conducted the experiment(s); V.T Tonelotto, V.Trapani and S.B. analysed the results; P.B., V.Tonelotto, V.Trapani, S.B., R.W., F.R. reviewed the manuscript.

COMPETING INTERESTS

The authors declare no competing interests.

FUNDINGS

This work was supported by the Italian Ministry of Education, University and Research (Grants RBAP11Z3YA_003 and 2015FBNB5Y), the Telethon Foundation (Grant GGP14202), the Cariparo Foundation (Starting Grants 2015) and the University of Padova (to P.B.); the “Centre National de la Recherche Scientifique” and the “Ecole Normale Supérieure de Lyon” (to F.R.); and the German Research Council (SFB 829-B2, FOR 2722-B1) (to R.W).

DATA AVAILABILITY

The datasets generated and analysed during the current study are available from the corresponding author on reasonable request.

REFERENCES

1. Cescon, M., Gattazzo, F., Chen, P. & Bonaldo, P. Collagen VI at a glance. *J. Cell Sci.* **128,** 3525–3531 (2015).

2. Bonaldo, P., Russo, V., Bucciotti, F., Bressan, G. M. & Colombatti, A. Alpha 1 chain of chick type VI collagen. The complete cDNA sequence reveals a hybrid molecule made of one short collagen and three von Willebrand factor type A-like domains. *J. Biol. Chem.* **264,** 5575–5580 (1989).

3. Bonaldo, P., Russo, V., Bucciotti, F., Doliana, R. & Colombatti, A. Structural and functional features of the alpha 3 chain indicate a bridging role for chicken collagen VI in connective tissues. *Biochemistry* **29,** 1245–1254 (1990).

4. Doliana, R., Bonaldo, P. & Colombatti, A. Multiple forms of chicken alpha 3(VI) collagen chain generated by alternative splicing in type A repeated domains. *J. Cell Biol.* **111,** 2197–2205 (1990).

5. Chu, M.-L. *et al.* Amino acid sequence of the triple-helical domain of human collagen type VI. *J. Biol. Chem.* **263,** 18601–18606 (1988).

6. Fitzgerald, J., Rich, C., Zhou, F. H. & Hansen, U. Three novel collagen VI chains, α4(VI), α5(VI), and α6(VI). *J. Biol. Chem.* **283,** 20170–20180 (2008).

7. Gara, S. K. *et al.* Differential and restricted expression of novel collagen VI chains in mouse. *Matrix Biol.* **30,** 248–257 (2011).

8. Gara, S. K. *et al.* Three novel collagen VI chains with high homology to the α3 Chain. *J. Biol. Chem.* **283,** 10658–10670 (2008).

9. Maaß, T. *et al.* Heterogeneity of collagen VI microfibrils: Structural analysis of non-collagenous regions. *J. Biol. Chem.* **291**, 5247–5258 (2016).

10. Colombatti, A., Bonaldo, P., Ainger, K., Bressan, G. M. & Volpin, D. Biosynthesis of chick type VI collagen. I. Intracellular assembly and molecular structure. *J. Biol. Chem.* **262,** 14454–14460 (1987).

11. Colombatti, A. & Bonaldo, P. Biosynthesis of chick type VI collagen. II. Processing and secretion in fibroblasts and smooth muscle cells. *J. Biol. Chem.* **262,** 14461–14466 (1987).

12. Doane, K. J., Howell, S. J. & Birk, D. E. Identification and functional characterization of two type VI collagen receptors, alpha 3 beta 1 integrin and NG2, during avian corneal stromal development. *Invest. Ophthalmol. Vis. Sci.* **39,** 263–275 (1998).

13. Petrini, S. *et al.* Altered expression of the MCSP/NG2 chondroitin sulfate

proteoglycan in collagen VI deficiency. *Mol. Cell. Neurosci.* **30,** 408–417 (2005).

14. Bürgi, J. *et al.* CMG2/ANTXR2 regulates extracellular collagen VI which accumulates in hyaline fibromatosis syndrome. *Nat. Commun.* **8,** 15861 (2017).

15. Bönnemann, C. G. in *Handbook of clinical neurology* **101,** 81–96 (2011).

16. Lamandé, S. R. & Bateman, J. F. Collagen VI disorders: Insights on form and function in the extracellular matrix and beyond. *Matrix Biol.* **71-72**, 348–367 (2017).

17. Bonaldo, P. *et al.* Collagen VI deficiency induces early onset myopathy in the mouse: an animal model for Bethlem myopathy. *Hum. Mol. Genet.* **7,** 2135–2140 (1998).

18. Irwin, W. A. *et al.* Mitochondrial dysfunction and apoptosis in myopathic mice with collagen VI deficiency. *Nat. Genet.* **35,** 367–371 (2003).

19. Grumati, P. *et al.* Autophagy is defective in collagen VI muscular dystrophies, and its reactivation rescues myofiber degeneration. *Nat. Med.* **16,** 1313–1320 (2010).

20. Angelin, A. *et al.* Mitochondrial dysfunction in the pathogenesis of Ullrich congenital muscular dystrophy and prospective therapy with cyclosporins. *Proc. Natl. Acad. Sci.* **104,** 991–996 (2007).

21. Merlini, L. & Bernardi, P. Therapy of collagen VI-related myopathies (Bethlem and Ullrich). *Neurotherapeutics* **5,** 613–618 (2008).

22. Chrisam, M. *et al.* Reactivation of autophagy by spermidine ameliorates the myopathic defects of collagen VI-null mice. *Autophagy* **11,** 2142–2152 (2015).

23. Castagnaro, S. *et al.* Autophagy activation in COL6 myopathic patients by a low-protein-diet pilot trial. *Autophagy* **12,** 2484–2495 (2016).

24. Lieschke, G. J. & Currie, P. D. Animal models of human disease: zebrafish swim into view. *Nat. Rev. Genet.* **8,** 353–367 (2007).

25. Bretaud, S., Nauroy, P., Malbouyres, M. & Ruggiero, F. Fishing for collagen function: About development, regeneration and disease. *Semin. Cell Dev. Biol.* **89**, 100–108 (2018).

26. Telfer, W. R., Busta, A. S., Bonnemann, C. G., Feldman, E. L. & Dowling, J. J. Zebrafish models of collagen VI-related myopathies. *Hum. Mol. Genet.* **19,** 2433–2444 (2010).

27. Ramanoudjame, L. *et al.* Two novel COLVI long chains in zebrafish that are

essential for muscle development. *Hum. Mol. Genet.* **24,** 6624–6639 (2015).

28. Radev, Z. *et al.* A TALEN-Exon Skipping Design for a Bethlem Myopathy Model in Zebrafish. *PLoS One* **10,** e0133986 (2015).

29. Marvulli, D., Volpin, D. & Bressan, G. M. Spatial and temporal changes of typeVI collagen expression during mouse development. *Dev. Dyn.* **206,** 447–454 (1996).

30. Steffen, L. S. *et al.* Zebrafish orthologs of human muscular dystrophy genes. *BMC Genomics* **8,** 79 (2007).

31. Nauroy, P., Hughes, S., Naba, A. & Ruggiero, F. The in-silico zebrafish matrisome: A new tool to study extracellular matrix gene and protein functions. *Matrix Biol.* **65,** 5–13 (2018).

32. Meyer, A. & Schartl, M. Gene and genome duplications in vertebrates: the one-to-four (-to-eight in fish) rule and the evolution of novel gene functions. *Curr. Opin. Cell Biol.* **11,** 699–704 (1999).

33. Braasch, I. *et al.* The spotted gar genome illuminates vertebrate evolution and facilitates human-teleost comparisons. *Nat. Genet.* **48,** 427–437 (2016).

34. Bader, H. L. *et al.* Zebrafish collagen XII is present in embryonic connective tissue sheaths (fascia) and basement membranes. *Matrix Biol.* **28,** 32–43 (2009).

35. Lawson, N. D. & Weinstein, B. M. In vivo imaging of embryonic vascular development using transgenic zebrafish. *Dev. Biol.* **248,** 307–318 (2002).

36. Moro, E. *et al.* (2012). In vivo Wnt signaling tracing through a transgenic biosensor fish reveals novel activity domains. *Dev. Biol.* **366**, 327–340 (2012).

37. Brunt, L. H., Begg, K., Kague, E., Cross, S. & Hammond, C. L. Wnt signalling controls the response to mechanical loading during zebrafish joint development. *Development* **144,** 2798–2809 (2017).

38. DeLaurier, A. *et al.* Zebrafish sp7:EGFP: A transgenic for studying otic vesicle formation, skeletogenesis, and bone regeneration. *genesis* **48,** 505–511 (2010).

39. Le Guellec, D., Morvan-Dubois, G. & Sire, J.-Y. Skin development in bony fish with particular emphasis on collagen deposition in the dermis of the zebrafish (Danio rerio). *Int. J. Dev. Biol.* **48,** 217–231 (2004).

40. Frka, K. *et al.* Lentiviral-mediated RNAi in vivo silencing of Col6a1, a gene with complex tissue specific expression pattern. *J. Biotechnol.* **141,** 8–17 (2009).

41. Howe, K. *et al.* The zebrafish reference genome sequence and its relationship to the human genome. *Nature* **496,** 498–503 (2013).

42. Kimmel, C. B., Ballard, W. W., Kimmel, S. R., Ullmann, B. & Schilling, T. F. Stages of embryonic development of the zebrafish. *Dev. Dyn.* **203,** 253–310 (1995).

43. Wu, J. J., Eyre, D. R. & Slayter, H. S. Type VI collagen of the intervertebral disc. Biochemical and electron-microscopic characterization of the native protein. *Biochem. J.* **248,** 373–381 (1987).

44. Keene, D. R., Sakai, L. Y. & Burgeson, R. E. Human bone contains type III collagen, type VI collagen, and fibrillin: type III collagen is present on specific fibers that may mediate attachment of tendons, ligaments, and periosteum to calcified bone cortex. *J. Histochem. Cytochem.* **39,** 59–69 (1991).

45. Goldring, M. B., Tsuchimochi, K. & Ijiri, K. The control of chondrogenesis. *J. Cell. Biochem.* **97,** 33–44 (2006).

46. Izu, Y. *et al.* Dysfunctional tendon collagen fibrillogenesis in collagen VI null mice. *Matrix Biol.* **30,** 53–61 (2011).

47. Sievers, J., Pehlemann, F. W., Gude, S. & Berry, M. Meningeal cells organize the superficial glia limitans of the cerebellum and produce components of both the interstitial matrix and the basement membrane. *J. Neurocytol.* **23,** 135–149 (1994).

48. Zimmermann, D. R., Trüeb, B., Winterhalter, K. H., Witmer, R. & Fischer, R. W. Type VI collagen is a major component of the human cornea. *FEBS Lett.* **197,** 55–58 (1986).

49. Liebner, S. *et al.* Wnt/β-catenin signaling controls development of the blood–brain barrier. *J. Cell Biol.* **183,** 409–417 (2008).

50. Obermeier, B., Daneman, R. & Ransohoff, R. M. Development, maintenance and disruption of the blood-brain barrier. *Nat. Med.* **19,** 1584–1596 (2013).

51. Iyengar, P. *et al.* Adipocyte-derived collagen VI affects early mammary tumor progression in vivo, demonstrating a critical interaction in the tumor/stroma microenvironment. *J. Clin. Invest.* **115,** 1163–1176 (2005).

52. Lettmann, S. *et al.* Col6a1 Null Mice as a Model to Study Skin Phenotypes in Patients with Collagen VI Related Myopathies: Expression of Classical and Novel Collagen VI Variants during Wound Healing. *PLoS One* **9,** e105686 (2014).

53. Chen, P., Cescon, M. & Bonaldo, P. Lack of Collagen VI Promotes Wound-Induced Hair Growth. *J. Invest. Dermatol.* **135,** 2358–2367 (2015).

54. Metz, J. R., Leeuwis, R. H. J., Zethof, J. & Flik, G. Zebrafish (Danio rerio) in calcium-poor water mobilise calcium and phosphorus from scales. *J. Appl. Ichthyol.* **30**, 617–677 (2014).

55. Zou, Y., Zhang, R.-Z., Sabatelli, P., Chu, M.-L. & Bönnemann, C. G. Muscle Interstitial Fibroblasts Are the Main Source of Collagen VI Synthesis in Skeletal Muscle: Implications for Congenital Muscular Dystrophy Types Ullrich and Bethlem. *J. Neuropathol. Exp. Neurol.* **67,** 144–154 (2008).

56. Sabatelli, P. *et al.* Expression of collagen VI α5 and α6 chains in human muscle and in Duchenne muscular dystrophy-related muscle fibrosis. *Matrix Biol.* **31,** 187–196 (2012).

57. Cescon, M. *et al.* Collagen VI is required for the structural and functional integrity of the neuromuscular junction. *Acta Neuropathol.* **136**, 483–499 (2018).

58. Guillon, E., Bretaud, S. & Ruggiero, F. Slow Muscle Precursors Lay Down a Collagen XV Matrix Fingerprint to Guide Motor Axon Navigation. *J. Neurosci.* **36,** 2663–2676 (2016).

59. Fox, M. A. Novel roles for collagens in wiring the vertebrate nervous system. *Curr. Opin. Cell Biol.* **20,** 508–513 (2008).

60. Thisse, C. & Thisse, B. High-resolution in situ hybridization to whole-mount zebrafish embryos. *Nat. Protoc.* **3,** 59–69 (2008).

61. Maertens, B. *et al.* Cleavage and oligomerization of gliomedin, a transmembrane collagen required for node of ranvier formation. *J. Biol. Chem.* **282,** 10647–10659 (2007).

62. Inoue, D. & Wittbrodt, J. One for All—A Highly Efficient and Versatile Method for Fluorescent Immunostaining in Fish Embryos. *PLoS One* **6,** e19713 (2011).

63. Facchinello, N. *et al.* nr3c1 null mutant zebrafish are viable and reveal DNA-binding-independent activities of the glucocorticoid receptor. *Sci. Rep.* **7,** 4371 (2017).

64. Gupta, T. & Mullins, M. C. Dissection of Organs from the Adult Zebrafish. *J. Vis. Exp.* **37,** e1717 (2010).

FIGURE LEGENDS

Figure 1. Phylogenetic analysis of zebrafish ColVI genes. (**A**) Phylogenetic trees of the ColVI α4, α5 and α6 chains in different species, obtained by amino acid sequence comparison of the regions spanning the C1 and C2 domains in the corresponding α chains. The sequences from zebrafish (z), mouse (m) and human (h) were aligned using the PILEUP program of the GCG package, using default parameters. The trees were constructed using the PROTEIN PARSIMONY, PROTEIN DISTANCE, FITCH and CONSENSE tools of the PHYLIP package version 3.69. Bootstrap analyses using 100 replicates were performed to show the significance. Numbers indicate the statistical weight of the individual branches. The C1 and C2 domains of zebrafish ColVI α1 chain were used as outgroup. (**B**) Comparative maps of syntenic regions of the zebrafish *col6a4b* gene. Genes encoding the corresponding α4 chain in different species are indicated by red arrows. Neighboring syntenic genes are indicated by blue arrows. For simplicity, the orientation of the genes on the chromosomes was adjusted to that of zebrafish chromosome 13. Members of the carp family (Cyprinidae) are boxed.

Figure 2. ColVI expression in zebrafish at different developmental stages. (**A**) qRT-PCR for *col6a1, col6a2, col6a3, col6a4a* and *col6a4b* transcripts in zebrafish embryos and larvae from 12 hpf to 96 hpf. Data were normalized to *arp*. The expression levels of the different genes were compared to *col6a1* expression at 24 hpf, which was arbitrarily set to 1, and represent the mean of at least three independent experiments. Error bars indicate s.e.m. (**, $P < 0.01$). (**B**) Whole-mount *in situ* hybridization for *col6a1* in zebrafish embryos and larvae. The top panels show lateral (lat) and dorsal (dors) views of 1- to 3-dpf embryos labeled with the *col6a1* probe. The bottom panels show transverse sections at different head and trunk levels (*i-iv*, as indicated on the lateral view at the top) and higher magnifications of the tail region (*v* and *vi*) of 2-dpf embryos labeled with the *col6a1* probe. At 1 dpf, labeling for *col6a1* mRNA is restricted to two lines of slow muscle fibers and to the pectoral fin buds (arrowhead). At 2 and 3 dpf, strong signals for *col6a1* transcript are detected in vertical myosepta, pectoral fins (arrowhead),

branchial arches, axial vasculature and gut. (**C**) Western blot for α1(VI) chain in protein extracts from zebrafish embryos and larvae at the indicated stages. β-actin was used as a loading control. Numbers on the left indicate sizes (in kDa) of protein standard markers. The cropped blots for α1(VI) chain and β-actin derive from different parts of the same gel. (**D**) Whole-mount immunofluorescence labeling with anti-ColVI antibody in zebrafish larvae at different developmental stages from 2 dpf to 10 dpf, as indicated. The panels show lateral (lat), ventral (ven) and dorsal (dors) views of different head and trunk regions. From 2 dpf onwards, ColVI immunoreactivity (red) is present in the connective tissue surrounding the eye, in the pectoral fins and in myosepta. At 3 dpf, ColVI deposition extends to craniofacial elements and intestine. From 6 dpf onwards, ColVI labeling is also detected in the connective tissue surrounding olfactory pits. Scale bar, 100 µm. ch, ceratohyal; ey, eye; fb, fin buds; m, myosepta; mc, Meckel's cartilage; no, notochord; op, olfactory pit; pf, pectoral fins; pq, palatoquadrate; sc, spinal cord; yo, yolk.

Figure 3. Characterization of ColVI deposition in 3- and 5-dpf developing zebrafish. (**a-h**) Immunofluorescence images of transverse sections (**a-f**) or whole-mount (**g, h**) 3-dpf embryos at the level of the trunk. Samples were labeled with anti-ColVI antibodies (red) and, where indicated, with phalloidin to reveal actin (green; panel c), or with antibodies against the epithelial marker cadherin (green; panel d) and the mesenchymal marker collagen XII (green; panels f-h). Nuclei were stained with Hoechst (blue; panels a-f). (**a**) Global view of ColVI immunoreactivity at the level of the trunk. (**b**, **c**) Zoomed image of the boxed region in **a**, showing myotomal muscle cells. (**d**) Epidermis. (**e**, **f**) Transverse section of the head. (**g**) Merge image of the vertical myosepta obtained from a z-projection of confocal stack of lateral views. (**h**) Orthogonal view of the vertical myosepta from the z-stack acquired on ImageJ. Scale bars, 25 µm (e-h), 20 µm (a), 10 µm (b, c) or 5 µm (d). SC, spinal cord; NT, notochord; My, myotome.

(**i-m**) Immunofluorescence images of sagittal sections of 5-dpf larvae. Samples were labeled with anti-α1(VI) antibodies (red) and, where indicated, with phalloidin (green; panels j, k, l', m'). Nuclei were stained with Hoechst (blue). (**i**) Global view of ColVI immunoreactivity. (**j**) Intestine. (**k**) Ceratobranchial cartilage. (**l-m'**) Skeletal muscle at the level of the pectoral fin (**l**, **l'**) and the trunk (**m**, **m'**). Scale

bars, 50 µm (i), 25 µm (j, k), 10 µm (l, l') or 5 µm (m, m'). br, brain, ey, eye, sk m, skeletal muscle; pc, pharyngeal cartilage, l, liver, pf, pectoral fin.

Figure 4. Spatio-temporal pattern of ColVI distribution in larvae from wild-type animals and transgenic reporter fish lines. (**a-d**) Confocal z-stacks of whole-mount immunofluorescence for ColVI (red) in 6-dpf *Tg(fli1:EGFP)* (fli1:EGFP, green) larvae, showing strong ColVI labeling in the connective tissue surrounding the eye and in the pericellular matrix surrounding chondrocytes of the jaw. Panel **d** is a magnification of the dotted area of panel c. The asterisk in panel **a** indicates nonspecific autofluorescence. (**e-h**) Confocal z-stacks of whole-mount immunofluorescence for ColVI (red) in 6-dpf *Tg(7xTCF-Xla.Siam:GFP)ia4* (TCF-GFP, green) larvae, showing ColVI labeling near Wnt-positive cells in jaw cartilages. Panel **h** is a higher magnification of an individual z-stack of panel **g** at the level of Meckel's and palatoquadrate cartilages. (**i-n**) Section of 7-dpf larvae stained with anti-α1(VI) antibodies (red), WGA (green) and anti-MF20 antibodies (gray). ColVI labeling is present in craniofacial cartilaginous elements, as well as in blood vessels (arrowhead). Panel **n** is a magnification of the dotted area of panel **m**, showing ColVI labeling in the perichondrium surrounding the cartilaginous elements of the pharyngeal arches, as revealed by co-localization with WGA. (**o-q**) Whole-mount immunostaining for ColVI (red) in 6-dpf *Tg(osx:nuGFP)* (osx:GFP, green) larvae. ColVI labeling surrounds dentary bone and ceratobranchial arches, as revealed by two individual z-stacks in panels **p** and **q**. (**r-t**) Section of a 7-dpf larva stained with anti-ColVI antibodies (red), WGA (green) and Hoechst (blue). ColVI labeling is present in the connective tissue around brain, olfactory pit and eye. (**u**) Section of a 7-dpf larva stained with anti-ColVI antibodies (red) and Hoechst (blue), showing ColVI labeling in the meninges (arrowhead). (**v-y**) Confocal z-stacks of whole-mount immunostaining for ColVI (red) in 6-dpf *Tg(fli1:EGFP)* (fli:EGFP, green) larvae. A strong pattern of ColVI labeling is found around blood vessels (arrowheads) of the intestine. Panel **y** is a magnification of the dotted area of panel **x**. Scale bar, 100 µm (a-g, v-x) or 50 µm (i-m, r-u). bsr, branchiostegal ray; cb, ceratobranchial; ch, ceratohyal; db, dentary bone; ey, eye; f,

forebrain; h, hindbrain; m, maxilla; mc, Meckel's cartilage; mid, midbrain; op, olfactory pit; ope, operculum; pq, palatoquadrate; sc, spinal cord.

Figure 5. ColVI expression in adult zebrafish tissues. (**A**) qRT-PCR for *col6a1, col6a2, col6a3, col6a4a* and *col6a4b* transcripts in different tissues of adult (8- to 12-mpf) fish. Data were normalized to *eif1axb* expression and represent the mean of at least three independent experiments. Error bars indicate s.e.m. (**B**) Western blotting for α1(VI) chain in protein extracts of adult (8- to 12-mpf) fish tissues. Vinculin was used as a loading control. Number on the left indicate sizes (in kDa) of protein standard markers. The histogram on the bottom shows the densitometric quantification of α1(VI) vs. vinculin, as determined by three independent western blot experiments. Values for cartilage were arbitrarily set to 1. Error bars indicate s.e.m. The cropped blots for α1(VI) chain and vinculin derive from different parts of the same gel. (**c-k**) Sagittal sections of adult (8-to 12-mpf) fish tissues analyzed by haematoxylin-eosin staining (H&E, left panels) and by immunofluorescence labeling with anti-ColVI antibodies (red, middle and right panels). Nuclei were stained with Hoechst (blue, right panels). Scale bar, 50 µm. a, adipocyte; bs, bony scale; cb, ceratobranchial; ce, ceratohyal; cr, cryptae; endom, endomysium; en, endothelium; ep, epithelium; gc, goblet cell; ir, iris; me, mucosal epithelium, pl, primary lamella; sl, secondary lamella; st, stroma; te, telencephalon.

SUPPLEMENTARY DATA

Supplementary Figure S1. (**a**) Schematic diagram of the domain structure of ColVI α chains in zebrafish (*D. rerio*) and in mouse (*M. musculus*). The domain organization of the α1(VI), α2(VI) and α3(VI) chains (i.e., the main ColVI subunits) is largely conserved between fish and mammals, including humans. A distinctive feature of zebrafish and other cyprinid fish is the presence of two ohnolog genes coding for the α4(VI) chain (see also Fig. 1a, b). At difference from mouse α4(VI), the zebrafish α4(VI) chains display additional VWA modules at the N-terminal end (outlined in red in the diagram) and two Kunitz-like domains at the C-terminal end. Genes coding for the α5(VI) and α6(VI) chains are absent in zebrafish, suggesting

that they evolved later during evolution. (**b**) Multiple amino acid sequence alignment of the α1(VI) chain in mouse (MmCol6a1), humans (HsCol6a1), zebrafish (DrCol6a1) and fugu (TrCol6a1), as determined by analysis with the ClustalW software. Identical amino acid residues in all sequences are marked with '*', while conservative and semi-conservative substitutions are marked with ':' and '.', respectively. The three VWA domains are highlighted in green, the collagenous domain triple helix is highlighted in red, and the conserved cysteine residues are boxed.

Supplementary Figure S2. (**a**) Whole-mount *in situ* hybridization for *col6a2* and *col6a3* in zebrafish embryos and larvae. The panels show lateral (lat) and dorsal (dors) views of 1- to 3-dpf embryos labeled with *col6a2* or *col6a3* probes, as indicated. (**b**) Whole-mount *in situ* hybridization of a 24-hpf zebrafish embryo labeled with the *col6a1* riboprobe. The inset shows higher magnification of the boxed region, revealing labeling at the level of basal epidermal cells (arrow). (**c**) Immunofluorescence with anti-ColVI antibody in transverse sections of 6-dpf larvae at the level of the head, showing that ColVI is found in brain blood vessels, as also confirmed by the negative control (secondary antibody, II ab only), where no ColVI labeling was detected. Nuclei were stained with Hoechst (blue). (**d**) Immunofluorescence with anti-α1(VI) antibodies in transverse sections of 1-year old fish at the level of the trunk, showing the presence of strong ColVI labeling (red) in bony scales and dermis (left panel), in the endomysium of skeletal muscles (middle panel), and in the mucosa and muscular layers of the gut (right panel). Nuclei were stained with Hoechst (blue). Scale bar 50 μm (c) or 25 μm (d). de, dermis; ep, epimysium; fb, fiber; me, muscularis externa; sc, scale; v, villus.

Supplementary Figure S3. Immunofluorescence images of ColVI labeling in 5-mpf *Tg(7xTCF-Xla.Siam:GFP)ia4* zebrafish. Sections of 5-mpf *Tg(7xTCF-Xla.Siam:GFP)ia4* zebrafish were stained with anti-ColVI (red) and anti-GFP (green) antibodies. Nuclei were stained with Hoechst (blue). (**a-h**) Brain sections, showing ColVI labeling in blood vessels close to Wnt-responsive cells. (**i-p**) Section of basihyal cartilage. ColVI surrounds Wnt-responsive cells, as revealed by the magnification of the boxed areas in panels **m-p**. Scale bar, 50 μm (a-d) or 100 μm (e-l).

Supplementary Table 1. List of the primer sequences used for qRT-PCR.

Primer	Forward	Reverse
qPCRzf*col6a1*(1)	CATCAAGACCCTGACCGACC	GCACAGCACGTTTAATGGCA
qPCRzf*col6a1*(2)	CAAACGCTCTCAACTTCGCC	TGCTCCACGGCTTTCTCAAT
qPCRzf*col6a2*(1)	CGGTGCCCTGGATATTGTGT	GTTGAGTCGAATGGCCTGGA
qPCRzf*col6a2*(2)	CTGTGCTTTGTCCGGATCCT	AAGACCAGATCAACAGGCCG
qPCRzf*col6a3*(1)	CATCCTCGCCACTTGAAGGT	CCAACCGCCATCACCACTAT
qPCRzf*col6a3*(2)	GGACTTCTGTGCCCCTGATC	TGGTGGGATCTCTTCGGTCT
qPCRzf*col6a4*(1)	AACAGGGACATAGGGCAAGC	AGCCTCGATTCACTCTCCGA
qPCRzf*col6a4*(2)	CGGAGAGTGAATCGAGGCTC	AACCTGCATTGCTCGTCTCA
qPCRzf*col6a6*(1)	GCGCCGACTTTGAAGATGTG	TGAAGAGTGGGATTGCGGTC
qPCRzf*col6a6*(2)	CACTTCAAATCGCCGCAACA	TCCTCAGAGCAATGACCCCA
qPCRzf*ef1axb*	CTGGAGGCCAGCTCAAACAT	ATCAAGAAGAGTAGTACCGCTAGCATTAC
qPCR*arp*	CTGAACATCTCGCCCTTCTC	TAGCCGATCTGCAGACACAC

Supplementary Table 2. List of the primer sequences used for whole-mount *in situ* hybridization.

Probe	Forward	Reverse
zf*col6a1*	ATCGTGGACAGCTCTGAGAG	TCCGTGAGAAGTCCTTGGTC
zf*col6a2*	TGTGAAAAGAGATGCGGTGC	GATCCGGACAAAGCACAGTC
zf*col6a3*	AGGCTTTGCAAACCCGTAAG	TCCTCTAAGAAGCTGCGGAC

A

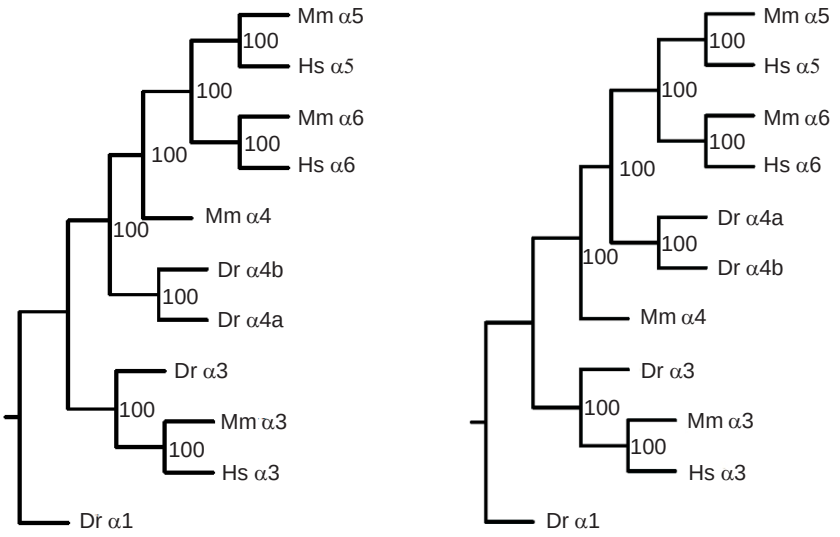
Mm α5
Hs α5
Mm α6
Hs α6
Mm α4
Dr α4b
Dr α4a
Dr α3
Mm α3
Hs α3
Dr α1
100
Protein distance
Protein parsimony

B

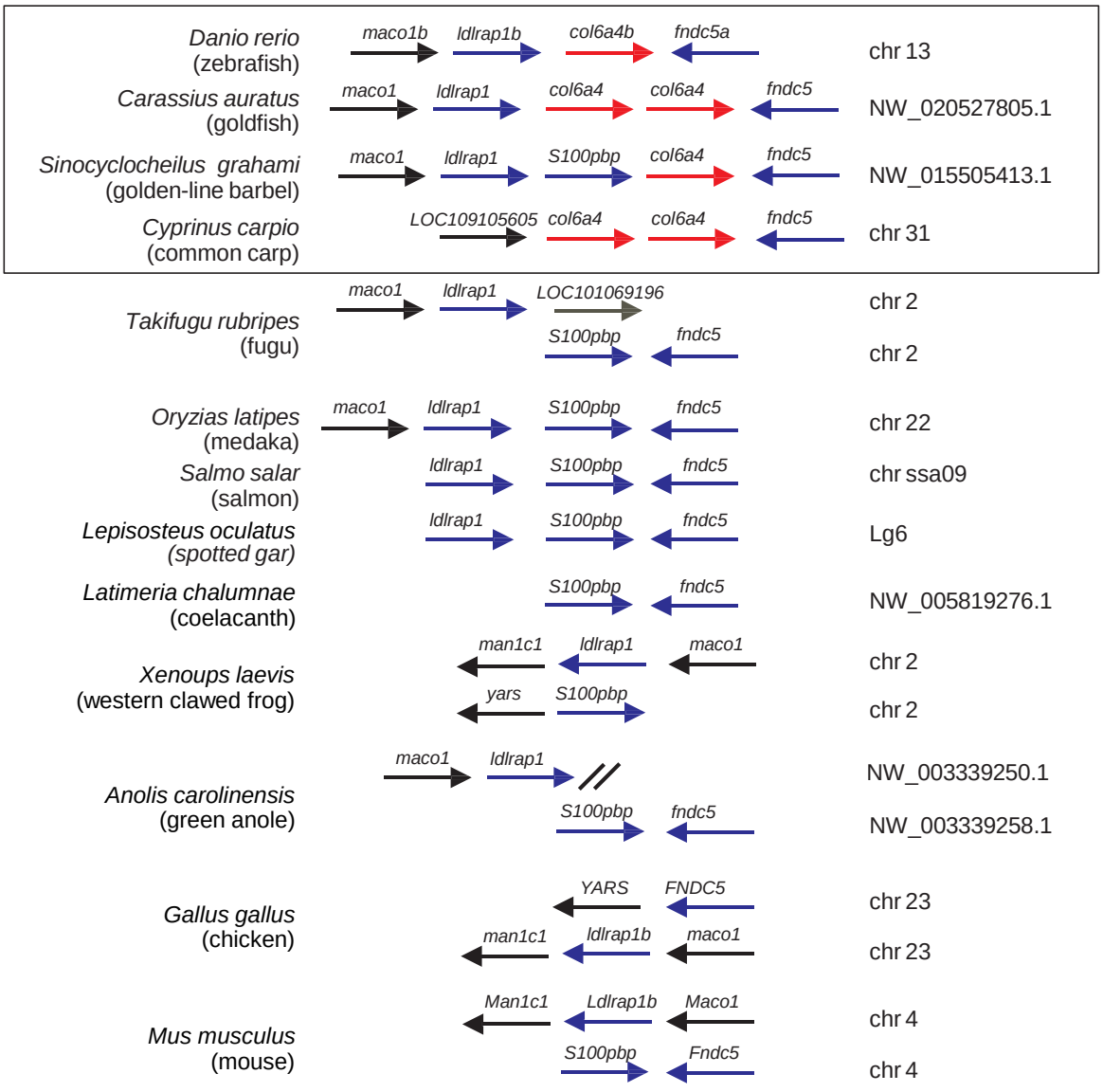
Danio rerio (zebrafish)
maco1b ldlrap1b col6a4b fndc5a
chr 13
Carassius auratus (goldfish)
maco1 ldlrap1 col6a4 col6a4 fndc5
NW_020527805.1
Sinocyclocheilus grahami (golden-line barbel)
maco1 ldlrap1 S100pbp col6a4 fndc5
NW_015505413.1
Cyprinus carpio (common carp)
LOC109105605 col6a4 col6a4 fndc5
chr 31
Takifugu rubripes (fugu)
maco1 ldlrap1 LOC101069196
chr 2
S100pbp fndc5
chr 2
Oryzias latipes (medaka)
maco1 ldlrap1 S100pbp fndc5
chr 22
Salmo salar (salmon)
ldlrap1 S100pbp fndc5
chr ssa09
Lepisosteus oculatus (spotted gar)
ldlrap1 S100pbp fndc5
Lg6
Latimeria chalumnae (coelacanth)
S100pbp fndc5
NW_005819276.1
Xenoups laevis (western clawed frog)
man1c1 ldlrap1 maco1
chr 2
yars S100pbp
chr 2
Anolis carolinensis (green anole)
maco1 ldlrap1
NW_003339250.1
S100pbp fndc5
NW_003339258.1
Gallus gallus (chicken)
YARS FNDC5
chr 23
man1c1 ldlrap1b maco1
chr 23
Mus musculus (mouse)
Man1c1 Ldlrap1b Maco1
chr 4
S100pbp Fndc5
chr 4

Figure 1

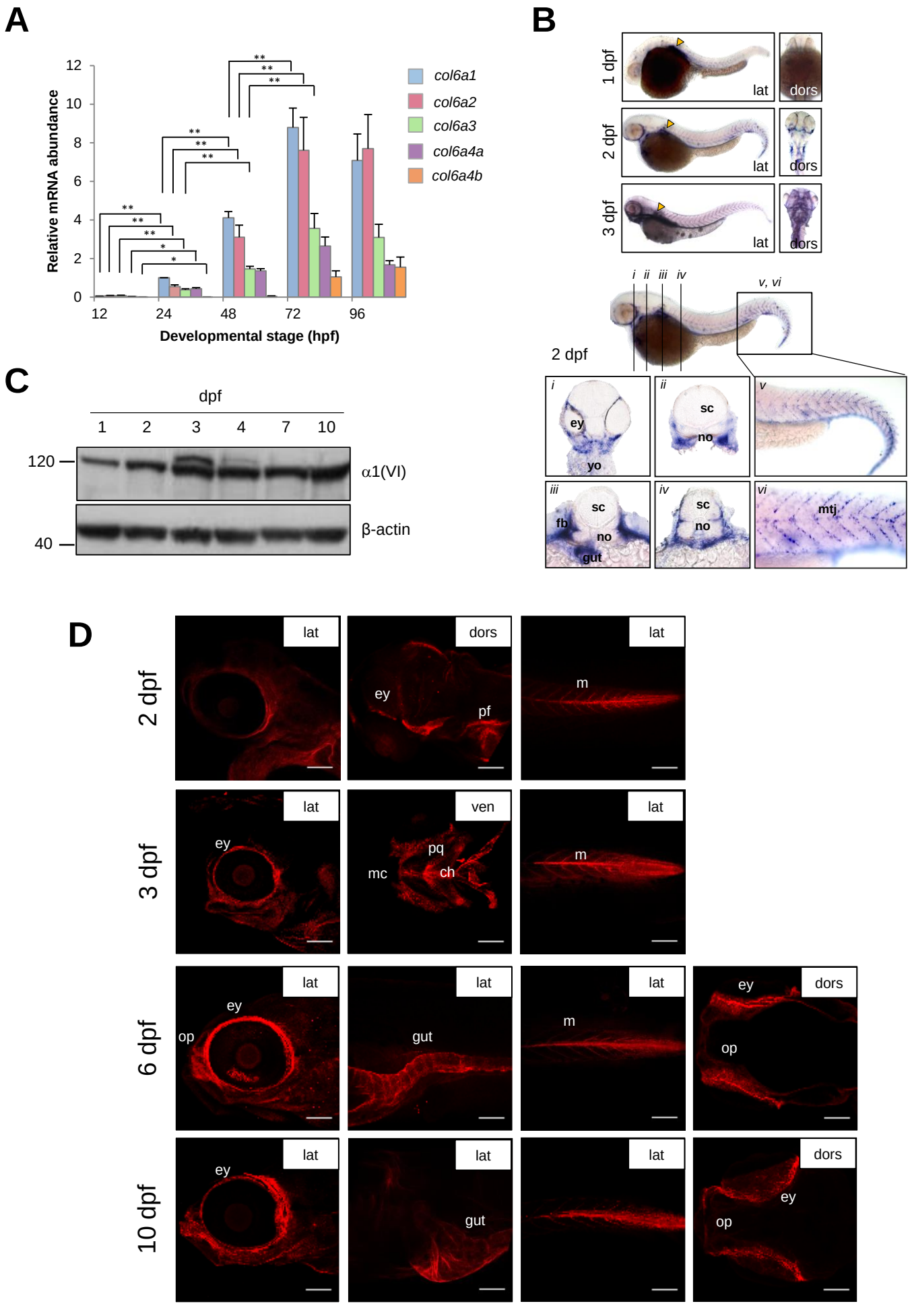
A
Relative mRNA abundance
Developmental stage (hpf)
col6a1
col6a2
col6a3
col6a4a
col6a4b
B
1 dpf
2 dpf
3 dpf
lat
dors
i ii iii iv
v, vi
ey
yo
sc
no
fb
gut
mtj
C
dpf
1 2 3 4 7 10
120
40
α1(VI)
β-actin
D
2 dpf
3 dpf
6 dpf
10 dpf
lat
dors
ven
ey
pf
m
pq
mc
ch
op
gut

Figure 2

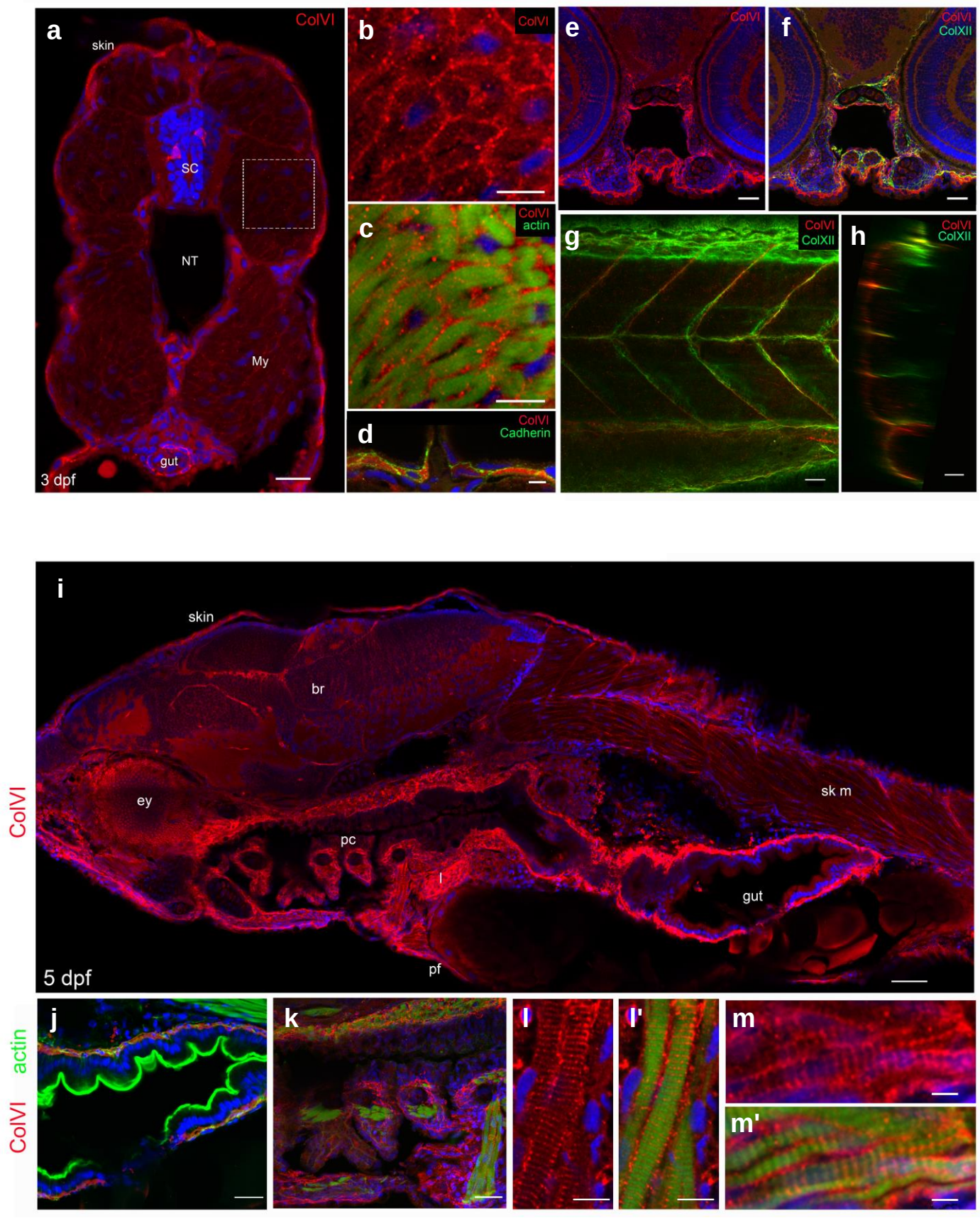
a
ColVI
skin
SC
NT
My
gut
3 dpf
b
ColVI
c
ColVI
actin
d
ColVI
Cadherin
e
ColVI
f
ColVI
ColXII
g
ColVI
ColXII
h
ColVI
ColXII
i
skin
br
ey
pc
l
sk m
gut
pf
5 dpf
ColVI
actin
ColVI
j
k
l
l'
m
m'

Figure 3

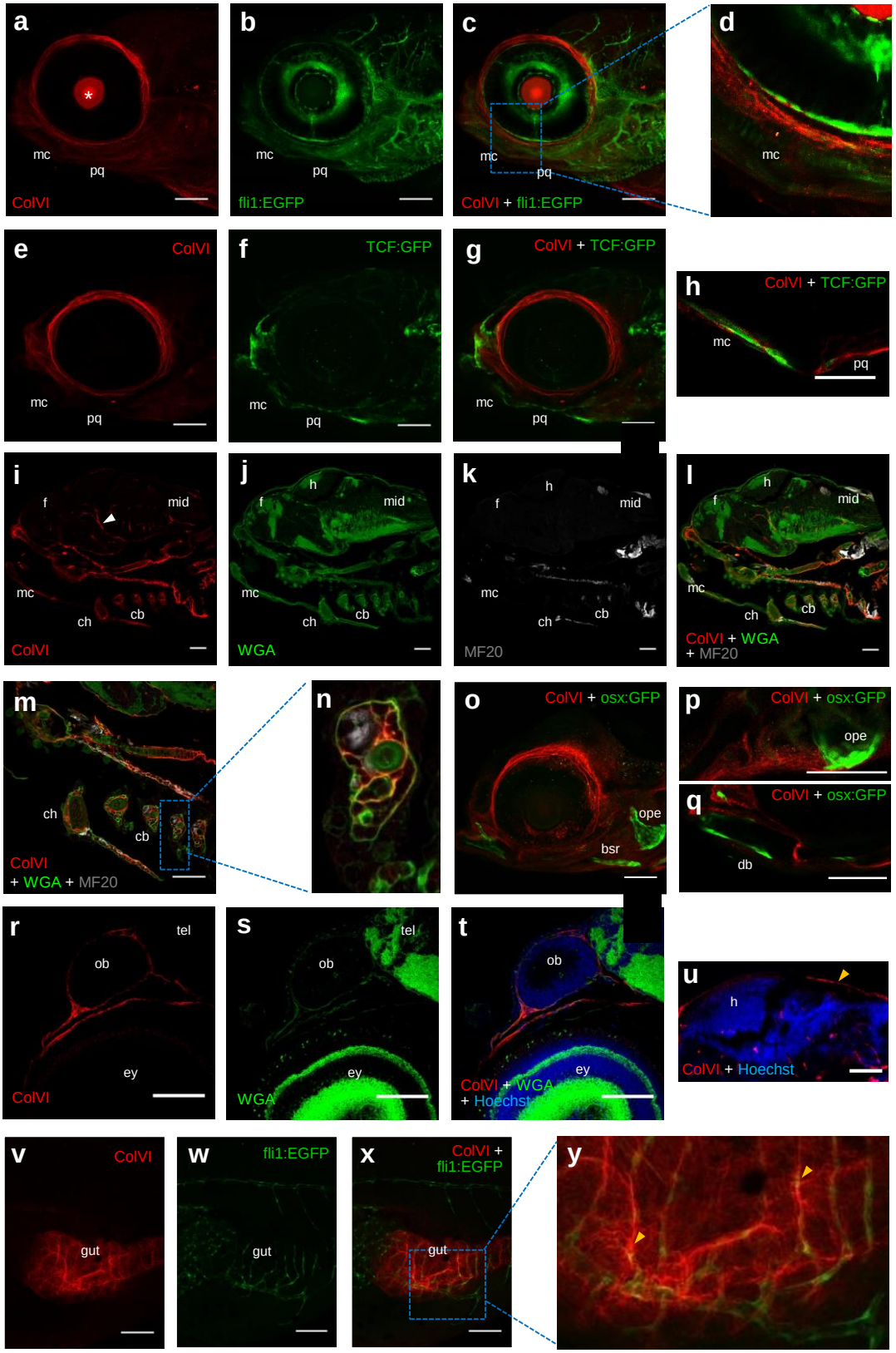
a
mc
pq
ColVI
b
mc
pq
fli1:EGFP
c
mc
pq
ColVI + fli1:EGFP
d
mc
e
ColVI
mc
pq
f
TCF:GFP
mc
pq
g
ColVI + TCF:GFP
mc
pq
h
ColVI + TCF:GFP
mc
pq
i
f
mid
mc
ch
cb
ColVI
j
h
f
mid
mc
ch
cb
WGA
k
h
f
mid
mc
ch
cb
MF20
l
h
f
mid
mc
ch
cb
ColVI + WGA
+ MF20
m
ch
cb
ColVI
+ WGA + MF20
n
o
ColVI + osx:GFP
ope
bsr
p
ColVI + osx:GFP
ope
q
ColVI + osx:GFP
db
r
tel
ob
ey
ColVI
s
tel
ob
ey
WGA
t
ob
ey
ColVI + WGA
+ Hoechst
u
h
ColVI + Hoechst
v
ColVI
gut
w
fli1:EGFP
gut
x
ColVI +
fli1:EGFP
gut
y

Figure 4

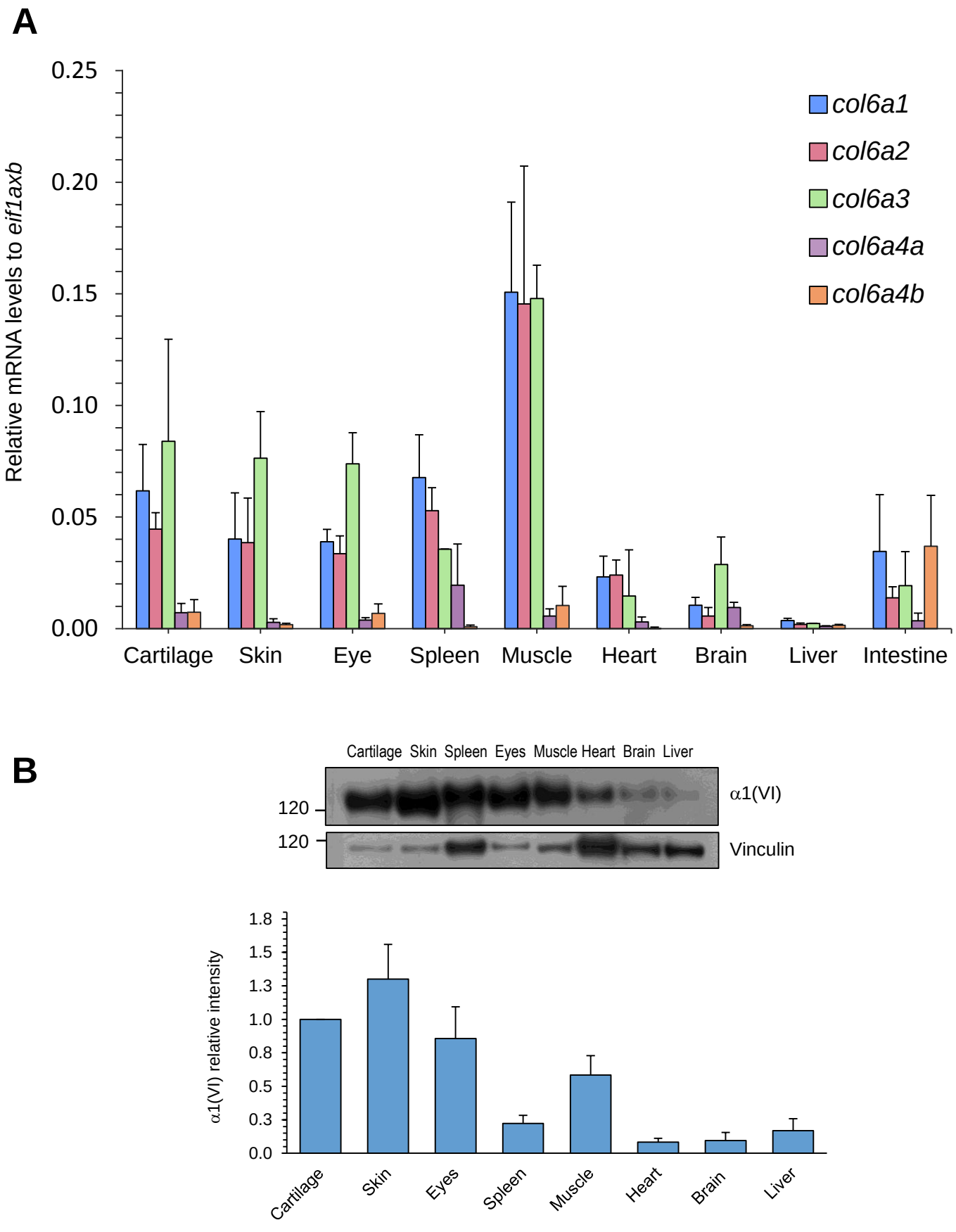
A
Relative mRNA levels to eif1axb
0.25
0.20
0.15
0.10
0.05
0.00
col6a1
col6a2
col6a3
col6a4a
col6a4b
Cartilage
Skin
Eye
Spleen
Muscle
Heart
Brain
Liver
Intestine
B
Cartilage Skin Spleen Eyes Muscle Heart Brain Liver
120
120
α1(VI)
Vinculin
α1(VI) relative intensity
1.8
1.5
1.3
1.0
0.8
0.5
0.3
0.0
Cartilage
Skin
Eyes
Spleen
Muscle
Heart
Brain
Liver

Figure 5

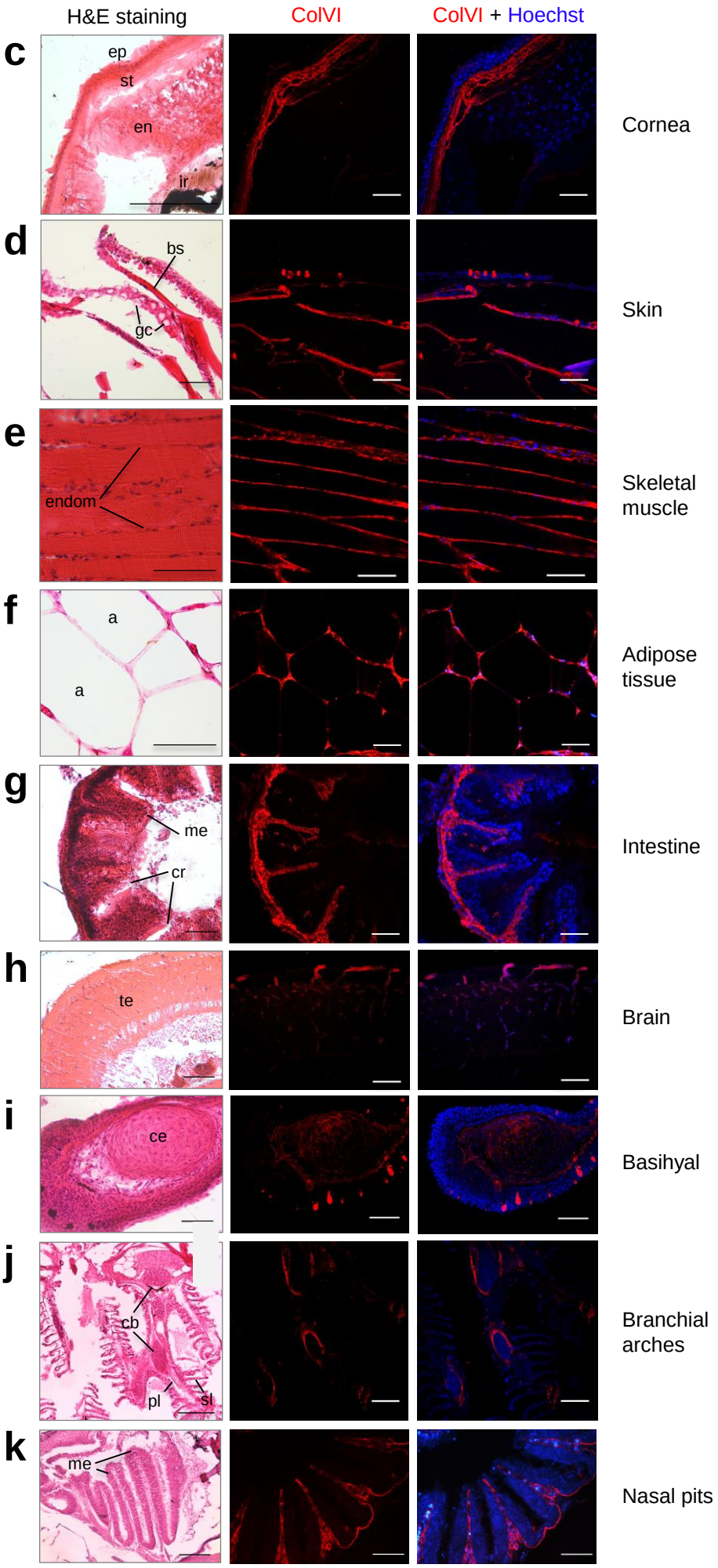
H&E staining
ColVI
ColVI + Hoechst
c
ep
st
en
ir
Cornea
d
bs
gc
Skin
e
endom
Skeletal muscle
f
a
a
Adipose tissue
g
me
cr
Intestine
h
te
Brain
i
ce
Basihyal
j
cb
pl
sl
Branchial arches
k
me
Nasal pits

Figure 5

a

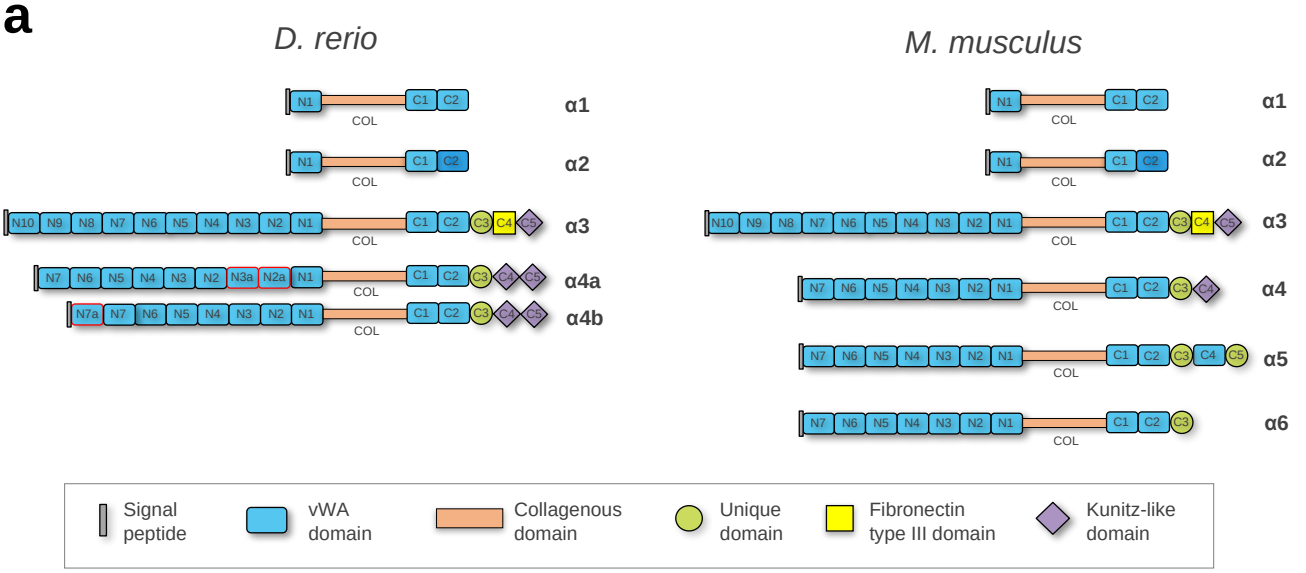

b

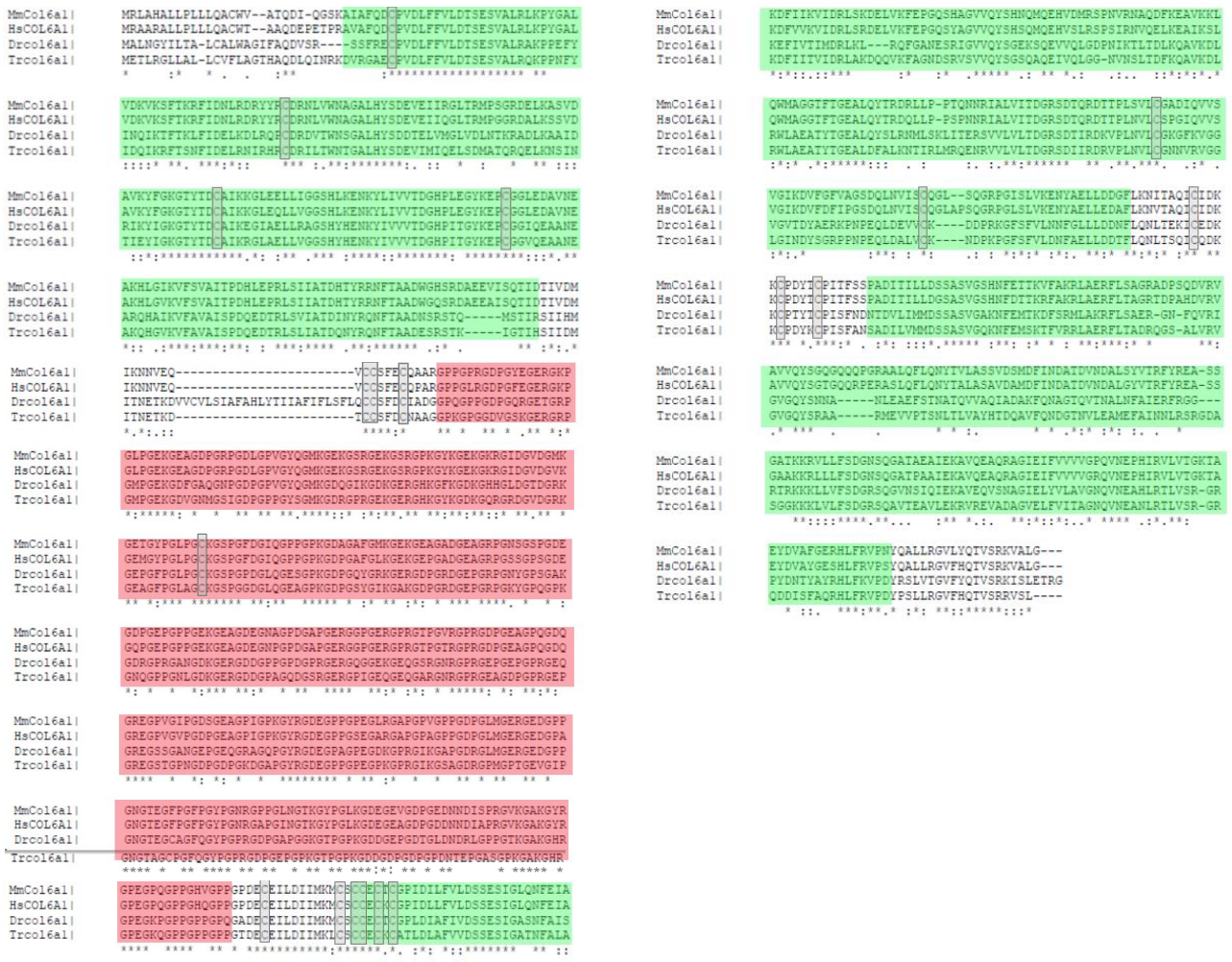

Supplementary Figure S1

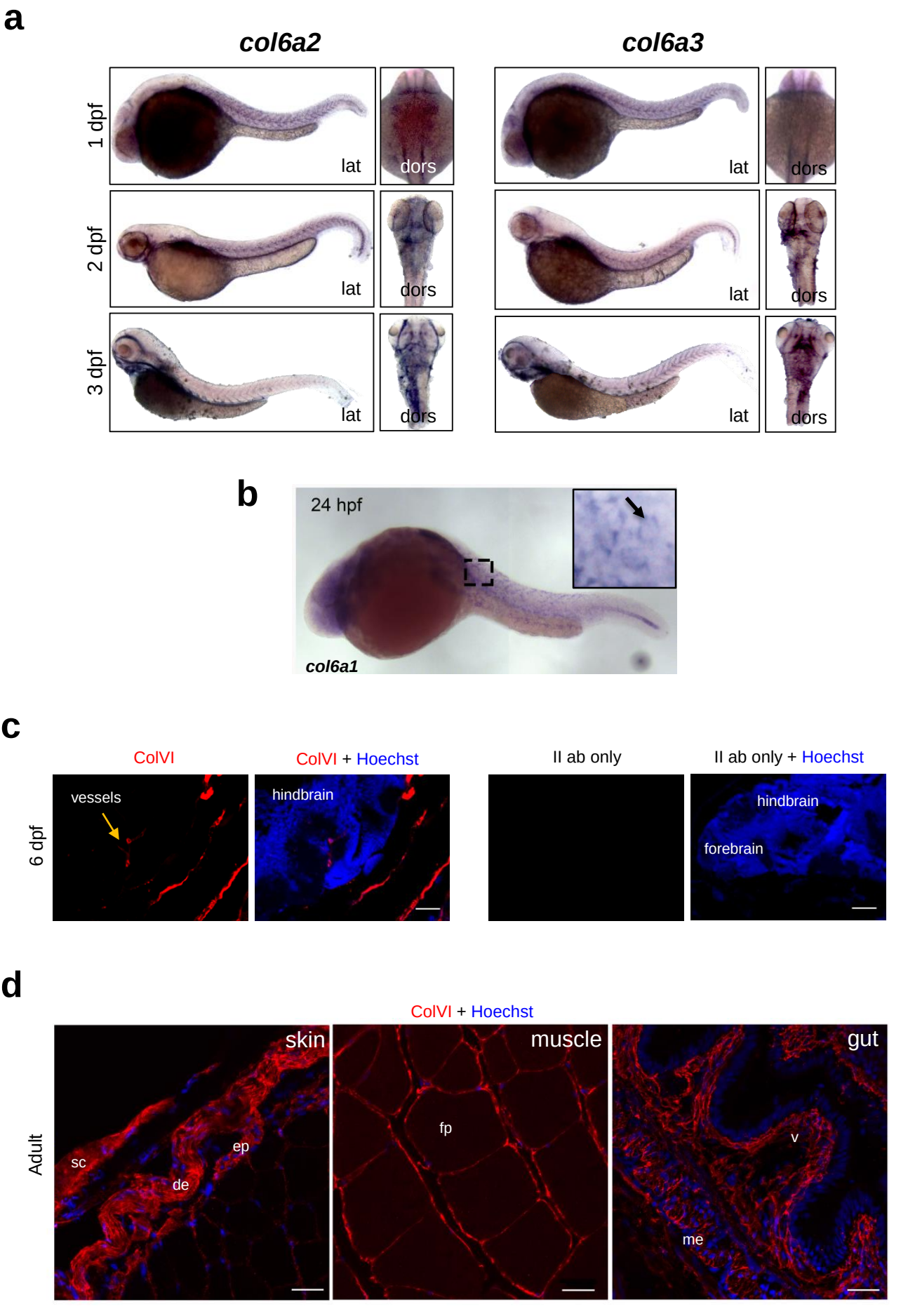

Supplementary Figure S2

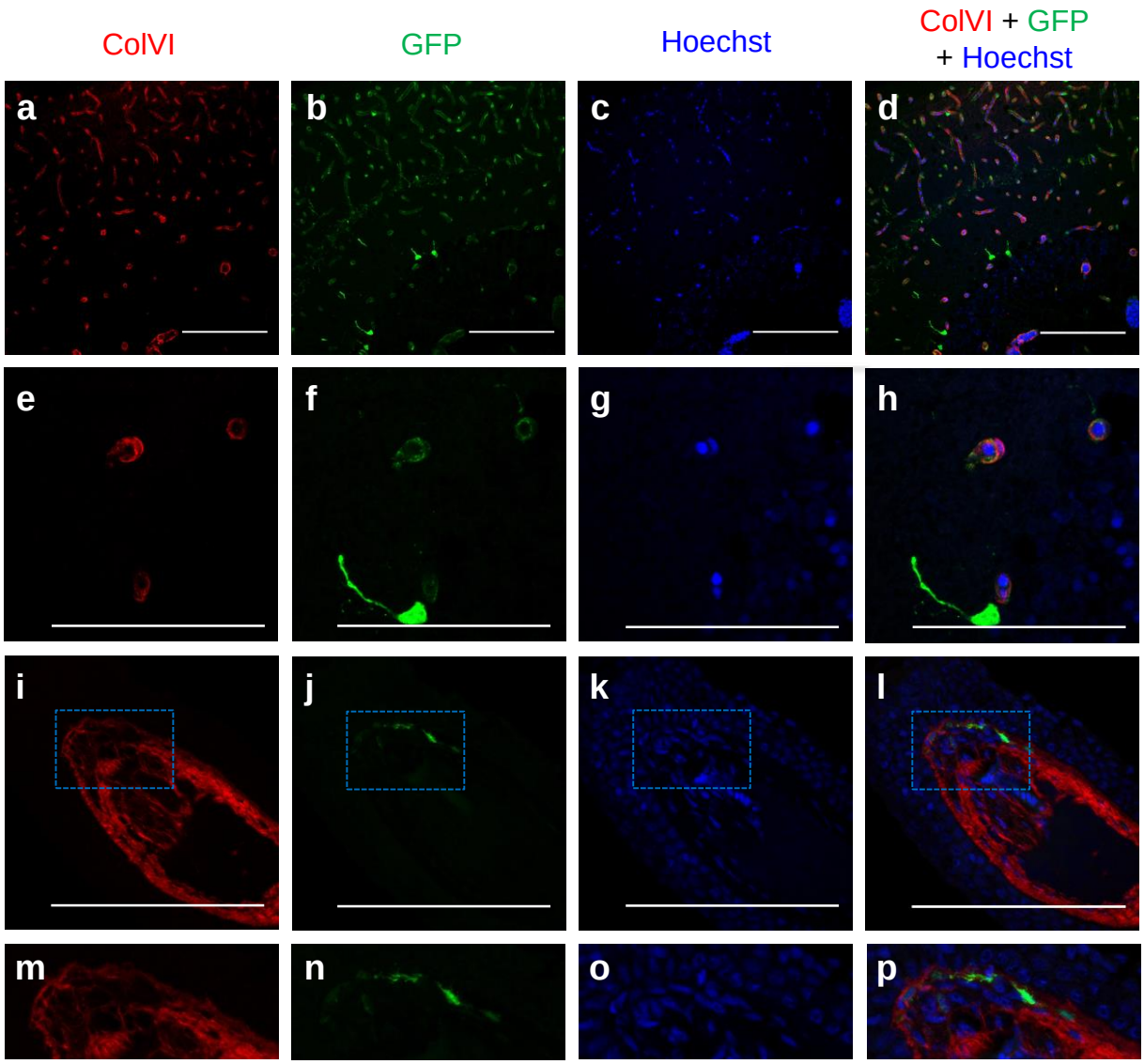

Supplementary Figure S3

Chapter II

1. Background

In the last few years, some studies on COL6 in zebrafish were published (Telfer et al., 2010; Radev et al., 2015; Ramanoudjame et al., 2015; Zech et al., 2015).

In 2010, Telfer and coll. used an antisense morpholino approach to generate zebrafish models for COL6 myopathies. In particular, the authors designed a morpholino to target exon 13 of *col6a1*, mimicking a dominant mutation frequently found in BM patients. In addition, they generated a morpholino targeting exon 9 of *col6a1*, with the aim to reproduce the effects of one of the most common mutations observed in UCMD. Exon 9 morphants displayed increased cell death and mitochondrial swelling, and these defects were attenuated by treatment with cyclosporin A (Telfer et al., 2010). It is well known that A has potent immunosuppressive effects, raising several concerns about its prospective use for the treatment of patients affected by COL6 myopathies (Merlini et al., 2008a). Based on this rationale, another study carried out on *col6a1* exon9 morphants demonstrated that N-methyl-4-isoleucine-cyclosporin (NIM811), a cyclophilin inhibitor devoid of immunosuppressive activity, is more effective than cyclosporin A in recovering structural and functional abnormalities (Zulian et al., 2014).

Another work described two COL6 genes coding for long chains in zebrafish (Ramanoudjame et al., 2015). The authors proposed that these two genes are homologous to the mammalian α4(VI) chain, and for this reason they named them *col6a4a* and *col6a4b*. They generated transient morphant models for *col6a4a*, *col6a4b* and *col6a2* deficiency in zebrafish, and showed that morphant embryos display abnormal muscle organization, reduced autophagic flux and impaired motility. In addition, neuronal outgrowth defects were observed, similarly to the axonal growth alterations recently described in *col6a3* zebrafish morphants mimicking dystonia (Zech et al., 2015).

Although these zebrafish models provided valuable information on the effects of transient COL6 deficiency in tissues such as skeletal muscle and nervous system, the use of morphants limited the study of phenotypes, since the activity of antisense morpholino oligonucleotides lasts very few days in the embryos. For this reason,

Radev and coll. exploited a transcription activator-like effector nuclease (TALEN) approach to generate a mutant *col6a1* zebrafish line. This line bears a mutation disrupting an essential splice site, resulting in an in-frame skipping of *col6a1* exon 14, which codes for the N-terminal portion of the collagenous domain of the α1(VI) chain, thus mimicking a dominant mutation frequently observed in BM patients. These zebrafish mutants exhibited histological and ultrastructural muscle alterations similar to those found in muscle cell cultures and biopsies from BM patients and in *Col6a1* null mice, and their symptoms worsened with ageing (Radev et al., 2015).
Altogether, these findings underline the importance of generating of stable zebrafish null lines, at difference from the previously exploited exon-skipping morphants and mutant models. Therefore, with the aim of dissecting in detail the impact of COL6 ablation in tissue homeostasis and development, Bonaldo's lab recently generated a zebrafish *col6a1* knockout line. During my PhD work I carried out a thorough characterization of this new zebrafish line.

2. Materials and methods

2.1. Zebrafish husbandry

Maintenance and staging of AB/TU wild-type, *col6a1* null and *Tg(7xTCF-Xla.Siam:GFP)ia4* zebrafish were carried out using established protocols (Kimmel et al., 1995). Fish were raised in a 14 h light cycle at approximately 28.5° C in embryo medium (0.5 mM NaH_2PO_4, 0.5 mM Na_2HPO_4, 1.5 g Instant Ocean in deionized water). From 24 hpf, embryos were treated with phenylthiourea (PTU) to block pigmentation.

2.2. PCR on embryos or fin clip lysates

At 24-72 hpf, single embryo was prepared genomic DNA using the HotSHOT protocol (Meeker et al., 2007). For fin clip lysates, adult fish (from 2 mpf) were anesthetized with 0.5 mg/mL tricaine buffered with sodium bicarbonate and biopsies from the caudal fin removed with a sharp blade. Briefly, 50 µl of 50 mM NaOH were added to single embryo or fin clip biopsies and incubated for 20 minutes at 95 ˚C, followed by cooling to 4 ˚C and addition of 5 µl of 1 M Tris HCl, pH 7.5. Subsequently, the genomic region surrounding the target exon was amplified using the following primers:

primer	Forward	Reverse
WT	TGACCATTTGACAGCCCTAGA	TCAGTCCGACTCATAAATCCG
ins7	AGAACTTCACCGCTGTGAACTA	TGTCCATGTTATGCGTTTCTC

The protocol used for PCR was the following:

Genomic DNA (20-80 ng)	1 µl
25 mM $MgCl_2$	1.5 µl
10x buffer	2.5 µl
10 µM forward primer	1 µl
10 µM reverse primer	1 µl
10 mM dNTPs	0.625 µl
Taq polymerase	0.5 µl
Water	16.875 µl
Total	25 µl

1) 94 ˚C 4 minutes
2) 94 ˚C 30 seconds
3) 56 ˚C 30 seconds
4) 72 ˚C 30 seconds
5) repeat steps 2 to 4 for 30 times
6) 72 ˚C 7 minutes

Specificity of the PCR products was verified by electrophoresis in a 1.5% agarose gel in 0.5 x TBE containing ethidium bromide at a final concentration of 0.5 µg/ml. To discriminate homozygous *col6a1* null fish from the heterozygous siblings, native PAGE (Harwood, 1996) of PCR products was carried out in 5% polyacrylamide gels.

2.3. Quantitative RT-PCR (qRT-PCR)

RNA extraction was performed by adding 1 ml TRIzol Reagent (Life Technologies) directly on anesthetized embryos and following the manufacturer's protocol. RNA was quantified using a Nanodrop ND-1000 instrument (Nanodrop Technologies) and 1 µg total RNA was retrotranscribed using the SuperScript III First-Strand Synthesis System for RT-PCR (Life Technologies), following manufacturer's instructions. Resulting cDNAs were used to perform quantitative real time PCR using Rotor-Gene SYBR Green PCR Kit mastermix (Qiagen) with the RotorGeneQ instrument (Qiagen). Primer sequences are shown below.

primer	Forward	Reverse
qPCRzf*col6a1*	CAAACGCTCTCAACTTCGCC	TGCTCCACGGCTTTCTCAAT
qPCRzf*col6a2*	CTGTGCTTTGTCCGGATCCT	AAGACCAGATCAACAGGCCG
qPCRzf*col6a3*	GGACTTCTGTGCCCCTGATC	TGGTGGGATCTCTTCGGTCT
qPCRzf*col6a4b*	CGGAGAGTGAATCGAGGCTC	AACCTGCATTGCTCGTCTCA
qPCRzf*col6a4a*	CACTTCAAATCGCCGCAACA	TCCTCAGAGCAATGACCCCA
qPCRzf*ef1axb*	CTGGAGGCCAGCTCAAACAT	ATCAAGAAGAGTAGTACCGCTAGCATTAC
qPCRzf*axin1*	GAGAGACAGCCATGGAGAGG	TGCTCATAGTGTCCCTGCACACCAAGCAC
qPCRzf*axin2*	ACCAAGCACAAGCCCCACAGC	ATGCCCACTGCTTCCGCCAC
qPCRzf*tcf4*	AGATGGAGGGCTGTTCAAGA	TGTGTGCTGGAGAAGGTGA
qPCRzf*tcf7*	CTGGCTCTCCAAAGAAATGC	CTTCCATCGGAAGAATGTGG
qPCRzf*myca*	CCAGCAGCAGTGGCAGCGAT	GGGGACTGGGGTACCTCGACTCT
qPCRzf*ccnd1*	AGGCTTTTGAAACGTAAGCCTGCGG	AGGTACACTTGGGCATCCGTGCA

2.4. Western blot analysis

Embryos and larvae were deyolked (except for 7- and 9-dpf larvae) and lysed in Tissue Extraction Reagent I (Invitrogen) and proteases inhibitors (Complete EDTA

free, Roche). Lysates were then processed through mechanical homogenization and protein concentration determined by the BCA Protein Assay kit (Pierce). Adult tissues were dissected following established protocols (Gupta and Mullins, 2010), and lysis was performed in Laemmli sample buffer containing 2 M urea and 50 mM dithiothreitol. SDS-PAGE of protein lysates (40-50 μg) was carried out in 3-8% or 4-12% polyacrylamide Novex NuPAGE Bis-Tris gels (Invitrogen), followed by electrotransfer onto PDVF membrane (Millipore). Membranes were blocked for 1 h in 5% milk in Tris-buffered saline/0.1% Tween 20 (TBST) and incubated overnight at 4° C with antibodies against zebrafish α1(VI) (1:500), LC3 (1:1000; PA1-16930, rabbit, Thermofisher); GAPDH (1:7000; TA802519, mouse, Origene) β-actin (1:1000; A2228, mouse monoclonal, Sigma-Aldrich). Membranes were then washed three times with TBST and incubated for 1 h at room temperature with HRP-conjugated anti-rabbit or antimouse antibodies (1:1000; Amersham Bioscience). Detection was performed by SuperSignal West Pico or Dura Chemiluminescent Substrate with CL-XPosure Film (Thermo Scientific).

2.5. Whole mount immunofluorescence

Embryos were fixed at the appropriate stage in 4% paraformaldehyde in 1x PBS. Immunohistochemical stainings were then performed by the One for All protocol (Inoue and Wittbrodt, 2011). Primary antibodies against zebrafish α1(VI) (1:50; except for Fig. 3g, 1:400; rabbit polyclonal), laminin (1:200; L9393, rabbit polyclonal, Sigma), slow MyHC and fast MyHC (1:50; F59 and F310 respectively, mouse, DSHB), engrailed 2 (1:10; 4D9, mouse, DSHB), synaptic vescicle glycoprotein 2A (1:20; SV2, mouse, DSHB) were used, followed by anti-rabbit Cy3/Cy5 (1:500; Jackson Immunoresearch) or anti-mouse Alexa Fluor 488 (1:500; Abcam) secondary antibodies. Rhodamine-coniugated α-bungarotoxin (αBTX, Invitrogen) was used to stain AChR clusters, diluted 1:200 together with secondary antibodies.

2.6. Methylcellulose incubation

Embryos were raised in 0.6% methyl-cellulose in embryo medium from 48 hpf to 6dpf. Then they were fixed in 4% paraformaldehyde in 1x PBS and used for immunohistochemical stainings.

2.7. Histology

Adult zebrafish and 7-dpf larvae were fixed for 24 h in Bouin's solution, following established protocols (Facchinello et al., 2017). The samples were dehydrated progressively in ethanol and embedded in paraffin. Sagittal sections (7 μm) were made with a microtome (Jung AG Heidelberg). Slices were then deparaffinized, rehydrated and stained with haematoxylin and eosin. Finally, sections were mounted with Eukitt (BioOptica) for microscopic examination.

2.8. Ultrastructural analysis

Wild type and *col6a1* null zebrafish embryos (48 hpf) and adults (16 mpf) were fixed with Karnovsky fixative (2.5% glutaraldehyde and 2% paraformaldehyde in 0.1 M cacodylate buffer) for 3 h at 4°C, washed with 0.1 M cacodilate buffer**,** post-fixed with osmium tetroxide for 2 h and embedded in EPON 812. Ultrathin sections were stained with uranyl acetate and lead citrate and observed with a Philips EM400 transmission microscope at 100 kV.

2.9. Whole-mount in situ hybridization

Whole-mount *in situ* hybridization on wild type or *col6a1* null embryos was performed following established protocols (Thisse and Thisse, 2008). The digoxygenin uridine-5′-triphosphate-labelled RNA probes used were *eng2* (Ekker et al., 1992) and *col2a1* (Yan et al., 1995).

2.10. Assays of motor function and behaviour

Spontaneous coiling was measured at 24 hpf by observing the number of coils in a 15-sec period, as previously described (Telfer et al., 2010).

Behavioural assays to analyse the escape responses to startling stimuli were performed using a DanioVision system running an Ethovision XT 14 software (Noldus, Wageningen, the Netherlands), following established protocols (Prats et al., 2017). To evaluate light-evoked movement, the distance moved by 48-hpf larvae was monitored during a 10-minute interval in the dark, and for additional 10 minutes after switching on the white light (at 100% intensity) located inside the DanioVision chamber. For tapping experiments, the DanioVision Tapping Device DVTD-0010 was exploited. Larvae (6 dpf) were adapted to the dark for at least 10 minutes inside the

DanioVision chamber, and then subjected to the following conditions: a) first tapping stimulus; b) 10 sec of movement monitoring; c) 20 sec interval; d) second tapping stimulus; e) 10 sec of movement monitoring. Distance covered in the 10 sec following each stimulus was measured by DanioVision-associated Ethovision XT 14 software, and statistics were calculated by taking into account, for each analyzed larva, the mean distance covered following the two tapping stimuli.

2.11. Pharmacological treatments

For analysis of the autophagic flux, NH_4Cl was dissolved in embryo medium to a final concentration of 100 mM from 44 to 48 hpf. For salbutamol treatment, embryos were exposed to 20 µM salbutamol (Sigma) dissolved in embryo medium from 7 to 24 hpf for coiling experiments and from 7 to 48 hpf for immunostaining experiments. Immediately before the treatment, chorion envelops were punctured to allow the exposure of embryos to the drug.

2.12. Alcian blue and Alizarin red staining

For Alcian blue experiments, larvae were fixed 2 h at room temperature in 4% paraformaldehyde in 1x PBS, dehydrated progressively in methanol at room temperature and then stored in 100% methanol at –20 °C (for at least 2 hours and up to several months). Larvae were stained overnight with Alcian solution (1% HCl, 70% ethanol, 0.1% Alcian blue) and then briefly cleared in 2% KOH and 3% H_2O_2. , they were dehydrated in ethanol and stored in 85% glycerol.

For Alizarin red experiments, 15-dpf larvae were fixed 2 h at room temperature in 4% paraformaldehyde in 1x PBS and then washed in PBS/0.1% Tween 20 (PBST). Larvae were dehydrated progressively in ethanol (from 50% to 95% EtOH). Subsequently, they were stained with Alizarin red solution (0.25% Alizarin red in 2% KOH) for 3 h, briefly cleared in 2% KOH, and finally stored in KOH/glycerol (20:80).

2.13. Imaging

Alcian blue- and Alizarin red-stained fish were mounted on slides in 80% glycerol in 1x PBS and then analyzed under a Leica DMR compound/Nomarski microscope equipped with a Leica DC500 digital camera. The same instruments were used for the analysis of transgenic fluorescent zebrafish. Whole mount immunofluorescence-labeled fish were mounted in 80% glycerol in 1x PBS between slide and coverslip and

images were acquired with Leica SP5, Nikon C2 or Zeiss LSM 700 confocal microscopes and analyzed with the ImageJ/Fiji software.
For all images, the same exposure parameters were chosen.

2.14. Micro-CT

Each wild-type and *col6a1* null fish was analyzed by an *ex vivo* high-resolution Micro-CT 1172 instrument (Skyscan, Aartselaar, Belgium). The following parameters were applied: 59 kV of voltage, 167 μA of current, 1 mm aluminum filter to reduce beam-hardening artifacts, 17 μm of isotropic voxel size and 1280 × 1024 pixel of field of view. All samples underwent a 180° rotation, with a 0.7 rotation step and a frame averaging of 2. The acquired raw data were reconstructed with the N-Recon Software (Skyscan, Aartselaar, Belgium). The bitmap images obtained after the reconstruction were then converted in Dicom files (Dicom Converter, Skyscan, Aartselaar, Belgium). Three-dimensional (3D) visualization and multiplanar reconstruction (MPR) were performed by CTVox (Skyscan, Aartselaar, Belgium) and Horos (Open Source Software, **https://www.horosproject.org**), respectively.

2.15. Statistics

All results are expressed as mean ± standard error. Statistical analysis of data was performed with Student's t test for unpaired data and a $P<0.05$ was considered as statistically significant (*, $P<0.05$; **, $P<0.01$; ***, $P<0.001$).

3. Results

3.1. Efficacy of targeted CRISPR/Cas9 *col6a1* mutagenesis in ablating COL6 in zebrafish embryos, larvae and adults

The new zebrafish *col6a1* null line produced in Bonaldo's lab was generated by exploiting the CRISPR/Cas9 technology. In this line, *col6a1* exon 5, coding for the N-terminal end of the α1 (VI) chain, has been targeted. As in mammals, *col6a1* encodes one of the essential chains required for COL6 assembly and secretion. Therefore, following the ablation of the α1 chain, COL6 cannot be secreted and deposited in the ECM. The designed sgRNA and cas9 mRNAs were injected into zebrafish zygotes (F0). Once the F0 fish founders were grown to fertile adults, they were outcrossed with wild type-fish, to obtain the F1 offspring. As a result of the CRISPR/Cas9 targeted approach, different *col6a1* mutations were identified in the heterozygous F1 progeny. Among them, a mutation corresponding to the insertion of 7 nucleotides within exon 5 was selected to generate the stable null line, as this insertion is predicted to generate a frameshift leading to a premature stop codon, thus preventing the translation of α1(VI) chain (Fig. 1A, B).

As a first step, I validated the presence of the null mutation and the effective ablation of COL6 in this new zebrafish line. RT-qPCR revealed a markedly lower amount of the *col6a1* transcripts in 48-hpf null zebrafish compared to wild-type ones (Fig. 1C). Western blot analysis with a novel antibody specific for zebrafish α1(VI) chain demonstrated that the protein was absent in zebrafish null embryos, larvae and adults (Fig. 1D, E). These results confirmed that the CRIPSR/Cas9 approach allowed to generate a *col6a1* null zebrafish line, which can be used for further functional studies.

3.2. Macroscopic phenotypic characterization of col6a1 null embryos.

First of all, I examined *col6a1* null embryos for gross morphological alterations, using live light microscopy. As shown in Figure 2, null embryos did not display overt morphological alterations in the first days of

development. However, at 24 hpf they had a significant reduction in length, which also persisted at 48 hpf and 6 dpf (Fig. 2A-F). Interestingly, this decrease in length was previously observed also in zebrafish embryos in which *col6a1* expression was transiently downregulated (Telfer et al., 2010).

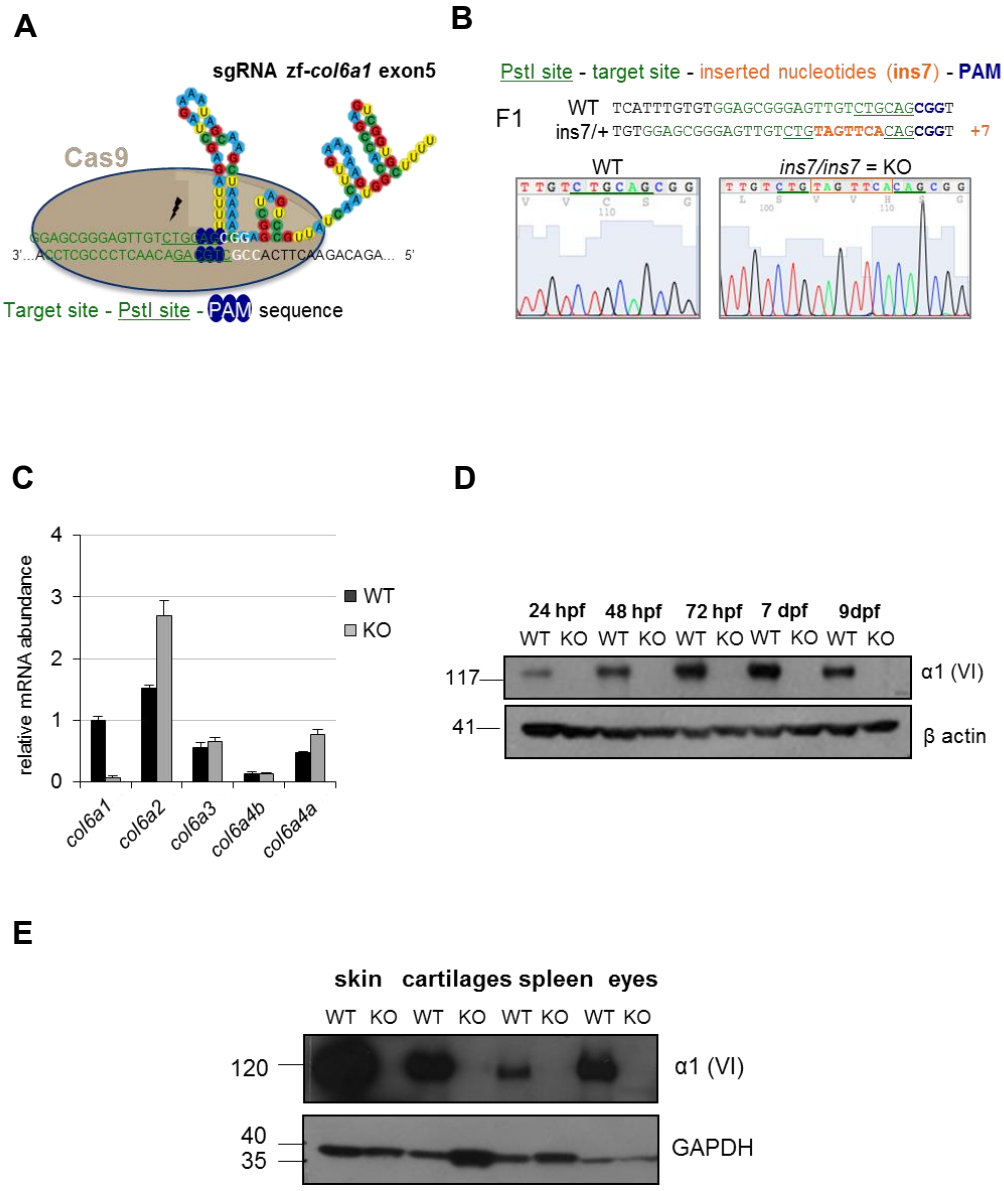

Figure 1. Generation of a stable *col6a1* null line with CRISPR/Cas9. **(A)** Scheme of the sgRNA on the target locus. **(B)** Nucleotide sequence and alignment of the mutation targeted by the CRISPR-Cas9. Each inserted nucleotides is represented in orange. The number of inserted bases is reported on the right-hand side of the alignment. **(C)** Relative abundance of COL6 transcripts in wild-type and *col6a1* null zebrafish embryos and larvae as determined by qRT-PCR. **(D)** Western blot of protein extracts from wild-type and *col6a1* null embryos (24

hpf, 48 hpf) and larvae (72 hpf, 7dpf, 9 dpf), confirming the absence of COL6. **(E)** Western blot of protein extracts from wild-type and null adult tissues (8-12 mpf), showing the complete ablation of COL6. KO, *col6a1* null; WT, wild-type.

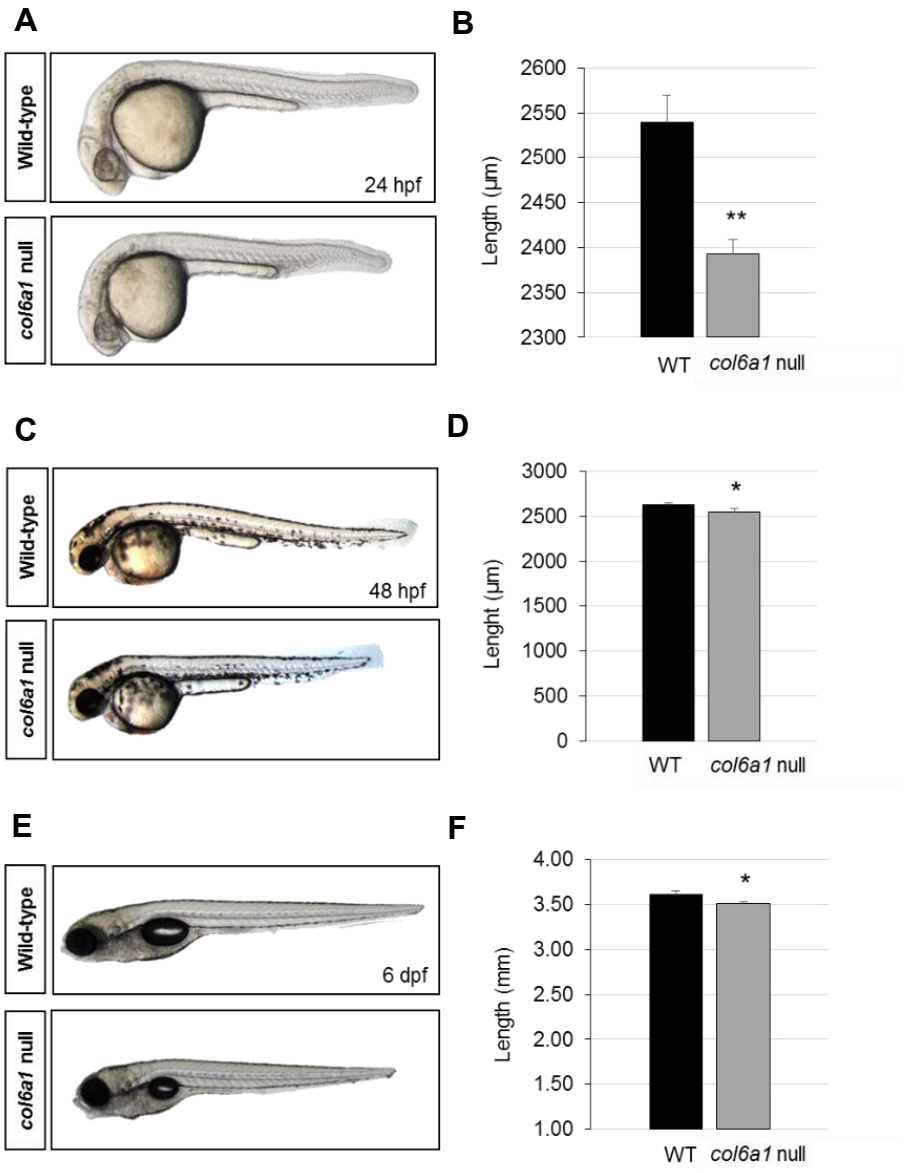

Figure 2. COL6 ablation does not overtly affect embryo morphology, except for body length. Representative images of 24-hpf **(A)**, 48-hpf **(C)** and 6-dpf **(E)** wild-type and *col6a1* null fish. The histograms on the right **(B, D, F)** report quantification of body length, showing a significant reduction in total length of embryos at 24 hpf, 48 hpf and 6 dpf (24 hpf, n = 16 per genotype, 48 hpf, n = 9 per genotype, 6 dpf, n = 19 per genotype). The graph reports mean ± SEM. Statistical significance was determined by Student's t-test (*, p <0.05; **, p <0.01). WT, wild-type.

3.3. Muscle development is affected in *col6a1* null fish

3.3.1. COL6 ablation affects myofibers and myosepta during development

COL6 is critical for the proper structure and function of skeletal muscles both in humans and in mice. Thus, I started investigating the muscular phenotype of the *col6a1* null zebrafish line by evaluating myofiber integrity. First, I analysed muscle fibers by immunostaining in 48-hpf embryos. Using F59 antibody, which labels slow myosin heavy chain, I found that although slow muscle fibers were still present in *col6a1* null embryos, they were highly disorganized, with several wavy myofibrils. Moreover, some myofibers were missing or detached from the myosepta. These defects primarily occurred in the slow muscle layer at the periphery of the myotome, which are the first myofibers in the embryo that differentiate and function (Fig. 3A). In addition to slow muscle fibers, I also analysed the patterning and the morphology of fast fibers by exploiting F310 antibody, which labels fast myosin isoforms. At difference from slow muscle fibers, the deeper fast muscle fibers appeared less affected in 48-hpf *col6a1* null embryos when compared to wild-type ones (Fig. 3B). To further evaluate the myosepta defects, I performed whole-mount double immunofluorescence with an antibody against laminin, a major basement membrane component, in order to examine whether laminin distribution was affected by COL6 depletion. Interestingly, laminin was still present in *col6a1* null myosepta, but the staining revealed that some myosepta had a U-shaped rather than the V or 'chevron' shape of the wild-type fish (Fig. 3B, arrow). This is a condition commonly found in zebrafish mutants lacking ECM components and receptors involved in muscle development, such as integrin β1 (Wood et al., 2018) and collagen XXII (Charvet et al., 2013).

Next, I evaluated whether the alterations of slow muscle fiber patterning was worsened by motor activity. Towards this aim, I stimulated larvae to swim through raising media to which an inert cellulose polymer, methyl-cellulose, was added to increase the viscosity (Hall et al., 2007). Raising embryos in 0.6% methyl-cellulose from 48 hpf to 6 dpf led to increased severity of the phenotype, with *col6a1* null fish displaying many detached fibers (Fig. 3C). These results are in full agreement with from 48 hpf to 6 dpf led to increased These results are in full agreement with what was reported for *Col6a1* null mice, where physical training exacerbated the myopathic phenotype (Grumati et al., 2011).

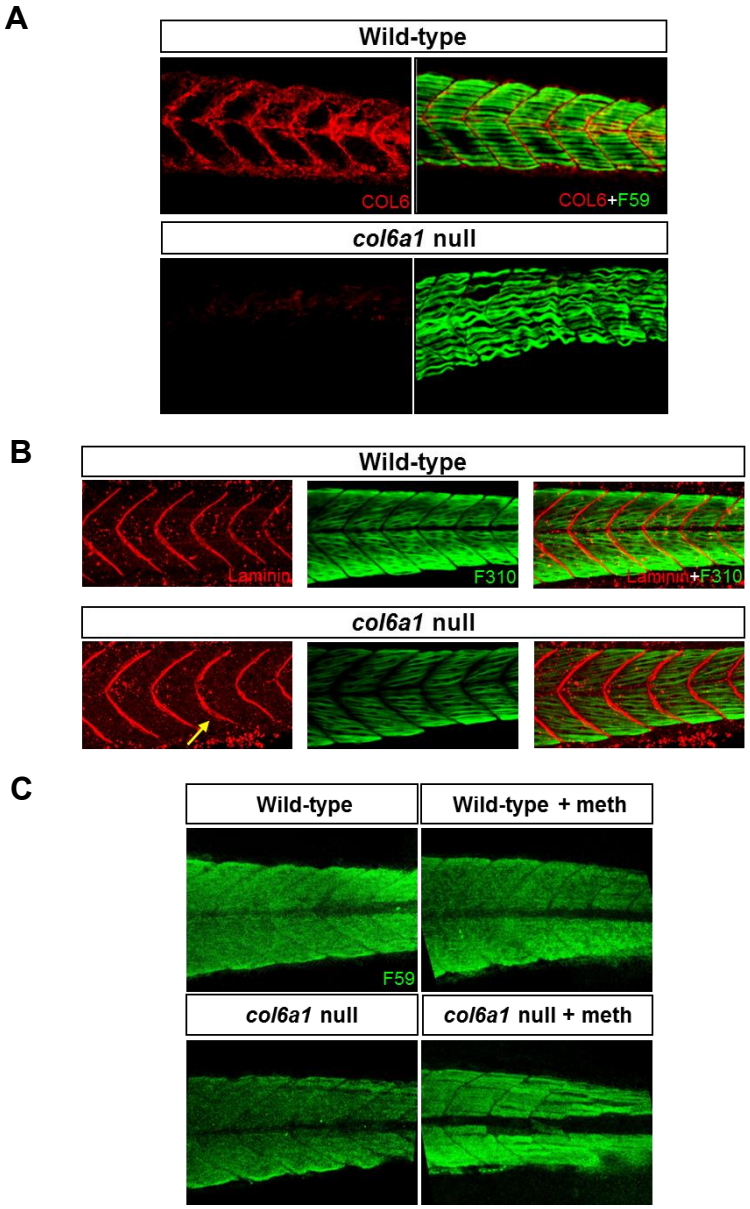

Figure 3. Slow muscle fibers and myosepta are affected in *col6a1* null embryos. (**A**) Wild-type and *col6a1* null embryos were stained with antibodies against COL6 (red) and slow myosin heavy chain (F59, green) at 48 hpf. In *col6a1* null embryos, myofibrils are not properly organized and display a wavy morphology with several gaps in myofiber arrangement. (**B**) 48-hpf wild-type and *col6a1* null embryos were stained with antibodies against anti-fast myosin light chain (F310, green) and laminin (red) antibodies. Fast muscle do not appear to be overtly affected in *col6a1* null embryos. Laminin staining shows the presence of some U-shaped myosepta in *col6a1* null fish (arrow). **(C)** Immunofluorescence for slow myosin heavy chain (F59, green) of wild-type and *col6a1* null embryos raised from 48 hpf to 6 dpf in the absence or presence of 0.6% methyl-cellulose (meth). The incubation in a highly viscous medium increased the severity of phenotype, with *col6a1* null embryos displaying many detached fibers.

To evaluate whether the organization of slow muscle fibers was still affected in adult *col6a1* null zebrafish, I performed hematoxylin-eosin staining of sections from 3-mpf animals (Fig. 4A, B). The layer of slow muscle fibers appeared thinner and disorganized in *col6a1* null adults compared to wild-type, suggesting a reduced amount of this muscle cell type.

Ultrastructural characterization of skeletal muscles from 16-mpf fish revealed a significantly increased length of sarcolemmal foldings at the level of myotendinous junctions (MTJ) in *col6a1* null animals (Fig. 4C, D). MTJ are specialized structures located at the muscle-tendon interface, which represent the primary site of force transmission (Charvet et al., 2012). MTJs are considered a mechanically critical feature in the muscle-tendon unit, as they help reducing membrane stress during muscle contraction (Tidball, 1991). Thus, the increased length of foldings at the level of MTJs in *col6a1* null animals may represent a compensatory mechanism through which fish sustain muscle contraction.

3.3.2. COL6 ablation affects the migration and differentiation of muscle precursor cells, leading to motor abnormalities

With the aim of investigating when slow muscle fibers start to be affected in *col6a1* null fish, I analysed the differentiation of this cell type by evaluating the patterning of a subpopulation of muscle pioneer cells, the so-called adaxial cells. Importantly, these cells are required for the specification of slow muscle cells (Devoto et al., 1996; Honjo and Eisen, 2005; Jackson and Ingham, 2013). Thus, I performed *in situ* hybridization and immunofluorescence analysis at 24 hpf to analyse the distribution of engrailed-2, a specific marker expressed only by adaxial cells. The amount of both *eng2* transcript (Fig. 5A) and engrailed-2 protein (Fig. 5B) was decreased in *col6a1* null embryos. These results indicated that a deficit in the adaxial cells, or in the signalling that regulates adaxial cells migration and differentiation, may be a primary trigger for the onset of the myopathic phenotype displayed by *col6a1* knockout embryos.

To evaluate whether the alterations in slow muscle fibers could lead to motor abnormalities, I measured the number of coiling events performed by wild-type and *col6a1* null embryos at 24 hpf. The choice of this assay relies on the fact that coiling events are spontaneous, alternating contractions of the trunk specifically mediated by slow muscle fibers (Naganawa and Hirata, 2011). Interestingly, the average

number of spontaneous coiling events was significantly lower in *col6a1* null embryos when compared to wild-type one (Fig. 5D), thus revealing that the impairment of slow muscle fibers also affected also embryo motility.

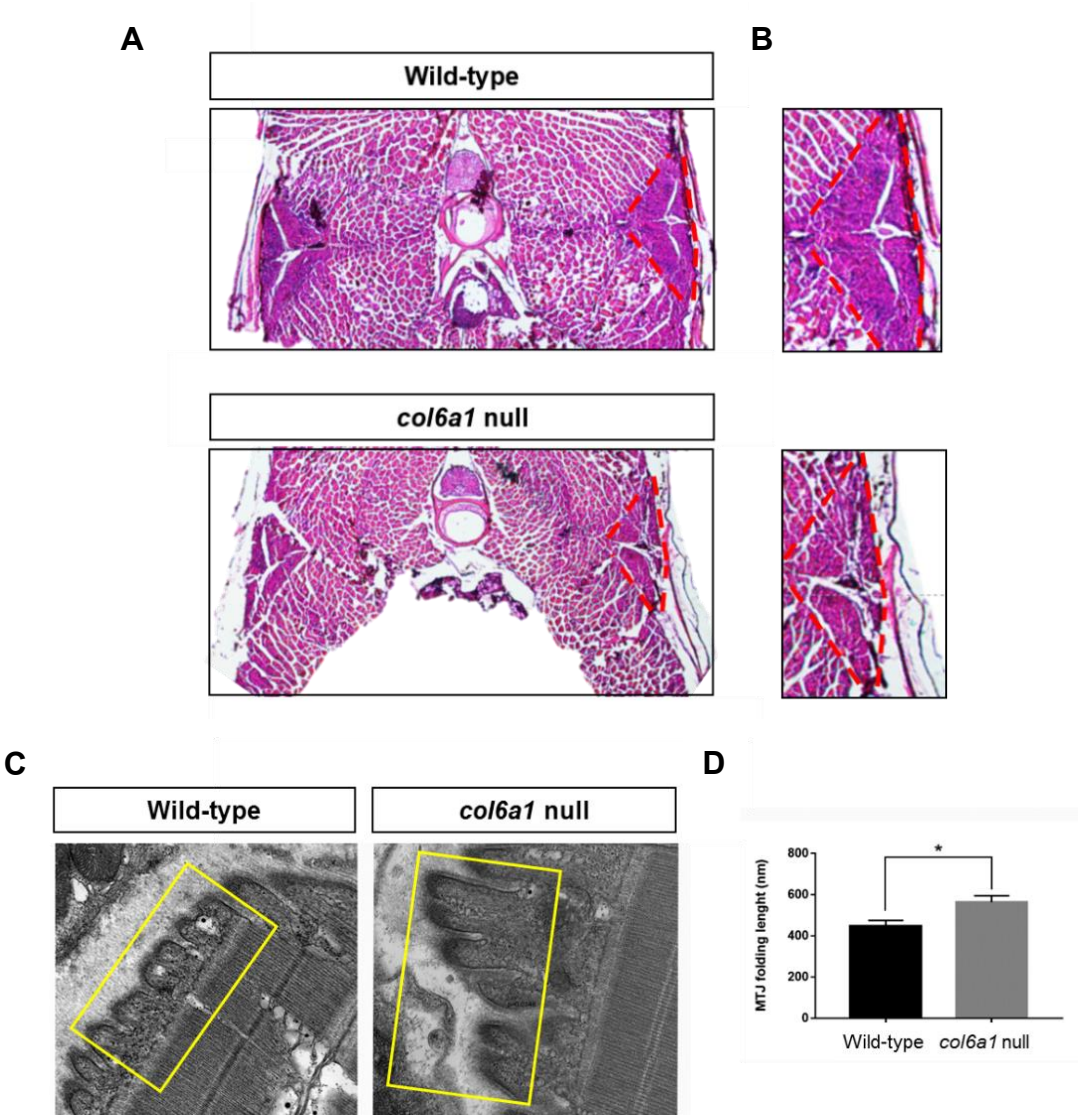

Figure 4. Myofibers and MTJ are affected in adult *col6a1* null fish. (A). Hematoxylin-eosin staining performed on sections of 3-mpf wild-type and *col6a1* null zebrafish. The layer of slow muscle fibers appears thinner in *col6a1* null fish when compared to wild-type animal, as shown in the red dotted area. A magnification of this area is shown in (**B**). **(C)** Ultrastructural analysis by transmission electron microscopy of skeletal muscles of 16-mpf wild-type and *col6a1* null fish at the level of MTJ. The length of sarcolemmal foldings (yellow squares) is significantly higher in *col6a1* null MTJs when compared to wild-type MTJs, as revealed by the quantification in (**D**) (*, $p < 0.05$; $n = 3$).

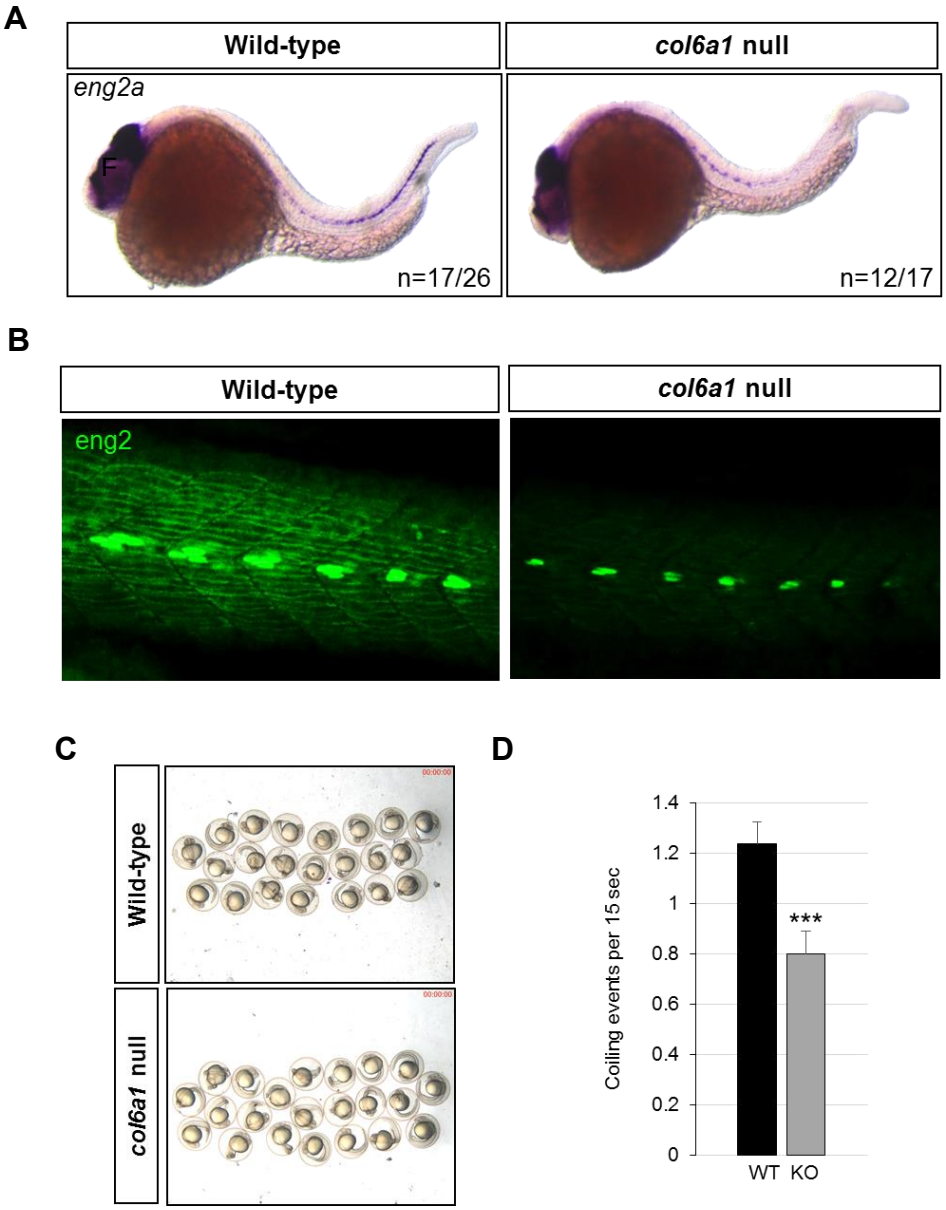

Figure 5. *col6a1* null embryos displayed a reduced amount of adaxial cells (A,B) and a decreased incidence of coiling events (C,D). (A) *In situ* hybridization for *eng2* in 24-hpf wild-type and *col6a1* null embryos. A decreased positivity for *eng2* is evident in *col6a1* null fish. **(B)** Representative immunofluorescence images of 24-hpf embryos stained with an antibody against engrailed-2 (green). *col6a1* null fish display a markedly reduced staining for engrailed-2. **(C)** Representative images of pools of 24-hpf wild-type and *col6a1* null embryos recorded for coiling events. **(D)** Quantification of the number of coilings in 15 sec, showing a significantly lower number of coiling events in *col6a1* null embryos (KO) when compared to wild-type embryos (WT) (***, p <0.001; wild-type, n = 194, *col6a1* null, n = 149). The graph reports mean ± SEM. Statistical significance was determined by Student's t-test.

3.4. Neuromuscular development is affected in *col6a1* null embryos

3.4.1. COL6 ablation leads to motor neuron defects and abnormal AChR patterning

The locomotor system is composed of both muscle fibers and neuronal cells (Umeda and Shoji, 2017). Myofibers and motor neurons develop in tight contact, and once functional neuromuscular contacts form, motor neurons have the capability to regulate muscle differentiation (Brennan et al., 2005). Therefore, having found that COL6 deficiency causes an impairment in skeletal muscle development and knowing that adaxial cells are also involved in driving motor neuron axons to their muscular targets, I investigated motor neuron development in *col6a1* null fish.

First, I performed immunofluorescence studies in 48-hpf embryos by exploiting an antibody against vesicle protein SV2, which labels the presynaptic terminals. Defects in axonal elongation were evident in *col6a1* null embryos, as they frequently displayed axons which failed to migrate correctly into the myotome (Fig. 6A). I then classified these defects, considering the extent of growth with respect to the horizontal myoseptum (Ramanoudjame et al., 2015). Altogether, 44% of *col6a1* null embryos displayed growth arrest of motor neuron axons before the horizontal myoseptum, whereas only 25% of wild-type embryos showed truncated axons (Fig. 6B). These data revealed that the migration of motor neuron axons toward the myotome is affected in *col6a1* null embryos.
Next, I analysed the NMJ compartment in 48-hpf wild-type and *col6a1* null embryos using α-bungarotoxin staining, which labels post-synaptic acetylcholine receptor (AChR) clusters. Together with the motor neuron outgrowth defects, AChRs clusters also appeared disorganized in *col6a1* null fish embryos (Fig. 6C), similarly to what displayed by *Col6a1* null mice and UCMD patients (Cescon et al., 2018).

3.4.2. *col6a1* null embryos display altered escape responses

Since it is known that fish mutants with neuromuscular defects display altered escape responses (Ono et al., 2002; Prats et al., 2017; McMacken et al., 2018), I measured the behavioural responses to startling stimuli. These responses are unconditioned behaviours consisting of rapid and massive acceleration resulting from the contraction of the axial muscles in response to visual, touch or acoustic stimuli (Tegelenbosch et al., 2012).

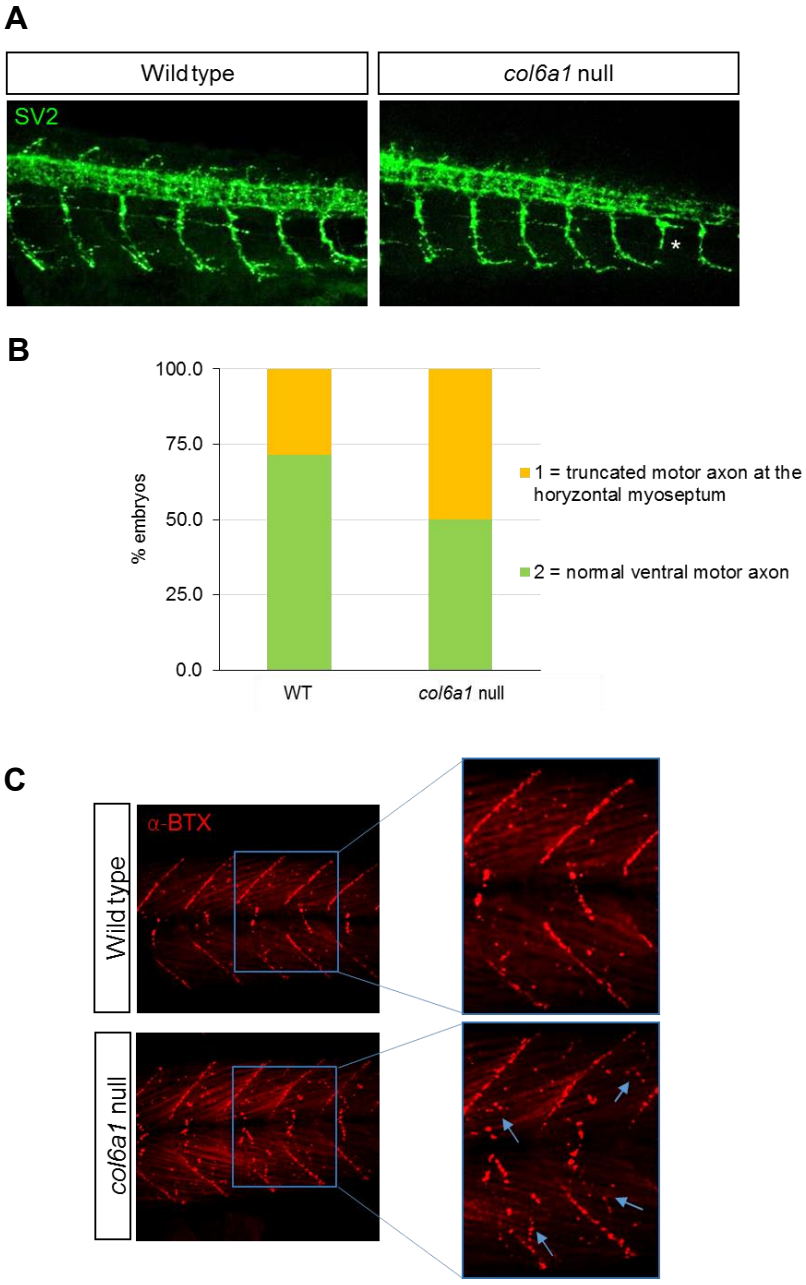

Figure 6. Neuromuscular development is affected in *col6a1* null embryos. (A) Lateral views of 48-hpf wild-type and col6a1 null embryos immunostained with anti-SV2 antibody, marking the presynaptic compartment. In col6a1 null embryos, some axons (asterisk) do not grow beyond the hemisegment (dotted blue line). (B) Graph of phenotypic classes of motor axons defects, based on the extent of axon growth. Motor axons were scored as follows: (1) truncated motor axon at the horizontal myoseptum; (2) normal ventral motor axon. Overall, 44% of col6a1 null embryos displayed truncated motor axons (wild-type, n = 16; col6a1 null, n = 18). (D) Lateral views of 48-hpf wild-type and col6a1 null embryos stained with α-bungarotoxin (α-BTX), to label AChR receptors. Arrows point at disorganized AChR clusters in col6a1 null embryos. KO, col6a1 null; WT, wild-type.

By exploiting the Noldus DanioVision instrument, I adopted an established protocol, in which 48-hpf embryos were monitored in a light/dark cycle within a time frame of 40 min, divided as follows: *i)* 10 min dark; *ii)* 20 min light; and *iii)* 10 min dark (Fig. 7A). To evaluate light-evoked movement, I measured the distance covered by the embryos during the first 10 min in the dark, and for the additional 10 min after switching on the light located inside the DanioVision chamber (Prats et al., 2017). Interestingly, *col6a1* null embryos showed a significantly reduced response to a light stimulus in comparison to wild-type siblings (Fig. 7B). Moreover, I also analysed the motor response evoked by a vibrational/acoustic stimulus (commonly referred to as "tapping stimulus") in 6-dpf larvae (Prats et al., 2017). For tapping experiments, I established a protocol in which 6-dpf larvae were adapted to the dark for at least 10 min inside the DanioVision chamber, and then subjected to the following conditions: *a)* first tapping stimulus; *b)* 10 sec of movement monitoring; *c)* 20 sec interval; *d)* second tapping stimulus; *e)* 10 sec of movement monitoring. The distance covered during the ten seconds following each stimulus was measured by DanioVision-associated Ethovision XT 14 software, and statistics were calculated by considering, for each analyzed larva, the mean distance covered following the two tapping stimuli. Interestingly, the data obtained by these experiments showed a clear tendency of *col6a1* null mutants to a reduced response when compared with wild-type larvae (Fig. 7C). Overall, these data revealed that *col6a1* null fish display altered escape responses, a condition commonly found in zebrafish models with neuromuscular alterations.

3.5. Salbutamol treatment of *col6a1* null embryos improves motility and alleviates axon pathfinding defects

Since NMJs are remarkably affected by COL6 deficiency (Cescon et al., 2018), it is reasonable to assume that the recovery of NMJ defects may improve muscle health. In a recent study, it was demonstrated that the β-adrenergic agonist salbutamol is able to counteract myasthenic syndromes, inherited neuromuscular conditions caused by alterations at the NMJ (McMacken et al., 2018). In the same study, the authors used zebrafish morphants with deficiency of two key postsynaptic proteins, Dok-7 and MuSK, and showed that salbutamol led to an improvement in AChR clustering, motor

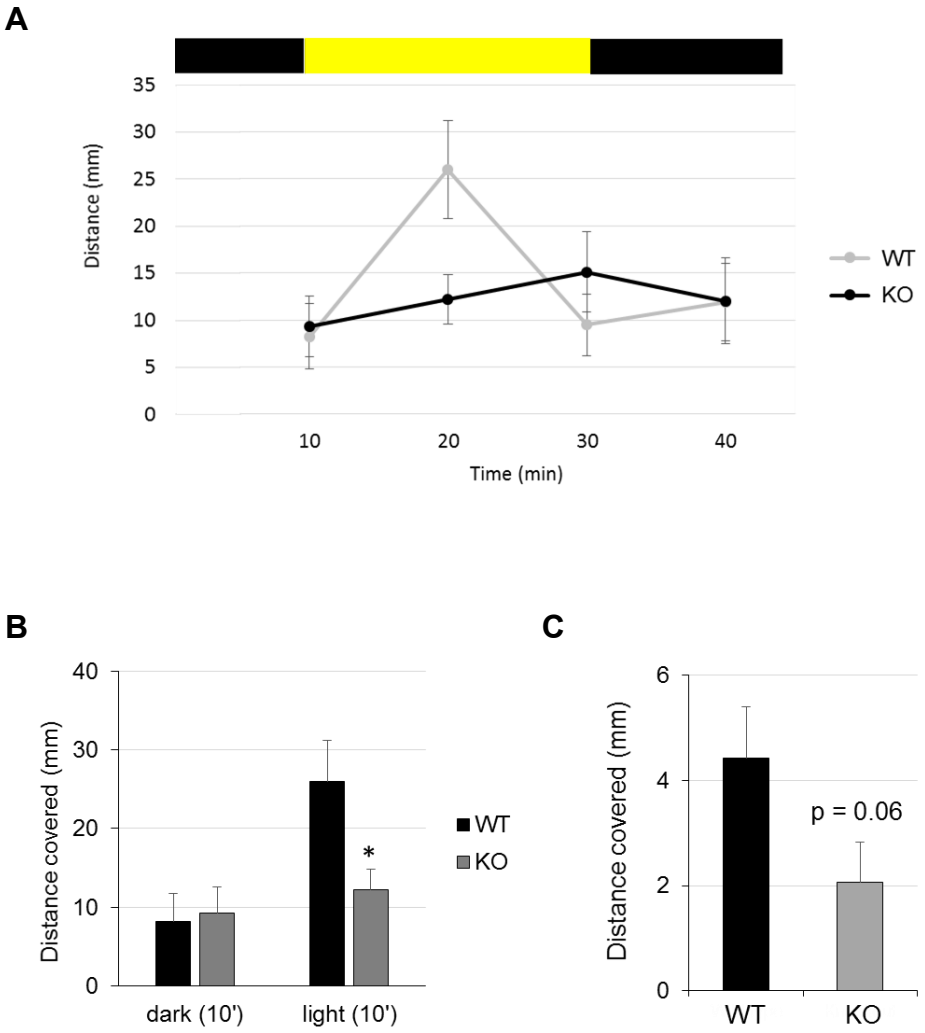

Figure 7. *col6a1* null embryos display impaired escape responses. (A) Distance covered by 48-hpf wild-type and *col6a1* null embryos during a dark-light cycle (10 min in the dark; 10 and 20 min in the light; 10 min in the dark). **(B)** Quantification of the distance covered during the first 10 min in the dark and the additional 10 min after switching on the light. *col6a1* null embryos display a significantly reduced distance covered in response to light stimulus (*, p <0.05; n = 16-24). The graph reports mean ± SEM. Statistical significance was determined by Student's t-test. **(C)** Quantification of the distance covered in the 10 sec following tapping stimulus at 6-dpf, showing a strong trend toward reduced distance covered by *col6a1* null larvae in response to tapping (p = 0.06; n = 18). The graph reports mean ± SEM. Statistical significance was determined by Student's t-test. KO, *col6a1* null; WT, wild-type.

axon guidance and swimming behaviours of morphant embryos (McMacken et al., 2018). Based on these concepts, I investigated whether salbutamol treatment could rescue some of the defects displayed by *col6a1* null fish. In particular, I analysed the number of coiling events of wild-type and *col6a1* null embryos after 20 µM salbutamol

exposure from 7 to 24 hpf. Spontaneous coiling events at 24 hpf were measured by observing each embryo for 15 sec and counting the total number of movements. Interestingly, salbutamol treatment was able to ameliorate the motility defects, leading to a significant increase of coiling frequency in treated *col6a1* null embryos when compared to untreated ones (Fig. 8A). Moreover, I performed immunofluorescence analysis of 48-hpf embryos treated with 20 µM salbutamol from 7 to 48 hpf. In particular, I analysed axon pathfinding by exploiting the anti-SV2 antibody. Overall, only 22% of salbutamol-treated *col6a1* null embryos displayed growth arrest of motor neuron axons before the horizontal myoseptum (Fig. 8B). Therefore, targeting the NMJ compartment by salbutamol treatment is able to elicit beneficial effects in *col6a1* null fish.

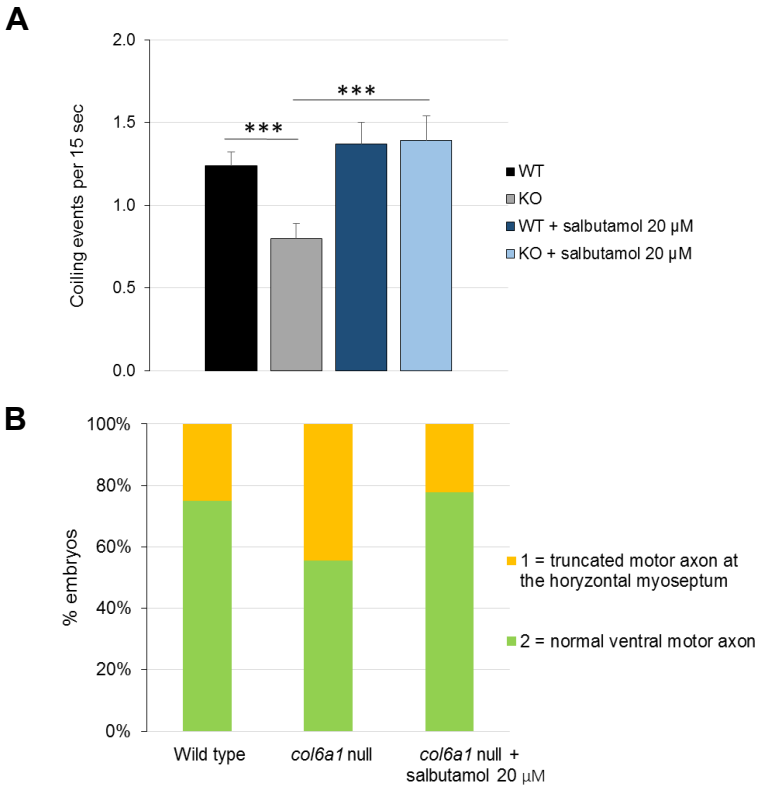

Figure 8. Salbutamol treatment improves motility and ameliorates axon pathfinding defects in *col6a1* null zebrafish. **(A)** Quantification of the number of coiling events in wild-type and *col6a1* null embryos in the absence or presence of 20 mm salbutamol. Following salbutamol treatment, *col6a1* null embryos tail twists show an increased frequency compared with untreated ones (***, p <0.001; wild-type, n = 194; *col6a1* null, n = 149; treated wild-type n = 133; treated *col6a1* null n = 94). The graph reports mean ± SEM. Statistical significance was determined by Student's t-test. **(B)** Graph of phenotypic repartition of motor axons defects considering the extent of growth. Motor axons were scored as follows: (1) truncated

motor axon at the horizontal myoseptum; (2) normal ventral motor axon. After salbutamol treatment, up to 78% of *col6a1* null embryos display normal ventral motor axons (wild-type, *n* = 16; *col6a1* null, *n* = 18; treated *col6a1* null *n* = 9). KO, *col6a1* null; WT, wild-type.

3.6. *col6a1* null zebrafish display autophagy and organelle defects

Previous studies demonstrated that COL6-deficient myofibers undergo spontaneous apoptosis with defective regulation of the autophagic machinery, leading to an accumulation of dysfunctional mitochondria and altered organelles (Irwin et al., 2003; Grumati et al., 2010). Based on these findings, I decided to investigate these cellular features in *col6a1* null fish. One of the 'gold standard' approaches currently used to evaluate the autophagic flux is based on the quantification of microtubule-associated protein light chain 3 (LC3) lipidation. The lipidated form of LC3 (LC3-II) is bound to the autophagosome membrane, where it remains until the fusion with the lysosome and, for this reason, it is an excellent marker of autophagy. Lysosomotropic reagents such as ammonium chloride, chloroquine, or bafilomycin A_1, which neutralize the lysosomal pH, block the degradation of LC3-II, resulting in the accumulation of LC3-II (Rubinsztein et al., 2009; Mizushima et al., 2010; Klionsky et al., 2016; Fodor et al., 2017; Mathai et al., 2017). Accordingly, the differences in the amount of LC3-II between samples in the presence and absence of lysosomal inhibitors represent the amount of LC3 that is delivered to lysosomes for degradation (i.e., autophagic flux) (Rubinsztein et al., 2009; Mizushima et al., 2010; Klionsky et al., 2016). Thus, I performed western blot experiments to monitor LC3-II levels in 48-hpf wild-type and *col6a1* null embryos, both in basal conditions and after treatment with 100 mM NH_4Cl (Mathai et al., 2017). Interestingly, I detected a higher level of LC3-II in untreated *col6a1* null embryos when compared with untreated wild-type embryos, and this level did not increase after exposure to NH_4Cl. Conversely, NH_4Cl treatment led to a higher amount of LC3-II in wild-type embryos, as expected (Fig. 9A). These results strongly suggest an impairment of the autophagic flux in *co6a1* null embryos. To assess for the possible presence of organelle defects, I analysed the ultrastructure of muscle fibers in wild-type and *col6a1* null embryos at 48 hpf. Notably, these experiments revealed the presence of swollen mitochondria in muscle fibers and an increased ECM deposition at the level of myosepta in *col6a1* null embryos when compared to wild-type ones (Fig. 9B). I also analysed the ultrastructure of muscle fibers in adult fish at 16 mpf. Interestingly, altered mitochondria were still present in

adult *col6a1* null fish (Fig. 9C, asterisks). The presence of mitochondrial ultrastructural defects is quite interesting, since similar alterations were also observed in muscle cells of BM and UCMD patients (Tagliavini et al., 2013), as well as in *Col6a1* knockout mice (Irwin et al., 2003). Of note, I also detected the accumulation of some autophagic vacuoles (Fig. 9C, arrow), in close apposition to defective mitochondria, thus reinforcing the hypothesis of a block in the terminal steps of autophagy in muscle fibers of COL6 null fish.

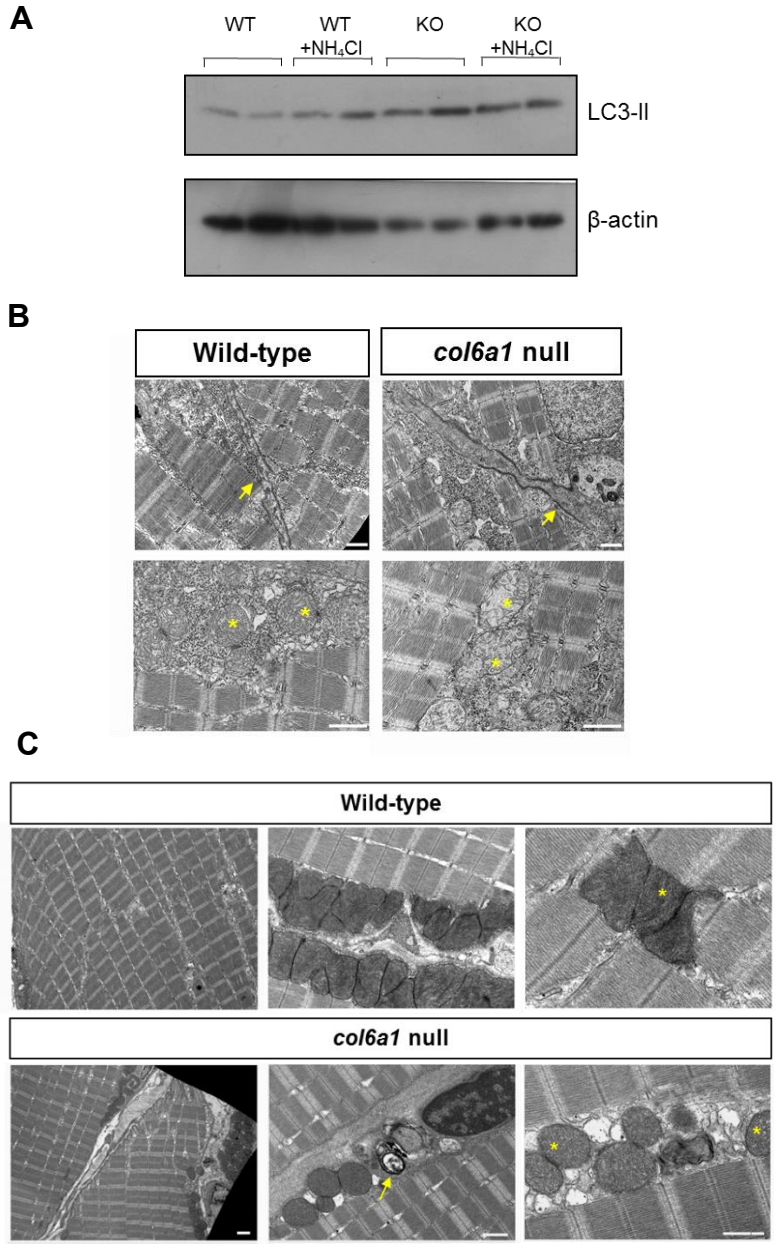

Figure 9. Ultrastructural defects in muscles of col6a1 null zebrafish. (A) Western blot of protein extracts from 48-hpf wild-type and col6a1 null embryos. To assess the autophagic flux,

fish were maintained for 4 hr (from 44 to 48 hpf) in embryo medium in the absence or presence of 100 mM NH_4Cl. The treatment leads to the accumulation of LC3-II in wild-type embryos, but not in col6a1 null embryos, where a higher level of LC3-II is already present in untreated condition. β-actin was used as a loading control. (B) Transmission electron microscopy analysis of 48-hpf embryos, showing swollen mitochondria (asterisks) in muscle fibers and an increased deposition of ECM at the level of myosepta (arrows) in col6a1 null embryos. (C) Transmission electron microscopy analysis of 16-mpf adult fish, showing altered mitochondria in col6a1 null muscle fibers (asterisks). Autophagic vacuoles are present near defective mitochondria (arrow). Scale bar 1 μm. KO, col6a1 null; WT, wild-type.

3.7. COL6 ablation interferes with Wnt signaling

Among the different ECM component, COL6 displays a remarkable and distinctive role in regulating key cell processes in different tissues, and in particular skeletal muscle, including differentiation, apoptosis and autophagy. However, signaling pathways affected by COL6 deficiency remains largely unknown. As mentioned above, zebrafish is an ideal tool for the *in vivo* analysis of signaling pathways, thanks to the availability of transgenic fish expressing fluorescent proteins under the control of responsive cis-elements for a number of different signaling pathways.

To start evaluating which signaling pathways are affected by COL6 ablation, I crossed *col6a1* null fish with *Tg(7xtcf-Xla.siam:EGFP)ia4*, a reporter fish line for the Wnt signaling pathway in which TCF responsive elements are linked to the enhanced green fluorescent protein (eGFP) (Moro et al., 2012). The wild-type adult offspring were then outcrossed with wild-type fish (i.e., not in reporter background), and the same procedure was adopted with *col6a1* null fish, and embryos obtained by these crossings were isolated and analysed by live microscopy. Interestingly, I consistently detected an increased Wnt reporter activity in the caudal region of 24-hpf *col6a1* null trunks, when compared to the corresponding wild-type samples (Fig. 10A). In spite of this, RT-qPCR for genes involved in Wnt signal transduction (*axin1*, *axin2*, *tcf4*, *tcf7*) performed on 24-hpf trunks did not reveal significant differences in the mRNA levels between wild type and *col6a1* null embryos, although the increase in the amount of *tcf7* transcripts was near significance ($p = 0.1$). Of note, also the levels of *ccnd1*, coding for cyclin D1, a transcriptional target downstream the Wnt pathway, were not affected by COL6 ablation (Fig. 10B). The reason for the discrepancy between these two sets of results may be explained by a highly regionalized change of Wnt activity, which can be easily detected by live imaging but is lost when performing RT-qPCR on whole trunks. On the other hand, RT-qPCR performed on 24-hpf heads revealed that

tcf4 and *tcf7* mRNA levels were significant upregulated ($p < 0.5$ and $p < 0.01$, respectively) in *col6a1* null embryos, suggesting that in this body region the absence of COL6 may lead to a stronger upregulation of Wnt signaling (Fig. 10D), as revealed also by live imaging (Fig. 10C).

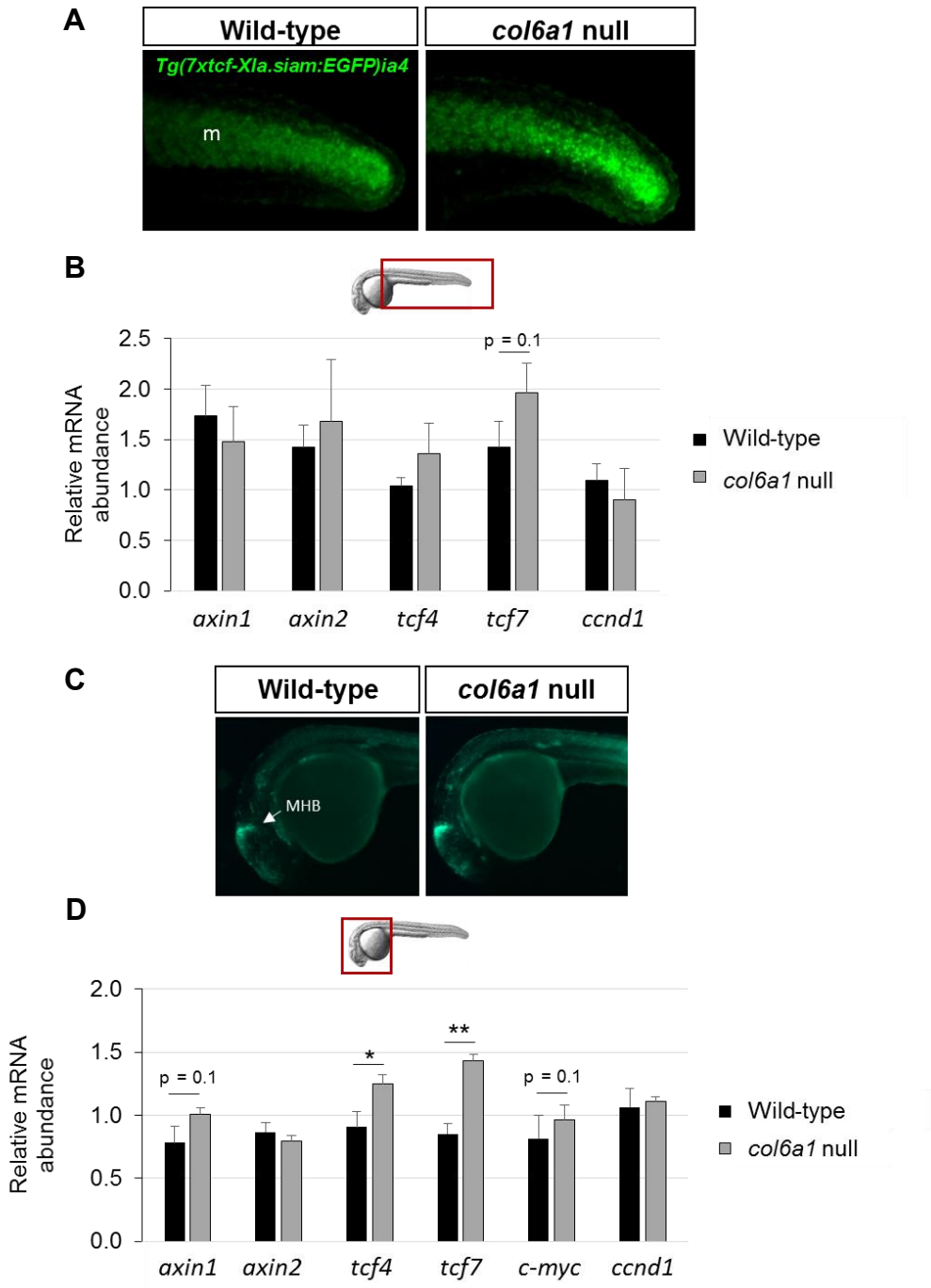

Figure 10. COL6 ablation leads to upregulation of Wnt signaling. (A) Representative images of 24-hpf Tg(7xtcf-Xla.siam:EGFP)ia4 wild-type and col6a1 null trunks. In col6a1 null embryos, increased Wnt reporter activity is observed in the caudal part of the myotome. m,

myotome. (B) qRT-PCR showing the amount of axin1, axin2, tcf4, tcf7 and ccnd1 transcripts in wild-type and col6a1 null trunks at 24 hpf. The upper part of the panel shows a 24-hpf embryo, where the region dissected to perform the qRT-PCR is delimited by a red square. No significant differences are observed between the two genotypes, even if there is a tendency to increased tcf7 levels in null trunks. The graph reports mean ± SEM. Statistical significance was determined by Student's t-test. (C) Representative images of 24-hpf Tg(7xtcf-Xla.siam:EGFP)ia4 wild-type and col6a1 null heads. In col6a1 null embryos, increased Wnt reporter activity is observed in the midbrain-hindbrain boundary (MHB). (D) qRT-PCR showing the expression of axin1, axin2, tcf4, tcf7, c-myc and ccnd1 transcripts in wild-type and col6a1 null heads at 24 hpf. The upper part of the panel shows a 24-hpf embryo, where the region dissected to perform the qRT-PCR is delimited by a red square. Null embryos display a significant increase in the level of tcf4 and tcf7 mRNAs compared to wild-type ones. The graph reports mean ± SEM. Statistical significance was determined by Student's t-test (*, $p < 0.05$; **, $p < 0.01$).

Interestingly, this increased Wnt reporter activity was still present in 48-hpf null heads, as revealed by live imaging on reporter fish (Fig. 11A). In addition, a significant increase of *tcf7* transcript levels in this region was detected by RT-qPCR on 48-hpf wild type and *col6a1* null fish (Fig. 10B). Interestingly, no major differences in the reporter activity were found in 48-hpf trunks, even if Wnt targets appeared slightly upregulated at the transcriptional level (Fig. 10C, D). Altogether, these results indicate that in the absence of COL6, the Wnt signaling pathway is upregulated during development at 24-hpf and 48-hpf, particularly in the head region. Of note, in the head region Wnt reporter expression of *Tg(7xtcf-Xla.siam:EGFP)ia4* fish was shown to be associated to hypothalamus, tectum, midbrain-hindbrain boundary and fronto-nasal ectoderm (Moro et al., 2012).

3.8. The three-dimensional architecture of craniofacial cartilages is affected in col6a1 null larvae and adults

As reported above, COL6 is also critical for the proper structure and function of cartilage and bone, since it has been demonstrated that *Col6a1* null mice display an accelerated development of osteoarthritic joint degeneration, as well as a delayed secondary ossification process and reduced bone mineral (Alexopoulos et al., 2009). On the basis of these findings, I also characterized also skeletal development of *col6a1* null fish.

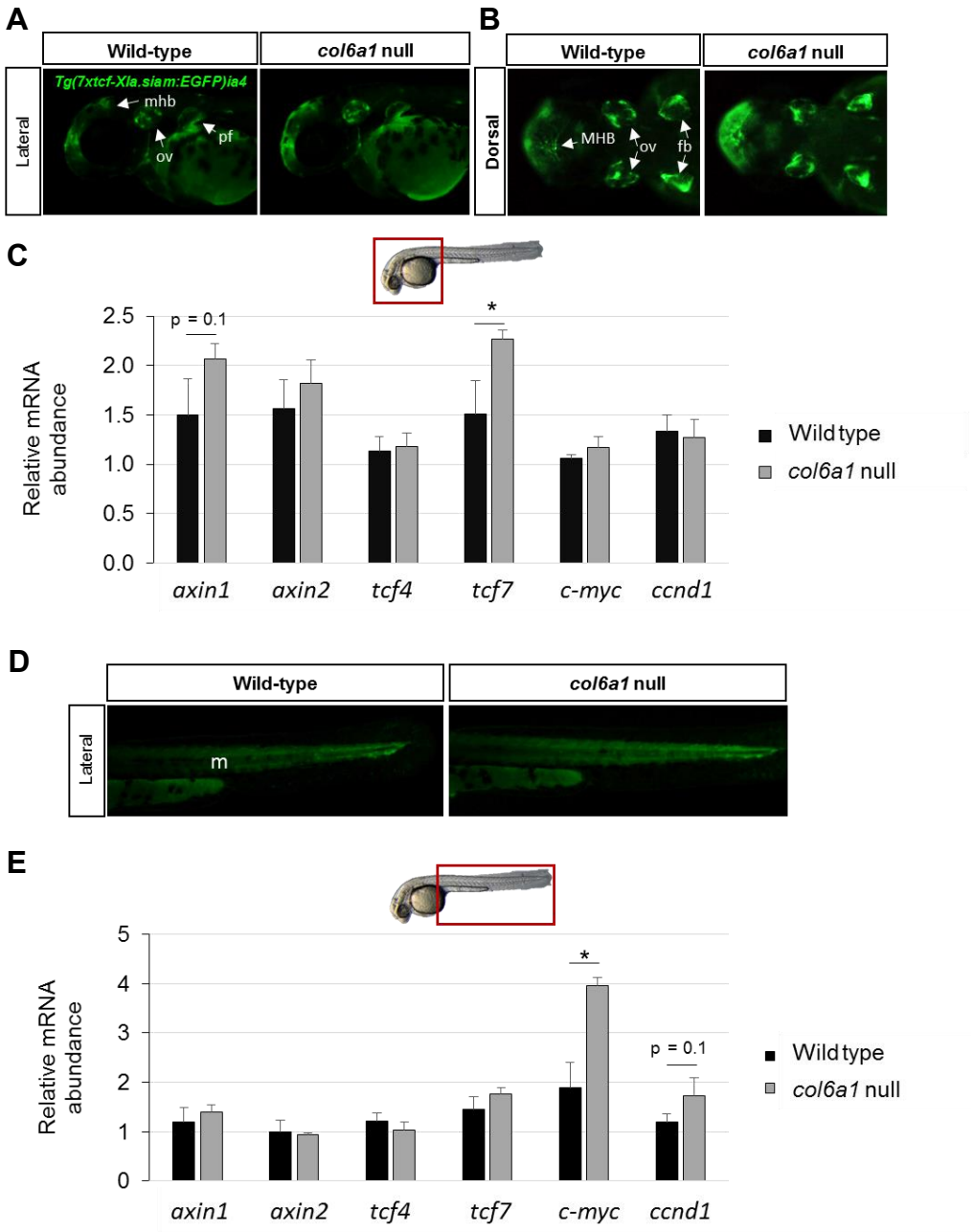

Figure 11. COL6 ablation leads to upregulation of Wnt signaling. **(A,B)** Representative images of 48-hpf *Tg(7xtcf-Xla.siam:EGFP)ia4* wild-type and *col6a1* null heads. **(A)** Lateral view, **(B)** Dorsal view. An increased Wnt reporter activity is observed In *col6a1* null embryos. MHB, midbrain-hindbrain boundary; ov, otic vesicle; pf, pectoral fin. **(C)** qRT-PCR showing the expression of *axin1*, *axin2*, *tcf4*, *tcf7*, *c-myc* and *ccnd1* transcripts in wild-type and *col6a1* null heads at 48 hpf. The upper part of the panel shows a 48-hpf embryo, where the region dissected to perform the qRT-PCR is delimited by a red square. Null embryos display a significant increase in the level of *tcf7* mRNA compared to wild-type ones. The graph reports mean ± SEM. Statistical significance was determined by Student's t-test (*, $p < 0.05$). **(D)** Representative images of 48-hpf *Tg(7xtcf-Xla.siam:EGFP)ia4* wild-type and *col6a1* null trunks. No major differences are observed in GFP labeling between the two genotypes. m, myotome.

(E) qRT-PCR showing the abundance of *axin1*, *axin2*, *tcf4*, *tcf7*, *c-myc* and *ccnd1* transcripts in wild-type and *col6a1* null trunks at 48 hpf. The upper part of the panel shows a 48-hpf embryo, where the region dissected to perform the qRT-PCR is delimited by a red square. Wnt targets (*c-myc*, *ccnd1*) are upregulated in *col6a1* null trunks. The graph reports mean ± SEM. Statistical significance was determined by Student's t-test **(***p* = 0.1).

First, I performed *in situ* hybridization of wild-type and *col6a1* null embryos with a probe against the cartilage marker *col2a1* at 48 hpf, since the first cartilages (i.e. pharyngeal arches and pectoral fin) start to develop at this developmental stages (Kimmel et al., 1995). This analysis did not show any overt difference in the amount or distribution of *col2a1* transcript between wild-type and *col6a1* null embryos (Fig. 12A). However, these experiments revealed some remarkable craniofacial features in null embryos. Indeed, I noticed that the angle formed by two pharyngeal cartilages, known as ceratohyals, was narrower in *col6a1* null fish (Fig. 13B, C). To support these findings and to investigate whether the defect was still present at later stages, I performed Alcian blue staining, a technique that allows analysing cartilage development in embryos and complete larvae (Walker and Kimmel, 2007). Interestingly, in 3-, 7- and 10-dpf *col6a1* null larvae I confirmed that the ceratohyal angle was significantly smaller compared to wild-type (Fig. 13D, G). In addition, I performed Alizarin red in 15-dpf larvae, to visualize mineralized bones (Walker and Kimmel, 2007). Normally, ossification of ceratohyal begins on the anterior margin of the element and extends along the cartilage until around 12 dpf (Cubbage and Mabee, 1996; Eames et al., 2013). Interestingly, I did not detect any significant difference between wild-type and *col6a1* null fish at this later developmental stage (Fig. 13E, G), suggesting that during the development, the ceratohyal angle defect displayed by early *col6a1* null larvae is somehow recovered.

To extend the analysis also to adult fish, which are no longer transparent, I exploited high-resolution micro–computed tomography (μ-CT), a very useful tool to assess trabecular and cortical bone morphology in animal and human specimens (Bouxsein et al., 2010). Of note, at 3 mpf the ceratohyal angle was significantly wider in *col6a1* null fish compared to wild-type, and at 15 mpf the angle became even larger (Fig. 3F, G). These results are particularly interesting, since it seems that the cartilaginous elements altered in the larvae were still defective also in the adult, although the entity of alteration changed. A possible explanation for the observed changes in the phenotypic defects may rely on the fact that from about 7 dpf zebrafish start to eat, thus the jaw is subjected to mechanical stress. Since COL6 in mammals is highly

expressed in tendons and ligaments (Keene, 1988; Sardone et al., 2016), the absence of this major ECM component may impact on the entire 3D architecture of jaws. In particular, when the fish start to eat, the pre-existent skeletal alterations may worsen as a consequence of mechanical stress.

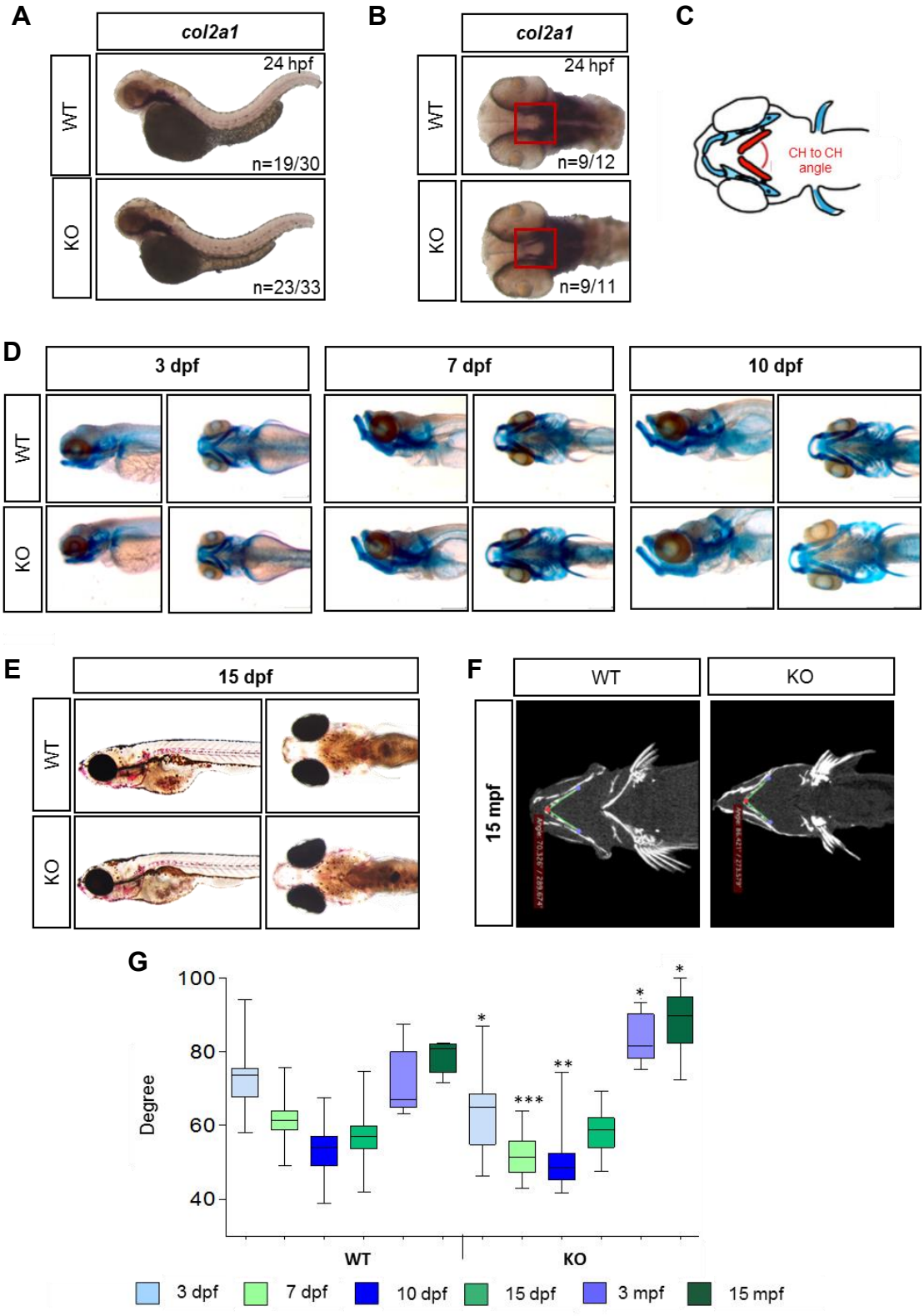

Figure 12. Characterization the skeletal phenotype of of *col6a1* null zebrafish. (A,B) *In situ* hybridization for *col2a1* expression in 48-hpf wild-type and *col6a1* null embryos. (**A**) Lateral view, (**B**) ventral view. The red square in B denotes ceratohyal cartilages. The distance between the two ceratohyal elements is smaller in *col6a1* null embryos. **(C)** Schematic representation of the angle formed by left and right ceratohyals (CH; modified from Petrey et al., 2012). **(D)** Alcian blue staining of 3-, 7- and 10-dpf larvae, showing that *col6a1* null fish display a narrower angle formed by left and right ceratohyal cartilages, when compared to wild-type ones. **(E)** Alizarin staining of 15-dpf wild-type and *col6a1* null larvae. No significant differences are observed in the width of CH angle between the two genotypes. **(F)** Three-dimensional bone reconstruction of micro-CT scans of 15-mpf adult zebrafish, showing that *col6a1* null fish display a wider angle formed by left and right ceratohyal elements, when compared to wild-type fish. **(G)** Graph showing the significant decrease in the width of CH angle in 3-, 7- and 10-dpf *col6a1* larvae and the increasing width of CH angle in 3- and 15-mpf *col6a1* null adults (3-dpf: wild type, $n = 11$, *col6a1* null, $n = 13$; 7-dpf: wild-type, $n = 23$, *col6a1* null, $n = 17$; 10-dpf, wild type, $n = 29$, *col6a1* null, $n = 17$; 15-dpf, wild-type, $n = 14$, *col6a1* null, $n = 13$; 3-mpf, wild-type, $n = 5$, *col6a1* null, $n = 6$; 15-mpf, wild-type. $n = 6$, *col6a1* null, $n = 6$). Statistical significance was determined by Student's t-test. p values refer to the same developmental stage (*, $p < 0.05$; **, $p < 0.01$; ***, $p < 0.001$). KO, *col6a1* null; WT, wild-type.

4. Discussion

COL6 is a major ECM protein forming a microfibrillar network in many tissues, in which it exerts several key roles (Cescon et al., 2015). In particular, COL6 is fundamental for the proper structure and function of skeletal muscle, and inherited mutations of the COL6 genes cause different forms of myopathies in humans, including UCMD and BM (Bönnemann, 2011a). A number of animal models have been generated for myopathies with a spectrum of phenotypes (Lamandé and Bateman, 2017). In particular, the generation of a *Col6a1* null mouse model provided a valuable tool for dissecting the *in vivo* functions of COL6 (Bonaldo et al., 1998). Indeed, studies on this model revealed that COL6 has several cytoprotective functions, which span from counteracting apoptosis and oxidative damage to regulating cell differentiation and autophagy (Bonaldo et al., 1998; Irwin et al., 2003; Urciuolo et al., 2013). Despite these notable findings, the information on the roles played by this ECM protein during development and in regulating intracellular signaling pathways are still very few. To obtain novel insights into these aspects, we decided to exploit *Danio rerio* (zebrafish), an animal model that has been widely used for studies of vertebrate development and gene function. Indeed, thanks to its transparency and rapid development, zebrafish represents a powerful tool to visualize the expression pattern of a gene in the whole organism. In addition, the availability of transgenic biosensor lines makes zebrafish an ideal model for the *in vivo* study of signaling pathways. Therefore, during my PhD work, I took advantage of this model organism to unveil signaling pathways and tissues affected by the absence of COL6.

In the last few years some studies on COL6 in zebrafish were published (Telfer et al., 2010; Radev et al., 2015; Ramanoudjame et al., 2015; Zech et al., 2015). These works exploited zebrafish morphants and mutant models with a reduced capability to produce COL6 chains to throw light on the effects of a reduced expression of COL6 in tissues such as skeletal muscle and nervous system. Although these studies provided new interesting findings, they also underlined the importance of the generation of stable zebrafish null lines, in which COL6 protein is permanently ablated, from embryonic to adult stages. Therefore, Bonaldo's team recently generated a stable zebrafish *col6a1* null line, that I validated and characterized during my PhD work.

The zebrafish *col6a1* null line was generated exploiting the CRISPR/Cas9 technology, a system that has become the most used genome editing approach in various species.

In particular, the planned approach was designed to target exon 5 of the zebrafish *col6a1* gene, coding for the N-terminal part of the α1(VI) chain. The *col6a1* gene encodes one of the essential chains required for COL6 assembly and secretion, and therefore no COL6 can be assembled secreted in the ECM following α1(VI) ablation. CRISPR/Cas9-mediated targeting of *col6a1* generated different mutations in the selected region of exon 5. Among them, a mutation corresponding to the insertion of 7 nucleotides was selected to generate the stable zebrafish *col6a1* null line, as this insertion was predicted to generate a frameshift and, as a consequence, a premature stop codon, thus preventing the translation of α1(VI) chain. By RT-qPCR and western blot experiments I demonstrated that the obtained zebrafish line effectively lacks COL6 expression in all analysed developmental stages and in the different tissues. Thus, this new zebrafish null line provides the possibility to dissect the roles of COL6 in a thorough manner throughout zebrafish life, taking a major step forward in comparison with the previously generated COL6 zebrafish models. During my PhD work, I investigated the histological, cellular and molecular phenotype of the *col6a1* null line, by focusing on some of the most relevant tissues and molecular aspects.

The data I obtained indicate that ablation of COL6 in zebrafish results in neuromuscular defects, which share some similar features with other previously described fish models for neuromuscular disorders and with impaired muscular development (Berger et al., 2010; Hall et al., 2007; Charvet et al., 2013; Smith et al., 2013; Smith et al., 2017; Wood et al., 2018; Bose et al., 2019). Indeed, although *col6a1* knockout fish do not display overt macroscopic alterations, they have remarkable defects in the three-dimensional organization and in the number of slow muscle fibers, during both embryonic development and adult life. In particular, 48-hpf *col6a1* null embryos display several muscle fibers detached from myosepta. Notably, myosepta are also misshapen in *col6a1* fish, with an expansion in the thickness of MTJ with increased matrix spaces. The myosepta represent characteristic structures separating myotomes and involved in force transmission during movement, and they are considered homologous to mammalian tendons based on similarities in their architectures and gene expression profiles (Kudo et al., 2004). Therefore, these findings indicate that COL6 is required for the stability of muscle attachments and that myofiber detachment can be a major cause of muscle degeneration. Interestingly, this phenotype is very similar to that observed in *candyfloss* (*caf*) mutants lacking laminin α2, another key ECM protein expressed in zebrafish myosepta, and mimicking muscular dystrophy congenital type 1A (MDC1A) (Hall et al., 2007). In the *caf* model,

it has been shown that myofiber detachment is worsened by motor activity. Thus, to evaluate whether COL6 ablation effectively makes the embryos more susceptible to myofiber detachment after motor activity, I incubated wild-type and *col6a1* null embryos from 48 to 6 dpf in a highly viscous medium that increases mechanical strain. Consistently, this led to a marked exacerbation of the muscular phenotype, thus demonstrating that mechanically overloading the muscles of COL6 null larvae increased the severity of myofiber pathology in these animals. Of note, physical training led to detrimental effects also in *Col6a1*$^{-/-}$ mice, which in standard housing conditions display a BM-like phenotype, leading to a muscle disease which is closer to the human UCMD pathology (Grumati et al., 2011). Therefore, *col6a1* null zebrafish model well mimics the murine and human COL6-related phenotypes, representing a valuable tool for the understanding of the pathophysiological mechanisms causing these phenotypes and for the screening and evaluation of drugs and therapeutic treatments. Intriguingly, a recent work demonstrated that the treatment of *caf* mutants with RGD (Arg-Gly-Asp) peptide, a potent inhibitor of integrin-β1, was able to improve myofiber stability (Wood et al., 2018). Wood and coll. showed that integrin-β1 is required for the correct localization of laminin and collagen I in the myosepta and that blocking integrin-β1 signalling in *caf* leads to the accumulation at the vertical myosepta of specific ECM components that stabilize muscle attachment. Based on this, the authors proposed that integrin-β1 could be a pharmacological target in different myopathic diseases, among which BM and UCMD (Wood et al., 2018). Therefore, it would be very interesting to test RGD peptides also on our *col6a1* null fish line and see whether this treatment can rescue muscle pathology, also in light of the fact that integrin-β1 is one of the COL6 interactors (Pfaff et al., 1993; Doane et al., 1998).

Increased mechanical stress is likely to contribute also to the reduced amount of slow muscle fibers displayed by *col6a1* null fish. On the other hand, the specification of slow muscle fibers during embryogenesis and muscle differentiation may be affected by COL6 ablation. To experimentally address this question, I investigated the amount and deposition of adaxial cells, which are the progenitors of slow muscle fibers (Devoto et al., 1996; Honjo and Eisen, 2005; Jackson and Ingham, 2013). Notably, the results indicate a remarkable reduction of adaxial cells density in 24-hpf *col6a1* null fish embryos. Thus, an intrinsic deficit in the adaxial cells, or in the signalling that regulates adaxial cells migration and differentiation, may be the primary cause for the onset of the myopathic phenotype displayed by *col6a1* null fish embryos, which is worsened by

locomotor activity. Of note, two major intracellular signaling pathways are involved in adaxial cells specification and migration, namely bone morphogenetic protein (BMP) and sonic hedgehog (Shh) pathways. Indeed, adaxial cells are allocated to the slow-twitch muscle lineage (Devoto et al., 1996) in response to prolonged notochord-derived Shh signals, while this specification can be suppressed by BMP-mediated signaling (Maurya et al., 2011). Therefore, it would be very interesting to investigate whether COL6 can have a role in modulating the availability of Shh and BMP ligands, since it has been shown that some ECM components affect the gradients of morphogens released from the notochord, such as Shh (Corallo et al., 2013). Toward this aim, I have already crossed *col6a1* null fish with reporter zebrafish lines for Shh and BMP pathways, and in the next future I will evaluate whether these signaling pathways are effectively dysregulated in COL6 deficiency. These studies are particularly relevant since the identification of signaling pathways affected by the ablation of this major ECM component are likely to have a strong impact on the thorough understanding of the mechanisms contributing to the onset and progression of muscle pathology in COL6-related myopathies.

Importantly, adaxial cells are also required to drive motor neuron axon toward their muscular targets (Zeller et al., 2002). In agreement with this, mutant models lacking adaxial cells display multiple and severe axonal pathfinding defects. For instance, in *you-too* (*yot*) zebrafish mutants, motor nerves are able to migrate within the spinal cord, but they do not extend into the periphery (Zeller et al., 2002). This is due to the fact that adaxial cells provide essential cues for axons projections into the somites. Interestingly, one of this cue is collagen XV (Pagnon-Minot et al., 2008), and a recent study in zebrafish demonstrated that both loss- and gain-of-function of *col15a1b* elicit pathfinding errors in motor neuron axons, resulting in muscle atrophy and compromised swimming behaviour (Guillon et al., 2016). This evidence is very intriguing, since we found that also COL6 ablation causes pathfinding errors beyond the choice point where axon pathway selection takes place. Of note, our findings are perfectly in line with the motor neuron guidance defects reported in transient *col6a4a* and *col6a4b* morphants (Ramanoudjame et al., 2015) and in *col6a3* mutants (Zech et al., 2015). Therefore, COL6 may be one of the cues released by adaxial cells to guide axon navigation in the ECM from the spinal cord to muscle targets. In addition, we also detected disorganization of AChR clusters in *col6a1* null embryos, a condition recently shown also in *Col6a1* null mice and UCMD patients (Cescon et al., 2018). Thus, together with axon guidance, COL6 could also have a role in the AChR pre-

patterning, both essential processes in the formation of neuromuscular synapses. Concerning this latter aspect, in literature it is reported that Wnt-induced trafficking of the muscle-specific kinase (MuSK) receptor triggers a signaling cascade that is crucial for AChR accumulation at future synaptic sites. Of note, a key secreted ligand involved in this process is Wnt11, expressed by adaxial cells (Jing et al., 2009; Gordon et al., 2012). In this respect, it will be interesting to determine whether in *col6a1* null fish embryos there is a mechanistic link between defective neuromuscular development and Wnt signaling alterations. Thus, the *col6a1* null fish line in the Wnt reporter background, which I generated during this PhD work, will be a highly valuable tool to experimentally address these aspects.

In order to evaluate whether the neuromuscular defects detected in *col6a1* null fish lead to functional alterations, I subjected them to motility and behavioural assays. In particular, I found that spontaneous coiling events are significantly decreased in 24-hpf COL6 null embryos. Interestingly, these movements are specifically mediated by slow muscle fibers (Naganawa and Hirata, 2011), suggesting that the defects observed in this cell type inevitably impact on motility. Of note, this functional parameter was found to be altered also in transient *col6a1* morphants (Telfer et al., 2010). In the light of fact that high-throughput drug screening and drug discovery in zebrafish is highly dependent on the identification of phenotypical readout suitable for chemical screening, a recent work proposed coiling defects as an ideal early phenotypic marker of *caf* mutants in large-scale drug screens (Smith et al., 2017). Based on this and on the data I obtained, the number of coiling events may be considered a useful and rapid readout in future drug screenings and testing in *col6a1* null embryos. In addition to coiling events, I also analysed startle responses, unconditioned behaviours consisting of rapid acceleration derived from the contraction of the axial muscles. This response is evoked by visual, touch or acoustic stimuli, and provides a measure of sensory and motor integration (Farooq et al., 2012). Intriguingly, the results I obtained show that *col6a1* null fish respond less to these stimuli when compared to wild-type siblings. These findings suggest that together with motor functions impairment we should also consider a possible involvement of the sensory component. Indeed, in spontaneous locomotor activity, the nervous system plays a central role (Saint-Amant and Drapeau, 1998; Xi et al., 2010). For instance, since I found that COL6 is abundantly expressed in zebrafish cornea, consistently with the pattern of COL6 distribution found in mammals (Zimmermann et al., 1986; Marvulli et al., 1996; Gara et al., 2011), it would be

interesting to investigate whether this ECM component plays a role in the transmission of light to the lens. Interestingly, a recent study reported that a 61-year-old woman with apolipoprotein A-I deficiency suffering from blurred vision with a corneal opacity showed several vesicles in the corneal stroma with a high content of COL6, and the authors suggested that structural changes in corneal COL6 deposition may contribute to corneal opacity (Namba et al., 2017).

Since NMJs are affected by COL6 deficiency (Cescon et al., 2018), it is reasonable to assume that the recovery of NMJ defects may ameliorate the neuromuscular phenotypes observed in absence of COL6. In a recent study, it was demonstrated that salbutamol, a β-adrenergic agonist, is able to counteract myasthenic syndromes, inherited neuromuscular conditions caused by alterations at the NMJ (McMacken et al., 2018). The authors knocked down two key postsynaptic proteins, Dok-7 and MuSK, in zebrafish and showed that salbutamol treatment leads to a notable improvement in AChR clustering, motor axon guidance and development of pre-patterned AChR clusters, with also a functional benefit in the motility and swimming behaviours of fish embryos (McMacken et al., 2018). Other literature studies reported that salbutamol displays beneficial effects in the respiratory function of children affected by type II spinal muscular atrophy (Khirani et al., 2017), as well as in Becker and Duchenne muscular dystrophy, by eliciting muscle strength improvement and increasing lean body mass (Fowler et al., 2004). Based on these evidence, I subjected *col6a1* null embryos to salbutamol treatment, to evaluate whether this treatment could rescue some of the defects displayed by *col6a1* null fish. Interestingly, both coiling and axons pathfinding defects were rescued after salbutamol treatment. Considered that this drug is beneficial for a large number of neuromuscular disorders, the results I obtained with the COL6 null zebrafish model suggest that salbutamol could be a good candidate also for the treatment of COL6-related diseases. Thus, in the next future, I will carry out further experiments to determine whether salbutamol can ameliorate other structural and functional parameters of the zebrafish *col6a1* null line, such as myofibers patterning and AChR clustering. Of note, it has been demonstrated that salbutamol also improves mitochondrial biogenesis and function in amyotrophic lateral sclerosis (Bartus et al., 2016). Thus, once again this drug could display multiple beneficial effects on COL6-related phenotypes, since mitochondria ultrastructural and functional alterations have been demonstrated in muscle biopsies and muscle cells of BM/UCMD patients (Angelin et al., 2007; Tagliavini et al., 2013), as well as in *Col6a1* knockout mice (Irwin et al., 2003). In this respect, during my PhD

work I detected swollen mitochondria in muscles of adult *col6a1* null fish. Moreover, mitochondrial swelling was present in *col6a1* null embryos, thus demonstrating for the first time that mitochondrial abnormalities are also found in developing muscles. Interestingly, the data I obtained show that COL6 knockout zebrafish have an impairment of the autophagic flux, in agreement with what was found in *Col6a1* knockout mice and BM/UCMD patients, where the accumulation of defective mitochondria is accompanied by an altered regulation of the autophagic machinery. Indeed, by quantifying LC3-II amounts, a widely used marker of autophagy, I detected higher levels of this marker in *col6a1* null embryos when compared with wild-type embryos, and these levels did not increase after exposure to ammonium chloride, which in normal conditions induces the accumulation of LC3-II. These results support a defective autophagic flux in COL6 null fish and strongly suggest the presence of a block in the terminal steps of autophagy, although further experiments exploiting late autophagic markers are needed to confirm this hypothesis. Nevertheless, this set of data is in line with what observed in fibroblast cultures from COL6-deficient mice, where defects in the autophagy/lysosome machinery together with impaired clearance of autophagosomes and altered lysosomal function were found (Castagnaro et al., 2018). Altogether, these findings suggest the *col6a1* null fish line could be a valuable tool also to study the molecular and mechanistic links between COL6 deficiency and mitochondrial defects in COL6-related disorders, which have not fully elucidated yet. I am currently evaluating the effects of salbutamol also on mitochondria morphology and autophagic flux in the *col6a1* null zebrafish.

To assess whether COL6 depletion affects signaling pathways involved in embryonic development, we crossed the *col6a1* null line with the *Tg(7xtcf-Xla.siam:EGFP)ia4*, a reporter fish line for the Wnt signaling pathway (Moro et al., 2012). As mentioned above, this signalling pathway is crucial for the promotion of AChR clustering at the synaptic sites (Gordon et al., 2012). Different literature works reported some indirect evidence and suggested a possible correlation between COL6 and this major signaling pathway. One study demonstrated that adipocyte-derived COL6 promotes early mammary tumor progression by binding the NG2/CSPG4 cell surface receptor and triggering the activation of the Wnt/β-catenin pathway (Izu et al., 2011). In addition, wound-induced hair regrowth is highly induced in *Col6a1* knockout mice, and this process has been shown to involve the activation of the Wnt/β-catenin signaling pathway (Chen et al., 2015b). Interestingly, the data I obtained with *col6a1* null fish in the Wnt reporter background suggest that the Wnt pathway is upregulated in 24-

and 48-hpf embryos, particularly in the brain region. These data support the possibility of a functional interaction between COL6 and Wnt signaling, which in turn may play crucial roles in physiological process and pathological conditions. For instance, it has been demonstrated that COL6 promotes neural crest cells (NCC) adhesion and migration, supporting the concept that it could be a cue participating in the regulation of NCC movement (Perris et al., 1993). Other literature studies revealed that the canonical Wnt signaling is needed for NCC differentiation, while the non-canonical Wnt signaling is required for their migration (De Calisto et al., 2005). In particular, loss- and gain-of-function experiments showed that Wnt11 plays a crucial role in neural crest migration (De Calisto et al., 2005). Therefore, it would be very intriguing to investigate whether besides being a substrate that guides NCC in their migration, COL6 could also act on the availability of Wnt ligands, thus affecting NCC migration and/or specification. Toward this aim, I have crossed the *col6a1* null fish line in Wnt reporter background with a reporter fish line for Sox10, a transcription factor involved in NCC fate specification (Carney et al., 2006), with the purpose of determining the effects of COL6 deficiency and simultaneously Wnt upregulation on NCC behaviour. Moreover, our studies revealed that COL6 is expressed in zebrafish meninges and brain vessels (see Chapter I), reflecting the distribution previously observed in mammals (Roggendorf et al., 1988; Sievers et al., 1994; Marvulli et al., 1996). In particular, our immunofluorescence experiments showed COL6 in close apposition to Wnt-positive cells, previously reported as endothelial cells (Moro et al., 2012). In this context, given the fact that Wnt signaling regulates the induction and maintenance of blood-brain barrier (Liebner et al., 2008; Obermeier et al., 2013), it will be interesting to elucidate, for instance by immunoprecipitation experiments, whether COL6 also plays a role in trapping and accumulating Wnt ligands, thus contributing to the fine regulation of Wnt signaling within the blood-brain barrier.

Beside skeletal muscle and nervous system, COL6 is also involved in the homeostasis of cartilage and bone. Indeed, it has been demonstrated that *Col6a1* null mice display an accelerated development of osteoarthritic joint degeneration, as well as a delayed secondary ossification process and reduced bone mineral density (Alexopoulos et al., 2009). Moreover, UCMD patients often display contractures and skeletal deformities in proximal joints (Bönnemann, 2011a). Thus, I carefully investigated whether *col6a1* null zebrafish display cartilaginous and skeletal defects. Interestingly, these experiments showed that the ceratohyal cartilages form a mishappen angle in COL6 knockout fish. The ceratohyal cartilages are the ventral element of the hyoid arch and

represent supportive structures of the lower jaw (Mork and Crump, 2015). In 3-, 7- and 10-dpf COL6 knockout larvae, I detected a narrower ceratohyal angle compared to that displayed by wild-type fish, while at 15 dpf no significant differences were present in fish of the two genotypes. Intriguingly, in 3- and 15-mpf adult fish, the width of ceratohyal angle was significantly increased in *col6a1* null fish, revealing an opposite change to that displayed during development. A likely explanation for this relies on the fact that from about 7 dpf zebrafish start to eat, thus the jaw is subjected to mechanical stress. Since COL6 in mammals is highly expressed in tendons and ligaments (Keene et al., 1991; Sardone et al., 2016), the lack of this major ECM component may impact on the entire three-dimensional architecture of jaws. In particular, when the fish start to eat, the pre-existent skeletal alterations may worsen as a consequence of mechanical stress. This compelling hypothesis needs to be validated in the next future through a detailed characterization of *col6a1* null tendons and ligaments, to verify if indeed the alteration of ceratohyal angle is a consequence of defective joints. Interestingly, previous studies showed that the tendons of *Col6a1*$^{-/-}$ mice have disrupted microdomains and abnormal fibrillogenesis, with a decrease in maximum load and stiffness, thus indicating that COL6 contributes to the maintenance of the mechanical properties of tendons (Izu et al., 2011; Kohara et al., 2016). Of note, some patients with COL6-related myopathies display limitations in jaw opening, with feeding and swallowing difficulties (Nadeau et al., 2009), suggesting that this particular district is a good candidate to highlight new relevant functions of COL6. A recent study defined the spatio-temporal dynamics of NG2/COL6 interactions during the progression of temporo-mandibular joint osteoarthritis (Yotsuya et al., 2019), a clinical syndrome characterized by arthralgia, limitation in mouth opening and painful chewing (Tanaka et al., 2008; Kalladka et al., 2014).

In conclusion, in this PhD work I characterized the structure, gene organization and expression of COL6 chains during zebrafish development and adult life. In addition, I performed functional studies exploiting a new zebrafish *col6a1* null line generated through CRISPR/Cas9 site-specific mutagenesis. COL6 ablation in the zebrafish animal model allowed to identify neuromuscular defects and distinctive alterations in the three-dimensional architecture of craniofacial cartilages. These functional studies also allowed me to detect changes in Wnt signalling, pointing at a possible role of COL6 in regulating this key signal pathway. Based on these latter findings, I have

planned a number of *in vitro* and *in vivo* studies aimed at elucidating in further in detail the mechanistic interactions between COL6 and Wnt signaling.

The zebrafish *col6a1* null line represents a valuable tool for the thorough understanding of the functions of COL6 during development and in regulating signaling pathways, thus allowing to unveil previously unknown links between molecular and signalling defects and COL6 deficiency. Indeed, the data reported in this thesis work underline that zebrafish is a very useful model for investigating the role of this distinctive ECM protein in different physiological and pathological contexts, also representing a suitable model for future drug testing aimed at the urgent quest for efficacious treatments and therapeutic opportunities for COL6-related diseases.

References

Aigner, T., Hambach, L., Söder, S., Schlötzer-Schrehardt, U. and Pöschl, E. (2002). The C5 Domain of Col6A3 Is Cleaved Off from the Col6 Fibrils Immediately after Secretion. *Biochem. Biophys. Res. Commun.* **290**, 743–748.

Albadri, S., Del Bene, F. and Revenu, C. (2017). Genome editing using CRISPR/Cas9-based knock-in approaches in zebrafish. *Methods* **121–122**, 77–85.

Alexopoulos, L. G., Youn, I., Bonaldo, P. and Guilak, F. (2009). Developmental and osteoarthritic changes in *Col6a1* -knockout mice: Biomechanics of type VI collagen in the cartilage pericellular matrix. *Arthritis Rheum.* **60**, 771–779.

Amiel, J., Sproat-Emison, E., Garcia-Barcelo, M., Lantieri, F., Burzynski, G., Borrego, S., Pelet, A., Arnold, S., Miao, X., Griseri, P., et al. (2007). Hirschsprung disease, associated syndromes and genetics: a review. *J. Med. Genet.* **45**, 1–14.

Amitai, G. and Sorek, R. (2016). CRISPR–Cas adaptation: insights into the mechanism of action. *Nat. Rev. Microbiol.* **14**, 67–76.

Angelin, A., Tiepolo, T., Sabatelli, P., Grumati, P., Bergamin, N., Golfieri, C., Mattioli, E., Gualandi, F., Ferlini, A., Merlini, L., et al. (2007). Mitochondrial dysfunction in the pathogenesis of Ullrich congenital muscular dystrophy and prospective therapy with cyclosporins. *Proc. Natl. Acad. Sci.* **104**, 991–996.

Aumailley, M., Bruckner-Tuderman, L., Carter, W. G., Deutzmann, R., Edgar, D., Ekblom, P., Engel, J., Engvall, E., Hohenester, E., Jones, J. C. R., et al. (2005). A simplified laminin nomenclature. *Matrix Biol.* **24**, 326–332.

Barrangou, R., Fremaux, C., Deveau, H., Richards, M., Boyaval, P., Moineau, S., Romero, D. A. and Horvath, P. (2007). CRISPR Provides Acquired Resistance Against Viruses in Prokaryotes. *Science (80-.).* **315**, 1709–1712.

Bartus, R. T., Bétourné, A., Basile, A., Peterson, B. L., Glass, J. and Boulis, N. M. (2016). β2-Adrenoceptor agonists as novel, safe and potentially effective therapies for Amyotrophic lateral sclerosis (ALS). *Neurobiol. Dis.* **85**, 11–24.

Berger, J., Berger, S., Hall, T. E., Lieschke, G. J. and Currie, P. D. (2010). Dystrophin-deficient zebrafish feature aspects of the Duchenne muscular dystrophy pathology. *Neuromuscul. Disord.* **20**, 826–832.

Bidanset, D. J., Guidry, C., Rosenberg, L. C., Choi, H. U., Timpl, R. and Hook, M. (1992). Binding of the proteoglycan decorin to collagen type VI. *J. Biol. Chem.*

267, 5250–5256.

Bonaldo, P., Russo, V., Bucciotti, F., Bressan, G. M. and Colombatti, A. (1989). Alpha 1 chain of chick type VI collagen. The complete cDNA sequence reveals a hybrid molecule made of one short collagen and three von Willebrand factor type A-like domains. *J. Biol. Chem.* **264**, 5575–5580.

Bonaldo, P., Russo, V., Bucciotti, F., Doliana, R. and Colombatti, A. (1990). Structural and functional features of the alpha 3 chain indicate a bridging role for chicken collagen VI in connective tissues. *Biochemistry* **29**, 1245–1254.

Bonaldo, P., Braghetta, P., Zanetti, M., Piccolo, S., Volpin, D. and Bressan, G. M. (1998). Collagen VI deficiency induces early onset myopathy in the mouse: an animal model for Bethlem myopathy. *Hum. Mol. Genet.* **7**, 2135–2140.

Bönnemann, C. G. (2011a). The collagen VI-related myopathies. In *Handbook of clinical neurology*, pp. 81–96.

Bönnemann, C. G. (2011b). The collagen VI-related myopathies: muscle meets its matrix. *Nat. Rev. Neurol.* **7**, 379–390.

Bose, P., Armstrong, G. A. B. and Drapeau, P. (2019). Neuromuscular junction abnormalities in a zebrafish loss-of-function model of TDP-43. *J. Neurophysiol.* **121**, 285–297.

Bouxsein, M. L., Boyd, S. K., Christiansen, B. A., Guldberg, R. E., Jepsen, K. J. and Müller, R. (2010). Guidelines for assessment of bone microstructure in rodents using micro-computed tomography. *J. Bone Miner. Res.* **25**, 1468–1486.

Braghetta, P., Ferrari, A., Fabbro, C., Bizzotto, D., Volpin, D., Bonaldo, P. and Bressan, G. M. (2008). An enhancer required for transcription of the Col6a1 gene in muscle connective tissue is induced by signals released from muscle cells. *Exp. Cell Res.* **314**, 3508–3518.

Brennan, C., Mangoli, M., Dyer, C. E. F. and Ashworth, R. (2005). Acetylcholine and calcium signalling regulates muscle fibre formation in the zebrafish embryo. *J. Cell Sci.* **118**, 5181–5190.

Briñas, L., Richard, P., Quijano-Roy, S., Gartioux, C., Ledeuil, C., Lacène, E., Makri, S., Ferreiro, A., Maugenre, S., Topaloglu, H., et al. (2010). Early onset collagen VI myopathies: Genetic and clinical correlations. *Ann. Neurol.* **68**, 511–520.

Brodsky, B. and Persikov, A. V. (2005). Molecular Structure of the Collagen Triple Helix. *Adv. Protein Chem.* **70**, 301–339.

Brown, J. C., Golbik, R., Mann, K. and Timpl, R. (1994). Structure and stability of the triple-helical domains of human collagen XIV. *Matrix Biol.* **14**, 287–295.

Camacho Vanegas, O., Bertini, E., Zhang, R. Z., Petrini, S., Minosse, C., Sabatelli, P., Giusti, B., Chu, M. L. and Pepe, G. (2001). Ullrich scleroatonic muscular dystrophy is caused by recessive mutations in collagen type VI. *Proc. Natl. Acad. Sci. U. S. A.* **98**, 7516–7521.

Caria, F., Cescon, M., Gualandi, F., Pichiecchio, A., Rossi, R., Rimessi, P., Cotti Piccinelli, S., Gallo Cassarino, S., Gregorio, I., Galvagni, A., et al. (2019). Autosomal recessive Bethlem myopathy: A clinical, genetic and functional study. *Neuromuscul. Disord.* **29**, 657-663.

Carney, T. J., Dutton, K. A., Greenhill, E., Delfino-Machin, M., Dufourcq, P., Blader, P. and Kelsh, R. N. (2006). A direct role for Sox10 in specification of neural crest-derived sensory neurons. *Development* **133**, 4619–4630.

Castagnaro, S., Pellegrini, C., Pellegrini, M., Chrisam, M., Sabatelli, P., Toni, S., Grumati, P., Ripamonti, C., Pratelli, L., Maraldi, N. M., et al. (2016). Autophagy activation in COL6 myopathic patients by a low-protein-diet pilot trial. *Autophagy* **12**, 2484–2495.

Castagnaro, S., Chrisam, M., Cescon, M., Braghetta, P., Grumati, P. and Bonaldo, P. (2018). Extracellular Collagen VI Has Prosurvival and Autophagy Instructive Properties in Mouse Fibroblasts. *Front. Physiol.* **9**, 1129.

Cescon, M., Gattazzo, F., Chen, P. and Bonaldo, P. (2015). Collagen VI at a glance. *J. Cell Sci.* **128**, 3525–3531.

Cescon, M., Gregorio, I., Bonaldo, P., Gregorio, I. and Bonaldo, P. (2017). Lack of collagen VI promotes neurodegeneration by impairing autophagy and inducing apoptosis during aging. *Aging.* **8**, 1083–1101.

Cescon, M., Gregorio, I., Eiber, N., Borgia, D., Fusto, A., Sabatelli, P., Scorzeto, M., Megighian, A., Pegoraro, E., Hashemolhosseini, S., et al. (2018). Collagen VI is required for the structural and functional integrity of the neuromuscular junction. *Acta Neuropathol.* **136**, 483–499.

Charvet, B., Ruggiero, F. and Le Guellec, D. (2012). The development of the myotendinous junction. A review. *Muscles. Ligaments Tendons J.* **2**, 53–63.

Charvet, B., Guiraud, A., Malbouyres, M., Zwolanek, D., Guillon, E., Bretaud, S., Monnot, C., Schulze, J., Bader, H. L., Allard, B., et al. (2013). Knockdown of col22a1 gene in zebrafish induces a muscular dystrophy by disruption of the myotendinous junction. *Development* **140**, 4602–4613.

Chen, P., Cescon, M., Megighian, A. and Bonaldo, P. (2014). Collagen VI regulates peripheral nerve myelination and function. *FASEB J.* **28**, 1145-1156.

Chen, P., Cescon, M., Zuccolotto, G., Nobbio, L., Colombelli, C., Filaferro, M., Vitale, G., Feltri, M. L. and Bonaldo, P. (2015a). Collagen VI regulates peripheral nerve regeneration by modulating macrophage recruitment and polarization. *Acta Neuropathol.* **129**, 97-113.

Chen, P., Cescon, M. and Bonaldo, P. (2015b). Lack of Collagen VI Promotes Wound-Induced Hair Growth. *J. Invest. Dermatol.* **135**, 2358–2367.

Cheng, J. S., Dubal, D. B., Kim, D. H., Legleiter, J., Cheng, I. H., Yu, G.-Q., Tesseur, I., Wyss-Coray, T., Bonaldo, P. and Mucke, L. (2009). Collagen VI protects neurons against Aβ toxicity. *Nat. Neurosci.* **12**, 119–121.

Cheng, I. H., Lin, Y.-C., Hwang, E., Huang, H.-T., Chang, W.-H., Liu, Y.-L. and Chao, C.-Y. (2011). Collagen VI protects against neuronal apoptosis elicited by ultraviolet irradiation via an Akt/Phosphatidylinositol 3-kinase signaling pathway. *Neuroscience* **183**, 178–188.

Chrisam, M., Pirozzi, M., Castagnaro, S., Blaauw, B., Polishchuck, R., Cecconi, F., Grumati, P. and Bonaldo, P. (2015). Reactivation of autophagy by spermidine ameliorates the myopathic defects of collagen VI-null mice. *Autophagy* **11**, 2142–2152.

Christensen, S. E., Coles, J. M., Zelenski, N. A., Furman, B. D., Leddy, H. A., Zauscher, S., Bonaldo, P. and Guilak, F. (2012). Altered Trabecular Bone Structure and Delayed Cartilage Degeneration in the Knees of Collagen VI Null Mice. *PLoS One* **7**, e33397.

Chu, M.-L., Conway, D., Pan, T.-C., Baldwin, C., Manns, K., Deutzmanns, R. and Timpls, R. (1988). Amino acid sequence of the triple-helical domain of human collagen type VI. *J. Biol. Chem*. **263,** 18601–18606.

Colombatti, A. and Bonaldo, P. (1987). Biosynthesis of chick type VI collagen. II. Processing and secretion in fibroblasts and smooth muscle cells. *J. Biol. Chem.* **262**, 14461–14466.

Colombatti, A., Bonaldo, P., Ainger, K., Bressan, G. M. and Volpin, D. (1987). Biosynthesis of chick type VI collagen. I. Intracellular assembly and molecular structure. *J. Biol. Chem.* **262**, 14454–14460.

Cong, L., Ran, F. A., Cox, D., Lin, S., Barretto, R., Habib, N., Hsu, P. D., Wu, X., Jiang, W., Marraffini, L. A., et al. (2013). Multiplex Genome Engineering Using CRISPR/Cas Systems. *Science (80-.).* **339**, 819–823.

Corallo, D., Schiavinato, A., Trapani, V., Moro, E., Argenton, F. and Bonaldo, P. (2013). Emilin3 is required for notochord sheath integrity and interacts with

Scube2 to regulate notochord-derived Hedgehog signals. *Development* **140**, 4594–4601.

Costa-Silva, B., da Costa, M. C., Melo, F. R., Neves, C. M., Alvarez-Silva, M., Calloni, G. W. and Trentin, A. G. (2009). Fibronectin promotes differentiation of neural crest progenitors endowed with smooth muscle cell potential. *Exp. Cell Res.* **315**, 955–967.

Cubbage, C. C. and Mabee, P. M. (1996). Development of the cranium and paired fins in the zebrafishDanio rerio (Ostariophysi, Cyprinidae). *J. Morphol.* **229**, 121–160.

Dahm, R. and Geisler, R. (2006). Learning from Small Fry: The Zebrafish as a Genetic Model Organism for Aquaculture Fish Species. *Mar. Biotechnol.* **8**, 329–345.

Davis, E. C. and Mecham, R. P. (1998). Intracellular trafficking of tropoelastin. *Matrix Biol.* **17**, 245–254.

De Calisto, J., Araya, C., Marchant, L., Riaz, C. F. and Mayor, R. (2005). Essential role of non-canonical Wnt signalling in neural crest migration. *Development* **132**, 2587–2597.

De Wever, O., Demetter, P., Mareel, M. and Bracke, M. (2008). Stromal myofibroblasts are drivers of invasive cancer growth. *Int. J. Cancer* **123**, 2229–2238.

Devoto, S. H., Melançon, E., Eisen, J. S. and Westerfield, M. (1996). Identification of separate slow and fast muscle precursor cells in vivo, prior to somite formation. *Development* **122**, 3371–3380.

Doane, K. J., Howell, S. J. and Birk, D. E. (1998). Identification and functional characterization of two type VI collagen receptors, alpha 3 beta 1 integrin and NG2, during avian corneal stromal development. *Invest. Ophthalmol. Vis. Sci.* **39**, 263–275.

Doliana, R., Bonaldo, P. and Colombatti, A. (1990). Multiple forms of chicken alpha 3(VI) collagen chain generated by alternative splicing in type A repeated domains. *J. Cell Biol.* **111**, 2197–2205.

Dziadek, M., Darling, P., Bakker, M., Overall, M., Zhang, R.-Z., Pan, T.-C., Tillet, E., Timpl, R. and Chu, M.-L. (1996). Deposition of Collagen VI in the Extracellular Matrix during Mouse Embryogenesis Correlates with Expression of the α3(VI) Subunit Gene. *Exp. Cell Res.* **226**, 302–315.

Eames, B., DeLaurier, A., Ullmann, B., Huycke, T. R., Nichols, J. T., Dowd, J., McFadden, M., Sasaki, M. M. and Kimmel, C. B. (2013). FishFace: interactive atlas of zebrafish craniofacial development at cellular resolution. *BMC Dev. Biol.*

13, 23.

Eimon, P. M. and Rubinstein, A. L. (2009). The use of *in vivo* zebrafish assays in drug toxicity screening. *Expert Opin. Drug Metab. Toxicol.* **5**, 393–401.

Ekker, M., Wegner, J., Akimenko, M. A., Westerfield, M., Johnson, R. L., Scott, M. P. and Ingham, P. W. (1992). Coordinate embryonic expression of three zebrafish engrailed genes. *Development* **116**, 1001–1010.

El-Shabrawi, Y., Kublin, C. L. and Cintron, C. (1998). mRNA levels of alpha1(VI) collagen, alpha1(XII) collagen, and beta ig in rabbit cornea during normal development and healing. *Invest. Ophthalmol. Vis. Sci.* **39**, 36–44.

Facchinello, N., Skobo, T., Meneghetti, G., Colletti, E., Dinarello, A., Tiso, N., Costa, R., Gioacchini, G., Carnevali, O., Argenton, F., et al. (2017). nr3c1 null mutant zebrafish are viable and reveal DNA-binding-independent activities of the glucocorticoid receptor. *Sci. Rep.* **7**, 4371.

Farooq, A., J, N. L. P. J., J, T. R. A. and K, R. M. (2012). Zebrafish embryos and larvae in behavioural assays. *Behaviour* **149**, 1241–1281.

Finnis, M. L. and Gibson, M. A. (1997). Microfibril-associated glycoprotein-1 (MAGP-1) binds to the pepsin-resistant domain of the alpha3(VI) chain of type VI collagen. *J. Biol. Chem.* **272**, 22817–22823.

Fitzgerald, J., Rich, C., Zhou, F. H. and Hansen, U. (2008). Three Novel Collagen VI Chains, α4(VI), α5(VI), and α6(VI). *J. Biol. Chem.* **283**, 20170–20180.

Fodor, E., Sigmond, T., Ari, E., Lengyel, K., Takács-Vellai, K., Varga, M. and Vellai, T. (2017). Methods to Study Autophagy in Zebrafish. In *Methods in enzymology*, pp. 467–496.

Foley, A. R., Hu, Y., Zou, Y., Columbus, A., Shoffner, J., Dunn, D. M., Weiss, R. B. and Bönnemann, C. G. (2009). Autosomal recessive inheritance of classic Bethlem myopathy. *Neuromuscul. Disord.* **19**, 813–817.

Fowler, E. G., Graves, M. C., Wetzel, G. T. and Spencer, M. J. (2004). Pilot trial of albuterol in Duchenne and Becker muscular dystrophy. *Neurology* **62**, 1006–1008.

Frantz, C., Stewart, K. M. and Weaver, V. M. (2010). The extracellular matrix at a glance. *J. Cell Sci.* **123**, 4195–4200.

Frka, K., Facchinello, N., Del Vecchio, C., Carpi, A., Curtarello, M., Venerando, R., Angelin, A., Parolin, C., Bernardi, P., Bonaldo, P., et al. (2009). Lentiviral-mediated RNAi in vivo silencing of Col6a1, a gene with complex tissue specific expression pattern. *J. Biotechnol.* **141**, 8–17.

Gara, S. K., Grumati, P., Urciuolo, A., Bonaldo, P., Kobbe, B., Koch, M., Paulsson, M. and Wagener, R. (2008). Three Novel Collagen VI Chains with High Homology to the α3 Chain. *J. Biol. Chem.* **283**, 10658–10670.

Gara, S. K., Grumati, P., Squarzoni, S., Sabatelli, P., Urciuolo, A., Bonaldo, P., Paulsson, M. and Wagener, R. (2011). Differential and restricted expression of novel collagen VI chains in mouse. *Matrix Biol.* **30**, 248–257.

Garcia, G. R., Noyes, P. D. and Tanguay, R. L. (2016). Advancements in zebrafish applications for 21st century toxicology. *Pharmacol. Ther.* **161**, 11–21.

Gordon, L. R., Gribble, K. D., Syrett, C. M. and Granato, M. (2012). Initiation of synapse formation by Wnt-induced MuSK endocytosis. *Development* **139**, 1023–1033.

Gregorio, I., Braghetta, P., Bonaldo, P. and Cescon, M. (2018). Collagen VI in healthy and diseased nervous system. *Dis. Model. Mech.* **11**.

Grumati, P., Coletto, L., Sabatelli, P., Cescon, M., Angelin, A., Bertaggia, E., Blaauw, B., Urciuolo, A., Tiepolo, T., Merlini, L., et al. (2010). Autophagy is defective in collagen VI muscular dystrophies, and its reactivation rescues myofiber degeneration. *Nat. Med.* **16**, 1313–1320.

Grumati, P., Coletto, L., Schiavinato, A., Castagnaro, S., Bertaggia, E., Sandri, M. and Bonaldo, P. (2011). Physical exercise stimulates autophagy in normal skeletal muscles but is detrimental for collagen VI-deficient muscles. *Autophagy* **7**, 1415–1423.

Guillon, E., Bretaud, S. and Ruggiero, F. (2016). Slow Muscle Precursors Lay Down a Collagen XV Matrix Fingerprint to Guide Motor Axon Navigation. *J. Neurosci.* **36**, 2663–2676.

Gupta, T. and Mullins, M. C. (2010). Dissection of Organs from the Adult Zebrafish. *J. Vis. Exp.* **1717**.

Haffter, P., Granato, M., Brand, M., Mullins, M. C., Hammerschmidt, M., Kane, D. A., Odenthal, J., van Eeden, F. J., Jiang, Y. J., Heisenberg, C. P., et al. (1996). The identification of genes with unique and essential functions in the development of the zebrafish, Danio rerio. *Development* **123**, 1–36.

Hall, T. E., Bryson-Richardson, R. J., Berger, S., Jacoby, A. S., Cole, N. J., Hollway, G. E., Berger, J. and Currie, P. D. (2007). The zebrafish candyfloss mutant implicates extracellular matrix adhesion failure in laminin 2-deficient congenital muscular dystrophy. *Proc. Natl. Acad. Sci.* **104**, 7092–7097.

Hallmann, R., Horn, N., Selg, M., Wendler, O., Pausch, F. and Sorokin, L. M. (2005).

Expression and Function of Laminins in the Embryonic and Mature Vasculature. *Physiol. Rev.* **85**, 979–1000.

Hansen, U., Allen, J. M., White, R., Moscibrocki, C., Bruckner, P., Bateman, J. F. and Fitzgerald, J. (2012). WARP Interacts with Collagen VI-Containing Microfibrils in the Pericellular Matrix of Human Chondrocytes. *PLoS One* **7**, e52793.

Haq, R. U., Speer, M. C., Chu, M.-L. and Tandan, R. (1999). Respiratory muscle involvement in Bethlem myopathy. *Neurology* **52**, 174–174.

Harwood, A. J. (1996). Native Polyacrylamide Gel Electrophoresis. In *Basic DNA and RNA Protocols*, pp. 93–96.

Hay, E. D. (1981). Extracellular matrix. *J. Cell Biol.* **91**, 205s–223s.

Heldin, P. and Pertoft, H. (1993). Synthesis and Assembly of the Hyaluronan-Containing Coats around Normal Human Mesothelial Cells. *Exp. Cell Res.* **208**, 422–429.

Heumüller, S. E., Talantikite, M., Napoli, M., Armengaud, J., Mörgelin, M., Hartmann, U., Sengle, G., Paulsson, M., Moali, C. and Wagener, R. (2019). C-terminal proteolysis of the collagen VI α3 chain by BMP-1 and proprotein convertase(s) releases endotrophin in fragments of different sizes. *J. Biol. Chem.* **294**, 13769-13780.

Honjo, Y. and Eisen, J. S. (2005). Slow muscle regulates the pattern of trunk neural crest migration in zebrafish. *Development* **132**, 4461–4470.

Howe, K., Clark, M. D., Torroja, C. F., Torrance, J., Berthelot, C., Muffato, M., Collins, J. E., Humphray, S., McLaren, K., Matthews, L., et al. (2013). The zebrafish reference genome sequence and its relationship to the human genome. *Nature* **496**, 498–503.

Ingham, P. W. (2009). The power of the zebrafish for disease analysis. *Hum. Mol. Genet.* **18**, R107–R112.

Inoue, D. and Wittbrodt, J. (2011). One for All—A Highly Efficient and Versatile Method for Fluorescent Immunostaining in Fish Embryos. *PLoS One* **6**, e19713.

Iozzo, R. V. and Sanderson, R. D. (2011). Proteoglycans in cancer biology, tumour microenvironment and angiogenesis. *J. Cell. Mol. Med.* **15**, 1013–1031.

Iozzo, R. V. and Schaefer, L. (2015). Proteoglycan form and function: A comprehensive nomenclature of proteoglycans. *Matrix Biol.* **42**, 11–55.

Irwin, W. A., Bergamin, N., Sabatelli, P., Reggiani, C., Megighian, A., Merlini, L., Braghetta, P., Columbaro, M., Volpin, D., Bressan, G. M., et al. (2003). Mitochondrial dysfunction and apoptosis in myopathic mice with collagen VI

deficiency. *Nat. Genet.* **35**, 367–371.

Izu, Y., Ansorge, H. L., Zhang, G., Soslowsky, L. J., Bonaldo, P., Chu, M.-L. and Birk, D. E. (2011). Dysfunctional tendon collagen fibrillogenesis in collagen VI null mice. *Matrix Biol.* **30**, 53–61.

Izu, Y., Ezura, Y., Mizoguchi, F., Kawamata, A., Nakamoto, T., Nakashima, K., Hayata, T., Hemmi, H., Bonaldo, P. and Noda, M. (2012). Type VI collagen deficiency induces osteopenia with distortion of osteoblastic cell morphology. *Tissue Cell* **44**, 1–6.

Jackson, H. E. and Ingham, P. W. (2013). Control of muscle fibre-type diversity during embryonic development: The zebrafish paradigm. *Mech. Dev.* **130**, 447–457.

Jansen, R., Embden, J. D. A. van, Gaastra, W. and Schouls, L. M. (2002). Identification of genes that are associated with DNA repeats in prokaryotes. *Mol. Microbiol.* **43**, 1565–1575.

Jao, L.-E., Wente, S. R. and Chen, W. (2013). Efficient multiplex biallelic zebrafish genome editing using a CRISPR nuclease system. *Proc. Natl. Acad. Sci. U. S. A.* **110**, 13904–13909.

Jiang, F. and Doudna, J. A. (2017). CRISPR–Cas9 Structures and Mechanisms. *Annu. Rev. Biophys.* **46**, 505–529.

Jinek, M., Chylinski, K., Fonfara, I., Hauer, M., Doudna, J. A. and Charpentier, E. (2012). A Programmable Dual-RNA-Guided DNA Endonuclease in Adaptive Bacterial Immunity. *Science (80-.).* **337**, 816–821.

Jing, L., Lefebvre, J. L., Gordon, L. R. and Granato, M. (2009). Wnt Signals Organize Synaptic Prepattern and Axon Guidance through the Zebrafish unplugged/MuSK Receptor. *Neuron* **61**, 721–733.

Jöbsis, G. J., Boers, J. M., Barth, P. G. and de Visser, M. (1999). Bethlem myopathy: a slowly progressive congenital muscular dystrophy with contractures. *Brain* **122**, 649–655.

Kadler, K. E., Baldock, C., Bella, J. and Boot-Handford, R. P. (2007). Collagens at a glance. *J. Cell Sci.* **120**, 1955–1958.

Kalladka, M., Quek, S., Heir, G., Eliav, E., Mupparapu, M. and Viswanath, A. (2014). Temporomandibular joint osteoarthritis: diagnosis and long-term conservative management: a topic review. *J. Indian Prosthodont. Soc.* **14**, 6–15.

Karkheiran, S., Krebs, C. E., Makarov, V., Nilipour, Y., Hubert, B., Darvish, H., Frucht, S., Shahidi, G. A., Buxbaum, J. D. and Paisán-Ruiz, C. (2013).

Identification of COL6A2 mutations in progressive myoclonus epilepsy syndrome. *Hum. Genet.* **132**, 275–283.

Keene, D. R. (1988). Ultrastructure of type VI collagen in human skin and cartilage suggests an anchoring function for this filamentous network. *J. Cell Biol.* **107**, 1995–2006.

Keene, D. R., Sakai, L. Y. and Burgeson, R. E. (1991). Human bone contains type III collagen, type VI collagen, and fibrillin: type III collagen is present on specific fibers that may mediate attachment of tendons, ligaments, and periosteum to calcified bone cortex. *J. Histochem. Cytochem.* **39**, 59–69.

Khirani, S., Dabaj, I., Amaddeo, A., Olmo Arroyo, J., Ropers, J., Tirolien, S., Coudert, V., Estournet, B., Fauroux, B. and Quijano-Roy, S. (2017). Effect of Salbutamol on Respiratory Muscle Strength in Spinal Muscular Atrophy. *Pediatr. Neurol.* **73**, 78–87.e1.

Kimmel, C. B., Ballard, W. W., Kimmel, S. R., Ullmann, B. and Schilling, T. F. (1995). Stages of embryonic development of the zebrafish. *Dev. Dyn.* **203**, 253–310.

Kleinstiver, B. P., Prew, M. S., Tsai, S. Q., Topkar, V. V., Nguyen, N. T., Zheng, Z., Gonzales, A. P. W., Li, Z., Peterson, R. T., Yeh, J.-R. J., et al. (2015). Engineered CRISPR-Cas9 nucleases with altered PAM specificities. *Nature* **523**, 481–485.

Klionsky, D. J., Abdelmohsen, K., Abe, A., Abedin, M. J., Abeliovich, H., Arozena, A. A., Adachi, H., Adams, C. M., Adams, P. D., Adeli, K., et al. (2016). Guidelines for the use and interpretation of assays for monitoring autophagy (3rd edition). *Autophagy* **12**, 1.

Kohara, Y., Soeta, S., Izu, Y., Arai, K. and Amasaki, H. (2016). Distribution of type VI collagen in association with osteoblast lineages in the groove of Ranvier during rat postnatal development. *Ann. Anat. - Anat. Anzeiger* **208**, 58–68.

Koster, R. and Sassen, W. A. (2015). A molecular toolbox for genetic manipulation of zebrafish. *Adv. Genomics Genet.* **5**, 151.

Kudo, H., Amizuka, N., Araki, K., Inohaya, K. and Kudo, A. (2004). Zebrafish periostin is required for the adhesion of muscle fiber bundles to the myoseptum and for the differentiation of muscle fibers. *Dev. Biol.* **267**, 473–487.

Kuo, H.-J., Maslen, C. L., Keene, D. R. and Glanville, R. W. (1997). Type VI Collagen Anchors Endothelial Basement Membranes by Interacting with Type IV Collagen. *J. Biol. Chem.* **272**, 26522–26529.

Lamandé, S. R. and Bateman, J. F. (2017). Collagen VI disorders: Insights on form and function in the extracellular matrix and beyond. *Matrix Biol.* **71-72**, 348–

367.

Lamandé, S. R., Mörgelin, M., Adams, N. E., Selan, C. and Allen, J. M. (2006). The C5 Domain of the Collagen VI α3(VI) Chain Is Critical for Extracellular Microfibril Formation and Is Present in the Extracellular Matrix of Cultured Cells. *J. Biol. Chem.* **281**, 16607–16614.

Lampe, A. K. and Bushby, K. M. D. (2005). Collagen VI related muscle disorders. *J. Med. Genet.* **42**, 673–685.

Li, M., Zhao, L., Page-McCaw, P. S. and Chen, W. (2016). Zebrafish Genome Engineering Using the CRISPR–Cas9 System. *Trends Genet.* **32**, 815–827.

Liebner, S., Corada, M., Bangsow, T., Babbage, J., Taddei, A., Czupalla, C. J., Reis, M., Felici, A., Wolburg, H., Fruttiger, M., et al. (2008). Wnt/β-catenin signaling controls development of the blood–brain barrier. *J. Cell Biol.* **183**, 409–417.

Lucero, H. A. and Kagan, H. M. (2006). Lysyl oxidase: an oxidative enzyme and effector of cell function. *Cell. Mol. Life Sci.* **63**, 2304–2316.

Maaß, T., Bayley, C. P., Mörgelin, M., Lettmann, S., Bonaldo, P., Paulsson, M., Baldock, C. and Wagener, R. (2016). Heterogeneity of collagen VI microfibrils: Structural analysis of non-collagenous regions. *J. Biol. Chem.* **291**, 5247–5258.

Makarova, K. S., Wolf, Y. I., Alkhnbashi, O. S., Costa, F., Shah, S. A., Saunders, S. J., Barrangou, R., Brouns, S. J. J., Charpentier, E., Haft, D. H., et al. (2015). An updated evolutionary classification of CRISPR-Cas systems. *Nat. Rev. Microbiol.* **13**, 722–736.

Marraffini, L. A. and Sontheimer, E. J. (2010). Self versus non-self discrimination during CRISPR RNA-directed immunity. *Nature* **463**, 568–571.

Marvulli, D., Volpin, D. and Bressan, G. M. (1996). Spatial and temporal changes of typeVI collagen expression during mouse development. *Dev. Dyn.* **206**, 447–454.

Mathai, B. J., Meijer, A. H. and Simonsen, A. (2017). Studying Autophagy in Zebrafish. *Cells* **6**, 21.

Maurya, A. K., Tan, H., Souren, M., Wang, X., Wittbrodt, J. and Ingham, P. W. (2011). Integration of Hedgehog and BMP signalling by the engrailed2a gene in the zebrafish myotome. *Development* **138**, 755–765.

McCawley, L. J. and Matrisian, L. M. (2001). Matrix metalloproteinases: they're not just for matrix anymore! *Curr. Opin. Cell Biol.* **13**, 534–540.

McMacken, G., Cox, D., Roos, A., Müller, J., Whittaker, R. and Lochmüller, H. (2018). The beta-adrenergic agonist salbutamol modulates neuromuscular junction formation in zebrafish models of human myasthenic syndromes. *Hum.*

Mol. Genet. **27**, 1556–1564.

Meeker, N. D., Hutchinson, S. A., Ho, L. and Trede, N. S. (2007). Method for isolation of PCR-ready genomic DNA from zebrafish tissues. *Biotechniques* **43**, 610–614.

Mercuri, E., Yuva, Y., Brown, S. C., Brockington, M., Kinali, M., Jungbluth, H., Feng, L., Sewry, C. A., Muntoni, F., Mercuri, E., et al. (2002). Collagen VI involvement in Ullrich syndrome: a clinical, genetic, and immunohistochemical study. *Neurology* **58**, 1354–1359.

Merlini, L. and Bernardi, P. (2008). Therapy of collagen VI-related myopathies (Bethlem and Ullrich). *Neurotherapeutics* **5**, 613–618.

Merlini, L., Angelin, A., Tiepolo, T., Braghetta, P., Sabatelli, P., Zamparelli, A., Ferlini, A., Maraldi, N. M., Bonaldo, P. and Bernardi, P. (2008a). Cyclosporin A corrects mitochondrial dysfunction and muscle apoptosis in patients with collagen VI myopathies. *Proc. Natl. Acad. Sci.* **105**, 5225–5229.

Merlini, L., Martoni, E., Grumati, P., Sabatelli, P., Squarzoni, S., Urciuolo, A., Ferlini, A., Gualandi, F. and Bonaldo, P. (2008b). Autosomal recessive myosclerosis myopathy is a collagen VI disorder. *Neurology* **71**, 1245–1253.

Mizushima, N., Yoshimori, T. and Levine, B. (2010). Methods in mammalian autophagy research. *Cell* **140**, 313–26.

Mork, L. and Crump, G. (2015). Zebrafish Craniofacial Development: A Window into Early Patterning. *Curr. Top. Dev. Biol.* **115**, 235–269.

Moro, E., Ozhan-Kizil, G., Mongera, A., Beis, D., Wierzbicki, C., Young, R. M., Bournele, D., Domenichini, A., Valdivia, L. E., Lum, L., et al. (2012). In vivo Wnt signaling tracing through a transgenic biosensor fish reveals novel activity domains. *Dev. Biol.* **366**, 327–340.

Nadeau, A. and Muntoni, F. (2008). Skin changes in Ullrich congenital muscular dystrophy. *Neuromuscul. Disord.* **18**, 982.

Nadeau, A., Kinali, M., Main, M., Jimenez-Mallebrera, C., Aloysius, A., Clement, E., North, B., Manzur, A. Y., Robb, S. A., Mercuri, E., et al. (2009). Natural history of Ullrich congenital muscular dystrophy. *Neurology* **73**, 25–31.

Naganawa, Y. and Hirata, H. (2011). Developmental transition of touch response from slow muscle-mediated coilings to fast muscle-mediated burst swimming in zebrafish. *Dev. Biol.* **355**, 194–204.

Namba, H., Narumi, M., Susa, S., Ohe, R., Kato, T., Yamakawa, M. and Yamashita, H. (2017). Corneal vesicles accumulate collagen VI associated with tissue remodeling in apolipoprotein a-I deficiency: a case report. *BMC Ophthalmol.* **17**,

11.

Nishimura, Y., Inoue, A., Sasagawa, S., Koiwa, J., Kawaguchi, K., Kawase, R., Maruyama, T., Kim, S. and Tanaka, T. (2016). Using zebrafish in systems toxicology for developmental toxicity testing. *Congenit. Anom. (Kyoto).* **56**, 18–27.

Nonaka, I., Une, Y., Ishihara, T., Miyoshino, S., Nakashima, T. and Sugita, H. (1981). A clinical and histological study of Ullrich's disease (congenital atonic-sclerotic muscular dystrophy). *Neuropediatrics* **12**, 197–208.

Obermeier, B., Daneman, R. and Ransohoff, R. M. (2013). Development, maintenance and disruption of the blood-brain barrier. *Nat. Med.* **19**, 1584–1596.

Ono, F., Shcherbatko, A., Higashijima, S., Mandel, G. and Brehm, P. (2002). The Zebrafish motility mutant twitch once reveals new roles for rapsyn in synaptic function. *J. Neurosci.* **22**, 6491–6498.

Pagnon-Minot, A., Malbouyres, M., Haftek-Terreau, Z., Kim, H. R., Sasaki, T., Thisse, C., Thisse, B., Ingham, P. W., Ruggiero, F. and Le Guellec, D. (2008). Collagen XV, a novel factor in zebrafish notochord differentiation and muscle development. *Dev. Biol.* **316**, 21–35.

Palumbo, C., Massa, R., Panico, M. B., Di Muzio, A., Sinibaldi, P., Bernardi, G. and Modesti, A. (2002). Peripheral nerve extracellular matrix remodeling in Charcot-Marie-Tooth type I disease. *Acta Neuropathol.* **104**, 287–296.

Pankov, R. (2002). Fibronectin at a glance. *J. Cell Sci.* **115**, 3861–3863.

Park, J. and Scherer, P. E. (2012). Adipocyte-derived endotrophin promotes malignant tumor progression. *J. Clin. Invest.* **122**, 4243–4256.

Peltonen, J. T., Kalliomäki, M. A. and Muona, P. K. (1997). Extracellular matrix of peripheral nerves in diabetes. *J. Peripher. Nerv. Syst.* **2**, 213–226.

Perris, R., Kuo, H.-J., Glanville, R. W. and Bronner-Fraser, M. (1993). Collagen type VI in neural crest development: Distribution in situ and interaction with cells in vitro. *Dev. Dyn.* **198**, 135–149.

Pfaff, M., Aumailley, M., Specks, U., Knolle, J., Zerwes, H. G. and Timpl, R. (1993). Integrin and Arg-Gly-Asp Dependence of Cell Adhesion to the Native and Unfolded Triple Helix of Collagen Type VI. *Exp. Cell Res.* **206**, 167–176.

Prats, E., Gómez-Canela, C., Ben-Lulu, S., Ziv, T., Padrós, F., Tornero, D., Garcia-Reyero, N., Tauler, R., Admon, A. and Raldúa, D. (2017). Modelling acrylamide acute neurotoxicity in zebrafish larvae. *Sci. Rep.* **7**, 13952.

Radev, Z., Hermel, J.-M., Elipot, Y., Bretaud, S., Arnould, S., Duchateau, P., Ruggiero, F., Joly, J.-S. and Sohm, F. (2015). A TALEN-Exon Skipping Design for a Bethlem Myopathy Model in Zebrafish. *PLoS One* **10**, e0133986.

Ramanoudjame, L., Rocancourt, C., Lainé, J., Klein, A., Joassard, L., Gartioux, C., Fleury, M., Lyphout, L., Kabashi, E., Ciura, S., et al. (2015). Two novel COLVI long chains in zebrafish that are essential for muscle development. *Hum. Mol. Genet.* **24**, 6624–6639.

Roggendorf, W., Opitz, H. and Schuppan, D. (1988). Altered expression of collagen type VI in brain vessels of patients with chronic hypertension. *Acta Neuropathol.* **77**, 55–60.

Rozario, T. and DeSimone, D. W. (2010). The extracellular matrix in development and morphogenesis: A dynamic view. *Dev. Biol.* **341**, 126–140.

Rubinsztein, D. C., Cuervo, A. M., Ravikumar, B., Sarkar, S., Korolchuk, V. I., Kaushik, S. and Klionsky, D. J. (2009). In search of an "autophagomometer." *Autophagy* **5**, 585–589.

Sabatelli, P., Bonaldo, P., Lattanzi, G., Braghetta, P., Bergamin, N., Capanni, C., Mattioli, E., Columbaro, M., Ognibene, A., Pepe, G., et al. (2001). Collagen VI deficiency affects the organization of fibronectin in the extracellular matrix of cultured fibroblasts. *Matrix Biol.* **20**, 475–486.

Sabatelli, P., Gara, S. K., Grumati, P., Urciuolo, A., Gualandi, F., Curci, R., Squarzoni, S., Zamparelli, A., Martoni, E., Merlini, L., et al. (2011). Expression of the Collagen VI α5 and α6 Chains in Normal Human Skin and in Skin of Patients with Collagen VI-Related Myopathies. *J. Invest. Dermatol.* **131**, 99–107.

Saint-Amant, L. and Drapeau, P. (1998). Time course of the development of motor behaviors in the zebrafish embryo. *J. Neurobiol.* **37**, 622–632.

Sardone, F., Santi, S., Tagliavini, F., Traina, F., Merlini, L., Squarzoni, S., Cescon, M., Wagener, R., Maraldi, N. M., Bonaldo, P., et al. (2016). Collagen VI–NG2 axis in human tendon fibroblasts under conditions mimicking injury response. *Matrix Biol.* **55**, 90–105.

Sasaki, T., Göhring, W., Pan, T.-C., Chu, M.-L. and Timpl, R. (1995). Binding of Mouse and Human Fibulin-2 to Extracellular Matrix Ligands. *J. Mol. Biol.* **254**, 892–899.

Schaefer, L. and Schaefer, R. M. (2010). Proteoglycans: from structural compounds to signaling molecules. *Cell Tissue Res.* **339**, 237-246.

Shoulders, M. D. and Raines, R. T. (2009). Collagen Structure and Stability. *Annu.*

Rev. Biochem. **78**, 929–958.

Sievers, J., Pehlemann, F. W., Gude, S. and Berry, M. (1994). Meningeal cells organize the superficial glia limitans of the cerebellum and produce components of both the interstitial matrix and the basement membrane. *J. Neurocytol.* **23**, 135–149.

Silbert, J. E. and Sugumaran, G. (1995). Intracellular membranes in the synthesis, transport, and metabolism of proteoglycans. *Biochim. Biophys. Acta - Rev. Biomembr.* **1241**, 371–384.

Smeriglio, P., Lee, J. and Bhutani, N. (2017). Soluble Collagen VI treatment enhances mesenchymal stem cells expansion for engineering cartilage. *Bioeng. Transl. Med.* **2**, 278–284.

Smith, M. L., Gourdon, D., Little, W. C., Kubow, K. E., Eguiluz, R. A., Luna-Morris, S. and Vogel, V. (2007). Force-Induced Unfolding of Fibronectin in the Extracellular Matrix of Living Cells. *PLoS Biol.* **5**, e268.

Smith, L. L., Beggs, A. H. and Gupta, V. A. (2013). Analysis of skeletal muscle defects in larval zebrafish by birefringence and touch-evoke escape response assays. *J. Vis. Exp.* e50925.

Smith, S. J., Wang, J. C., Gupta, V. A. and Dowling, J. J. (2017). A novel early onset phenotype in a zebrafish model of merosin deficient congenital muscular dystrophy. *PLoS One* **12**, e0172648.

Soret, R., Mennetrey, M., Bergeron, K. F., Dariel, A., Neunlist, M., Grunder, F., Faure, C., Silversides, D. W., Pilon, N. and Ente-Hirsch Study Group (2015). A collagen VI–dependent pathogenic mechanism for Hirschsprung's disease. *J. Clin. Invest.* **125**, 4483–4496.

Specks, U., Mayer, U., Nischt, R., Spissinger, T., Mann, K., Timpl, R., Engel, J. and Chu, M. L. (1992). Structure of recombinant N-terminal globule of type VI collagen alpha 3 chain and its binding to heparin and hyaluronan. *EMBO J.* **11**, 4281–4290.

Stallcup, W. B., Dahlin, K. and Healy, P. (1990). Interaction of the NG2 chondroitin sulfate proteoglycan with type VI collagen. *J. Cell Biol.* **111**, 3177–3188.

Tagliavini, F., Sardone, F., Squarzoni, S., Maraldi, N. M., Merlini, L., Faldini, C. and Sabatelli, P. (2013). Ultrastructural changes in muscle cells of patients with collagen VI-related myopathies. *Muscles. Ligaments Tendons J.* **3**, 281–286.

Takahashi, T., Cho, H. I., Kublin, C. L. and Cintron, C. (1993). Keratan sulfate and dermatan sulfate proteoglycans associate with type VI collagen in fetal rabbit

cornea. *J. Histochem. Cytochem.* **41**, 1447–1457.

Tanaka, E., Detamore, M. S. and Mercuri, L. G. (2008). Degenerative Disorders of the Temporomandibular Joint: Etiology, Diagnosis, and Treatment. *J. Dent. Res.* **87**, 296–307.

Tavares, B. and Santos Lopes, S. The importance of Zebrafish in biomedical research. *Acta Med. Port.* **26**, 583–592.

Tegelenbosch, R. A. J., Noldus, L. P. J. J., Richardson, M. K. and Ahmad, F. (2012). Zebrafish embryos and larvae in behavioural assays. *Behaviour* **149**, 1241–1281.

Telfer, W. R., Busta, A. S., Bonnemann, C. G., Feldman, E. L. and Dowling, J. J. (2010). Zebrafish models of collagen VI-related myopathies. *Hum. Mol. Genet.* **19**, 2433–2444.

Theocharis, A. D., Skandalis, S. S., Tzanakakis, G. N. and Karamanos, N. K. (2010). Proteoglycans in health and disease: novel roles for proteoglycans in malignancy and their pharmacological targeting. *FEBS J.* **277**, 3904–3923.

Theocharis, A. D., Skandalis, S. S., Gialeli, C. and Karamanos, N. K. (2016). Extracellular matrix structure. *Adv. Drug Deliv. Rev.* **97**, 4-27.

Thisse, C. and Thisse, B. (2008). High-resolution in situ hybridization to whole-mount zebrafish embryos. *Nat. Protoc.* **3**, 59–69.

Tidball, J. G. (1991). Force transmission across muscle cell membranes. *J. Biomech.* **24**, 43–52.

Tsang, K. Y., Cheung, M. C. H., Chan, D. and Cheah, K. S. E. (2010). The developmental roles of the extracellular matrix: beyond structure to regulation. *Cell Tissue Res.* **339**, 93–110.

Tulla, M., Pentikäinen, O. T., Viitasalo, T., Käpylä, J., Impola, U., Nykvist, P., Nissinen, L., Johnson, M. S. and Heino, J. (2001). Selective binding of collagen subtypes by integrin alpha 1I, alpha 2I, and alpha 10I domains. *J. Biol. Chem.* **276**, 48206–48212.

Turley, E. A., Noble, P. W. and Bourguignon, L. Y. W. (2002). Signaling properties of hyaluronan receptors. *J. Biol. Chem.* **277**, 4589–4592.

Umeda, K. and Shoji, W. (2017). From neuron to behavior: Sensory-motor coordination of zebrafish turning behavior. *Dev. Growth Differ.* **59**, 107–114.

Urciuolo, A., Quarta, M., Morbidoni, V., Gattazzo, F., Molon, S., Grumati, P., Montemurro, F., Tedesco, F. S., Blaauw, B., Cossu, G., et al. (2013). Collagen VI regulates satellite cell self-renewal and muscle regeneration. *Nat. Commun.* **4**, 1964.

Varshney, G. K., Pei, W., LaFave, M. C., Idol, J., Xu, L., Gallardo, V., Carrington, B., Bishop, K., Jones, M., Li, M., et al. (2015). High-throughput gene targeting and phenotyping in zebrafish using CRISPR/Cas9. *Genome Res.* **25**, 1030–1042.

Vitale, P., Braghetta, P., Volpin, D., Bonaldo, P. and Bressan, G. M. (2001). Mechanisms of transcriptional activation of the col6a1 gene during Schwann cell differentiation. *Mech. Dev.* **102**, 145–156.

Voit, T. (1998). Congenital muscular dystrophies: 1997 update. *Brain Dev.* **20**, 65–74.

Walker, M. and Kimmel, C. (2007). A two-color acid-free cartilage and bone stain for zebrafish larvae. *Biotech. Histochem.* **82**, 23–28.

Wells, J. M., Gaggar, A. and Blalock, J. E. (2015). MMP generated matrikines. *Matrix Biol.* **44–46**, 122–129.

Wiberg, C., Hedbom, E., Khairullina, A., Lamandé, S. R., Oldberg, A., Timpl, R., Mörgelin, M. and Heinegård, D. (2001). Biglycan and decorin bind close to the n-terminal region of the collagen VI triple helix. *J. Biol. Chem.* **276**, 18947–18952.

Wise, S. G. and Weiss, A. S. (2009). Tropoelastin. *Int. J. Biochem. Cell Biol.* **41**, 494–497.

Wood, A. J., Cohen, N., Joshi, V., Li, M., Costin, A., Hersey, L., McKaige, E. A., Manneken, J. D., Sonntag, C., Miles, L. B., et al. (2018). RGD inhibition of itgb1 ameliorates laminin- $\boldsymbol{\alpha}$ 2-deficient zebrafish fibre pathology. *Hum. Mol. Genet.* **28**, 1403–1413.

Xi, Y., Ryan, J., Noble, S., Yu, M., Yilbas, A. E. and Ekker, M. (2010). Impaired dopaminergic neuron development and locomotor function in zebrafish with loss of *pink1* function. *Eur. J. Neurosci.* **31**, 623–633.

Yagihashi, S., Yamagishi, S.-I. and Wada, R. (2007). Pathology and pathogenetic mechanisms of diabetic neuropathy: Correlation with clinical signs and symptoms. *Diabetes Res. Clin. Pract.* **77**, S184–S189.

Yan, Y.-L., Hatta, K., Riggleman, B. and Postlethwait, J. H. (1995). Expression of a type II collagen gene in the zebrafish embryonic axis. *Dev. Dyn.* **203**, 363–376.

Yotsuya, M., Bertagna, A. E., Hasan, N., Bicknell, S., Sato, T. and Reed, D. A. (2019). Neuron/Glial Antigen 2-Type VI Collagen Interactions During Murine Temporomandibular Joint Osteoarthritis. *Sci. Rep.* **9**, 56.

Zech, M., Lam, D. D., Francescatto, L., Schormair, B., Salminen, A. V., Jochim, A., Wieland, T., Lichtner, P., Peters, A., Gieger, C., et al. (2015). Recessive Mutations in the α3 (VI) Collagen Gene COL6A3 Cause Early-Onset Isolated Dystonia. *Am. J. Hum. Genet.* **96**, 883–893.

Zelenski, N. A., Leddy, H. A., Sanchez-Adams, J., Zhang, J., Bonaldo, P., Liedtke, W. and Guilak, F. (2015). Type VI Collagen Regulates Pericellular Matrix Properties, Chondrocyte Swelling, and Mechanotransduction in Mouse Articular Cartilage. *Arthritis Rheumatol.* **67**, 1286–1294.

Zeller, J., Schneider, V., Malayaman, S., Higashijima, S., Okamoto, H., Gui, J., Lin, S. and Granato, M. (2002). Migration of Zebrafish Spinal Motor Nerves into the Periphery Requires Multiple Myotome-Derived Cues. *Dev. Biol.* **252**, 241–256.

Zimmermann, D. R., Trüeb, B., Winterhalter, K. H., Witmer, R. and Fischer, R. W. (1986). Type VI collagen is a major component of the human cornea. *FEBS Lett.* **197**, 55–58.

Zulian, A., Rizzo, E., Schiavone, M., Palma, E., Tagliavini, F., Blaauw, B., Merlini, L., Maraldi, N. M., Sabatelli, P., Braghetta, P., et al. (2014). NIM811, a cyclophilin inhibitor without immunosuppressive activity, is beneficial in collagen VI congenital muscular dystrophy models. *Hum. Mol. Genet.* **23**, 5353–5363.